ABSTRACT

Title of Document:	SUPERCRITICAL FLUID EXTRACTION OF HYDROCARBONS FROM THE MARCELLUS SHALE BY USING CO_2
	Palma Jean Jarboe, Master of Science, 2014
Directed By:	Professor Philip Candela Department of Geology

Supercritical carbon dioxide was used to extract n-aliphatic hydrocarbons from samples of Marcellus shale, and to evaluate recovery as a function of sample matrix particle size (sieve size). Results show that supercritical CO_2 has the potential to liberate diesel-range n-aliphatic hydrocarbons from high-maturity shale at estimated *in situ* pressure and temperature conditions. Total quantity of resolvable n-aliphatic hydrocarbons ranged from approximately 0.3 - 12 milligrams of hydrocarbon per gram of total organic carbon. No significant differences in extracted hydrocarbons were observed between crushed samples of different sieve sizes (1000 - 500 μm, 250 - 125 μm, and 63 - 25 μm). However, some increase in hydrocarbon extraction efficiency was seen as a function of exposed surface area. Additionally, a slight positive correlation was also observed between hydrocarbon recovery and S1 (free oil content) warranting further investigation.

SUPERCRITICAL FLUID EXTRACTION OF HYDROCARBONS FROM THE
MARCELLUS SHALE BY USING CO_2

By

Palma Jean Jarboe

Thesis submitted to the Faculty of the Graduate School of the
University of Maryland, College Park, in partial fulfillment
of the requirements for the degree of
Master of Science
2014

Advisory Committee:
Professor Philip Candela, Chair
Professor Wenlu Zhu
Professor Jay Kaufman

Dedication

To my parents, Stephanie and John Botterell, for their unending support and encouragement.

To my husband, Kevin Jarboe, for always standing by my side and believing in me.

To my high school chemistry teacher, Mrs. Sharon Hillery, for being an inspirational teacher and sparking my passion in chemistry.

Acknowledgements

Table of Contents

List of Tables

List of Figures

Chapter 1: Background

1.1 Introduction

Organic-rich shale reservoirs represent both a source rock and potential reservoir for petroleum hydrocarbons. Important factors controlling the resource potential of a reservoir include: 1) the type, thermal maturity and abundance of organic matter present; 2) reservoir thickness and areal extent; 3) matrix porosity and permeability; and 5) natural fracture spacing (Soeder, 1988; Peters & Cassa, 1994; McCarthy et al., 2011). Unconventional (continuous) shale reservoirs refer to low matrix porosity and permeability (< 0.1 millidarcy, mD) sediments, wherein hydrocarbons accumulate continuously within the stratigraphic unit, unlike conventional reservoirs that have discrete boundaries of natural gas, crude oil and water (Milici & Swezey, 2006; Boyer et al., 2011). Shales have typical porosities of approximately 1 - 12 %, mean pore sizes on the order of 10^{-3} to 10^{-1} μm, permeabilities from 10^{-19} to $10^{-24}\,\mathrm{m}^2$ (1 mD = 9.87 x $10^{-16}\,\mathrm{m}^2$), and a total organic carbon content (TOC) of $\geq$ 4 wt % (Lewis et al., 2004; Espinoza & Santamarina, 2012).

Hydraulic fracturing is a well stimulation technique that has successfully increased matrix permeability of unconventional reservoirs between 1 and 7 orders of magnitude (Lee et al., 2011), making possible the extraction of economically viable quantities of oil and natural gas. However, due to variability in both organic and inorganic matrix components found among different shale formations and within a single reservoir, there is a need to develop fracturing fluid systems that can optimize well productivity while minimizing damage to the reservoir. Conventional water-based fracturing fluids may not be the best option for water-sensitive formations (i.e.

those with an abundance of expanding clay minerals) or oil-wet formations that have a preferential attraction to oil (displacing water), clogging pores and reducing permeability, potentially damaging reservoirs, and reducing well productivity (Abdallah et al., 2007; Wang et al., 2012). Although carbon dioxide flooding is used to enhance oil recovery from conventional petroleum systems, CO_2-injection in unconventional shales is still under investigation. Research is ongoing for potential use of CO_2 as an extraction fluid alternative in both enhanced gas recovery (EGR) and enhanced oil recovery (EOR) initiatives (Oldenburg et al., 2001; Nuttall, et al., 2005; Nuttall, 2010; Sorenson et al., 2013).

The primary goal of this study is to examine the supercritical fluid extraction of resolvable n-aliphatic petroleum hydrocarbons from samples of Marcellus shale by using supercritical CO_2, and to evaluate how extraction efficiency varies as a function of sample matrix particle size (sieve size). Results are evaluated with regard to exposed surface area, organic matter content, and mineral composition of the samples. Knowledge of the chemical and physical interactions of high-density CO_2 with organic and inorganic shale matrices will help further evaluate controls on hydrocarbon mobilization by a fluid that contains a separate, dense, CO_2-bearing phase, within the Marcellus and other unconventional source rocks.

1.2 Organic Geochemistry

Petroleum, a collective term for crude oil, natural gas, and bitumen, is a complex mixture of gaseous, liquid, and solid hydrocarbons. Non-hydrocarbon constituents include nitrogen-sulfur-oxygen (NSO) heterocyclic compounds, and trace metals such as iron, vanadium and nickel. Classifications of hydrocarbon compounds are defined

by physical properties, such as solubility in common organic solvents, fusibility (softening point), or boiling point range. These physical differences are the results of variations in chemical composition, such as atomic hydrogen/carbon (H/C) and oxygen/carbon (O/C) ratios, molecular weight, degree of aromaticity, and polarity (Meyer & de Witt, Jr., 1990; Peters & Cassa, 1994).

Hydrocarbons are generally classified as aliphatic or aromatic compounds. Aliphatics (also known as saturates, alkanes, and paraffins) have single bonds between carbon molecules, with the molecular formula C_nH_{2n+2}. They exist in one of three main structural forms: n- (normal, straight-chain), iso- (branched), and cyclo- (cyclic, napthenes). Aromatic molecules (also known as aryls) include at least one 6-membered carbon ring (benzene, C_6H_6), a carbon-rich, resonance-stabilized structure characterized by pi (π)-electron delocalization among unsaturated carbon atoms. Polycyclic aromatic hydrocarbons (PAHs) have multiple fused benzene rings, and thus have more condensed structures (relative to aliphatic hydrocarbons). Isomers (compounds with the same molecular formula, but different chemical structures) further intensify the complexity of hydrocarbon compounds.

Heterocyclic compounds have another atom (heteroatom), most commonly nitrogen, sulfur or oxygen, attached to or substituted into the carbon backbone. Petroleum hydrocarbons and precursor kerogen polymers may include diverse combinations of aliphatic, aromatic and heterocyclic constituents depending upon the source of the organic matter and the degradation process (Meyer & de Witt, Jr., 1990; Peters & Cassa, 1994; Helgeson, 2009).

Bitumen is the fraction of organic matter that is soluble in common organic solvents such as carbon disulphide. A small portion of bitumen originates from lipids, but the major formation pathway is through the thermal degradation of kerogen (Peters & Cassa, 1994). In natural reservoirs, bitumen can undergo chemical and physical alterations to yield other forms of bitumen, crude oil, natural gas, and pyrobitumen (Meyers & de Witt, Jr., 1990; Lesueur, 2009).

Bitumen is a heavy petroleum hydrocarbon mixture with a non-crystalline, solid/semi-solid colloidal structure. Although its specific chemical composition is dependent upon the source of the organic matter, it generally consists of approximately 80-88 wt % carbon, 8-12 wt % hydrogen, 0-9 wt % sulfur, 0-2 wt % oxygen, and 0-2 wt % nitrogen. Trace metal constituents, namely vanadium, nickel, and iron, may be present as inorganic salts and oxides, or in porphyrin ring structures. Class fractions of crude oil and bitumen are commonly divided into the Saturate, Aromatic, Resin, and Asphaltene (SARA) fractions, based on differing chemical composition (polarity), physical structure (degree of aromaticity), and molecular weight (Meyer & de Witt, Jr., 1990; Read & Hunter, 2003; Lesueur, 2009).

	H/C	C (wt %)	H (wt %)	O (wt %)	N (wt %)	S (wt %)	Molecular Weight (g/mol)
Saturates	1.9	78 - 84	12 - 14	< 0.1	< 0.1	< 0.1	470 - 880
Aromatics	1.5	80 - 86	9 - 13	0.2	0.4	0.0 - 4.0	570 - 980
Resins	1.4	67 - 88	9 - 12	0.3 - 2.0	0.2 - 1.0	0.4 - 5.0	780 - 1,400
Asphaltenes	1.1	78 - 88	7 - 9	0.3 - 5.0	0.6 - 4.0	0.3 - 11.0	800 - 3,500

Table 1. Chemical properties of bitumen and SARA fractions (data from Lesueur, 2009). Hydrogen content (H/C) decreases with increasing aromaticity. Size and polarity also generally increase in the order (with some overlap): Saturates < Aromatics < Resins < Asphaltenes .

Saturate hydrocarbons are nonpolar, generally with the lowest molecular mass range of the class fractions. Aromatics are also predominantly nonpolar with a relatively low molecular weight, and are thus good liquid solvents for heavier hydrocarbon components. Resins are polar, aromatic molecules, with a non-crystalline solid/semi-solid structure. These molecules are slightly heavier with a more condensed structure and greater abundance of NSO constituents than saturate or aromatic fractions. Resins thus act as a solvating layer, to help stabilize the larger asphaltene suspension within bitumen. Together, saturates, aromatics and resins make up what is known as the 'maltenes' group (Meyer & de Witt, Jr., 1990; Lesueur, 2009).

Asphaltenes are an amorphous, highly aromatic and/or napthenic solid hydrocarbon mixture, with an abundance of NSO heteroatoms. They exist as a 'colloidal suspension', where they are suggested to form aggregated micelle structures dispersed or dissolved in the lower molecular weight maltene medium. Two general types of end-member bitumen structures, SOL and GEL type bitumens, are suggested to exist based upon interactions among the SARA hydrocarbon fractions (Read et al., 2003). The SOL type includes fully dispersed and non-interacting micelle units. In the GEL type, the micelles further link together to form larger, irregular interconnecting structures. The GEL model is suggested to form if there is a lower abundance of resin or aromatic fractions, or if those fractions have not sufficiently solvated the asphaltene micelles. Most bitumens have physical structures somewhere between these two end-member structures (Read et al., 2003).

The highly condensed aromatic character of asphaltenes also allows them to exist as planar sheet-like compounds that can associate with one another through π-π orbital bonding. This enables them to stack upon one another, further condensing and aggregating together (Lesueur, 2009). The distribution and interaction of hydrocarbon fractions present in bitumen and crude oil can impact their recovery from natural reservoirs (Meyer & de Witt, Jr., 1990; Read & Hunter, 2003).

Kerogen, a petroleum precursor, is commonly regarded as the portion of sedimentary organic matter that is insoluble in common organic solvents. Formed during diagenesis of buried organic matter, kerogen is considered a geopolymer, a heterogeneous mixture of reworked degradation products of organic polymers such as lipids, polypeptides, polysaccharides, and lignin. Macerals, the remains of various plant and animal matter, constitute the individual components of kerogen, and are categorized into groups according to their chemical and physical structure, and optical criteria. Three principal maceral groups are found in coals and sedimentary rocks: liptinite (formerly exinite), vitrinite, and inertinite (Hutton, et al., 1994; Peters & Cassa, 1994; Peters et al., 2005).

Sapropelic (marine or lacustrine) kerogen is composed of degraded and polymerized products of fatty lipid-rich organic material, usually deposited in anaerobic, subaqueous muds. Derived mainly from phytoplanktonic organisms (i.e. algae), this type of kerogen is amorphous in structure, rich in hydrogen, and oil-prone. Humic (terrestrial) kerogen, rich in woody material and plant tissues, originates mainly from land plants. Wood is composed mainly of cellulose and lignin, with an abundance of polysaccharides and aromatic compounds. They are thus found

to be richer in oxygen and more depleted in hydrogen, relative to marine organic matter. Natural gas and coal are the principal products formed from this type of kerogen via thermal degradation processes. However, plant waxes also produce long-chain aliphatic hydrocarbons found in crude oil (Nunez-Betelu & Baceta, 1994).

Kerogen is classified into four major types depending on its origin, hydrogen content, and predominant hydrocarbon products. Type I kerogens, composed of liptinite macerals, are derived from amorphous, lipid-rich algae (lacustrine or marine origin), and have the highest H/C and lowest O/C ratios of all kerogen types. Type II kerogens are also of marine origin, composed of liptinite macerals that include mixtures of plankton (algae), spores and waxy, resinous parts of plants. This type is also hydrogen-rich, but with lower H/C and wider O/C ranges than Type I kerogens. Type III kerogens are composed of vitrinite macerals, with a more poly-aromatic structure relative to Type I and II kerogens, due to significant proportions of lignin and cellulose from higher terrestrial plants. Although terrestrial in origin, this type of kerogen can still be found in marine source rocks, due to transportation from rivers, streams, and other erosional forces. Type IV kerogens originate from highly oxidized organic matter, altered by weathering, combustion, or biological oxidation before final deposition. They have the highest aromatic character and lowest H/C ratio of all types, with minimal (or no) potential for generating hydrocarbons (Nunez-Betelu & Baceta, 1994; Peters & Cassa, 1994; Peters et al., 2005).

Type	Principal Maceral Group	H/C	O/C	Main Product at Peak Maturity
I	Liptinite	> 1.5	< 0.1	Oil
II	Liptinite	1.2 - 1.5	0.05 - 0.15*	Oil
II/III	Liptinite/Vitrinite	1.0 - 1.2	---	Mixed Oil & Gas
III	Vitrinite	0.7 - 1.0	≤ 0.3	Gas (& Coal)
IV	Inertinite	< 0.7	≤ 0.3	None

Table 2. Kerogen types, with corresponding maceral groups, atomic H/C and O/C, and hydrocarbon products (*Hutton et al., 1994; Peters & Cassa, 1994).

Pyrobitumen is a term for insoluble, thermally-altered, solidified reservoir bitumen. It is a highly aromatic, carbonaceous residue formed as a by-product from the thermal degradation of petroleum (Huc et al., 2000; Wilson et al., 2000; Mort & Sanei, 2013). In petroleum systems where the reservoir and source rock are the same, organic matter is a mixture of original kerogen, petroleum, and pyrobitumen. However, in some highly mature, unconventional shale reservoirs (i.e. Marcellus Shale), pyrobitumen may be the only form of solid organic matter present (Mort & Sanei, 2013). Pyrobitumen has a highly condensed, graphite-like structure (Laughrey et al., 2011). It exhibits a void-filling texture, growing around mineral grains and thus reducing matrix porosity (Huc et al, 2000). It often contains mineral inclusions (i.e. pyrite framboids), and voids on its surface, filled mainly with calcite (or also quartz or metal sulfides) (Wilson et al., 2000).

1.3 Accumulation & Preservation of Organic Matter

Accumulation of organic matter in sediments is controlled by the interconnected factors of oxygen availability (redox conditions), level of biological activity, deposition rate, and mineralogy. Organic matter exists in aquatic environments either as colloidal, particulate, or dissolved matter (adsorbed onto clay minerals). Although

oxygen supports primary productivity, it also enhances oxidation and biodegradation of organic matter within the water column. In high-energy, oxygenated environments (i.e. shallow surface sediments), organic matter can be consumed by benthic scavengers and burrowing organisms. An anoxic, reducing environment is thus necessary to preserve organic matter, by limiting the availability of destructive oxidizing agents necessary for aerobic microbial degradation. A low energy environment also promotes deposition of fine-grained organic matter and sediments to settle within the water column. Co-deposition of transported and precipitated minerals can also affect the accumulation and preservation of organic matter, by reacting with organic compounds and diluting the relative abundance of organic matter within sediments (Nunez-Betelu & Baceta, 1994; McCarthy et al., 2011).

Shallow inland sedimentary basins, narrow seaways, stratified lakes, and low-energy coastal areas with anoxic, reducing bottom waters and attenuated circulation, enhance organic matter deposition, especially during periods of transgression where landward migration of the coastline occurs as a result of rising sea level and/or land subsidence. Fine-grained sediments such as shale, deposited in this type of setting, have the greatest potential for preservation (Nunez-Betelu & Baceta, 1994; Engelder & Lash, 2011).

1.4 Organic Metamorphism

Thermal maturity of a source rock refers to the degree of temperature-time driven reactions involved in the irreversible transformation of sedimentary organic matter into kerogen, petroleum, and pyrobitumen during burial (Peters & Cassa, 1994). Thermal maturation pathways are dependent upon a complex interplay of pressure,

temperature, time (extent of heat exposure), and source of organic matter. Increasing thermal maturity leads to the generation of progressively smaller, more volatile hydrocarbons, with a carbonaceous residue that becomes progressively more condensed, aromatic, and depleted in hydrogen (Peters & Cassa, 1994; Helgeson et al., 2009; McCarthy et al., 2011). Maturity is mainly associated with burial depth, but can also be influenced by 1) heat flow from crustal tectonic movements, igneous intrusions, or radioactive decay within the crust; and/or 2) basin uplift/subsidence (McCarthy et al., 2011).

Transformation of organic matter occurs in multiple stages. The first stage of metamorphism, diagenesis, includes all of the chemical, physical, and biological alterations made to the organic matter in shallow subsurface depths, up to approximately 50 ^{o}C. Source rocks in this stage are said to be thermally immature. In this zone, highly organized biopolymers are broken down and then polymerized and condensed into heterogeneous kerogen and small amounts of bitumen. Biogenic degradation by anaerobic, methanogenic bacteria can also produce dry gas (> 98 % methane). As burial and subsurface depths continue to increase, so does temperature. Starting at approximately 50 ^{o}C, catagenesis begins. Categenesis is a thermodynamic process involving the thermogenic degradation of kerogen, producing petroleum. During this stage (between approximately 50 ^{o}C and 150 ^{o}C), source rocks are considered effective and mature for oil production. This stage starts with the generation of oil, the oil window. With increasing temperature, the source rock enters the wet gas window, where secondary cracking of oil produces wet gas (< 98 % methane). Metagenesis, the last stage of petroleum generation, involves further

conversion of oil, kerogen and bitumen into dry gas and pyrobitumen, at temperatures ranging from approximately 150 $^{\circ}$C to 200 $^{\circ}$C. Non-hydrocarbon gases are also generated, including carbon dioxide, nitrogen, and hydrogen sulfide. Source rocks are labeled post-mature for oil, or spent, within this stage (Peters & Cassa, 1994; Vandenbroucke & Largeau, 2007; McCarthy et al., 2011).

Physical compaction, cementation, mineral formation, and conversion of kerogen into petroleum and pyrobitumen all reduce matrix porosity, pore and pore throat sizes, and ultimately permeability. Limited pore connectivity can be reduced even further with confining pressure at depth (Soeder, 1988; Nelson, 2009; Bruner & Smosna, 2011; Laughrey et al., 2011).

1.5 Marcellus Shale

1.5.1 Regional Geology

The Marcellus Shale, named after an outcrop near the village of Marcellus in Onandaga County, NY, is the most expansive natural gas reservoir in the United States. Covering an area of 75,000 square miles, the Marcellus Shale is located in the Appalachian Basin, on a northeast-southwest trending central axis from Ontario and New York through Pennsylvania and West Virginia; bordering Virginia and Maryland on the east and Ohio on the west. The Marcellus currently reaches over 9,000 ft along its structural axis (slightly basinward of the Appalachian Mountain range). Formation thickness can reach over 200 ft, with its thickest region in northeast Pennsylvania. The formation generally thins and becomes shallower to the north, west and south. Structural boundaries include the Allegheny Structural Front on the

east, and the Cincinnati Arch on the west (Milici & Swezey, 2006; Bruner & Smosna, 2011).
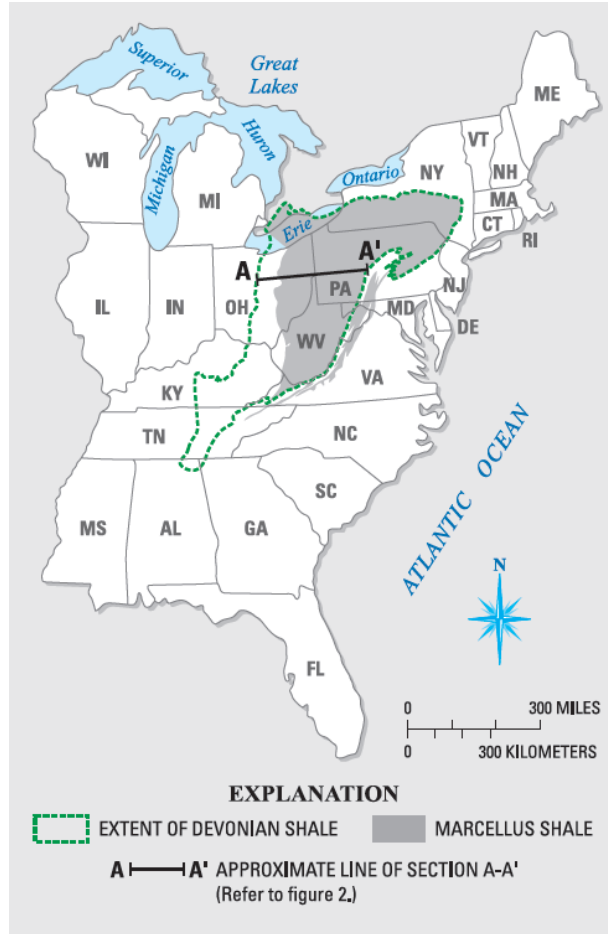
Figure 1. Regional distribution map of the Marcellus Shale (Soeder & Kappel, 2009).
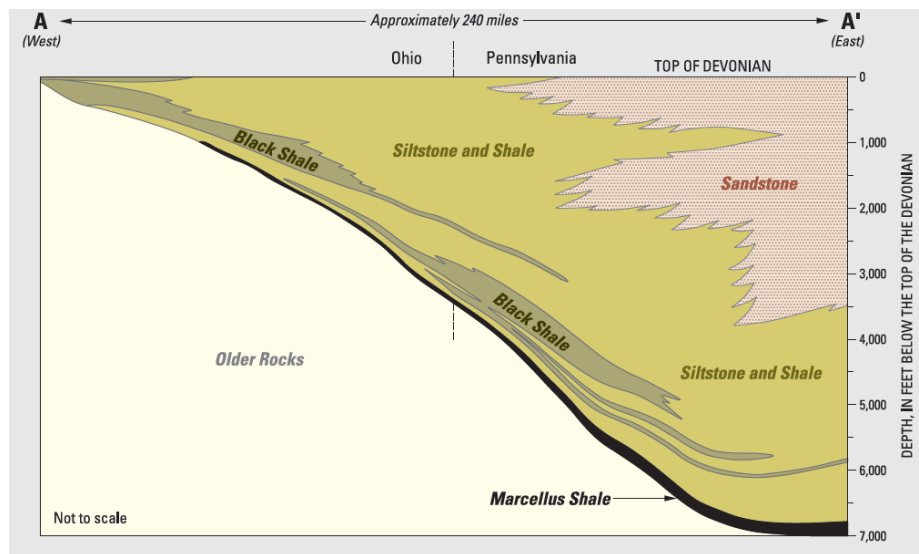
Figure 2. Cross-section of the Marcellus Shale from Ohio to Pennsylvania. (Soeder & Kappel, 2009).

The Marcellus was deposited approximately 385 million years ago (Ma) in the Middle Devonian Period during the Acadian Orogeny (a tectonic, structural event responsible for the formation of the present-day Appalachian Basin and eastward Appalachian Mountains). At the time of deposition, the Appalachian Basin was located in a shallow, epeiric seaway (< 200 meters deep). Tectonic stresses from the collision of lithospheric plates, Laurentia and Gondwana, caused crustal thickening at the site of plate convergence. Subsequent deepening of the foreland basin landward (west) of the elevated mountain belt on Laurentia occurred as the tectonic load bent the continental margin downward, creating the accommodation space for sediment and organic matter to accumulate (Engelder & Lash, 2008; Bruner & Smosna, 2011).

Due to land subsidence associated with the tectonic movements mentioned above and a eustatic rise in sea level, the foreland basin sank below the pycnocline water level to an oxygen-depleted, reducing environment. The Acadian Mountains disrupted river systems, reducing clastic and carbonate sediment supplies to the basin and current activity within the basin. The stagnant, stratified water column was a perfect environment for eutrophic algal blooms and primary production to flourish, further reinforcing the oxygen-depleted bottom waters. Accumulation of organic matter intermixed with the laminated fine-grained clay- and silt-sized shale particles, gave rise to the aforementioned 'black shale' intervals. Eventually, erosion from the adjacent mountains and river systems brought back an influx of clastic sediments to the basin, covering the organic-rich intervals with a mixture of gray shale, siltstone, and limestone. The Devonian shales of the Appalachian basin include at least 8

repetitions of this cycle within 20 Ma years. (Werne et al., 2002; Sageman et al., 2003; Engelder & Lash, 2008 & 2011).

The Appalachian Basin is also composed of a complex series of basement faults and grabens (most notably the Rome Trough), which developed in Late Precambrian-Early Cambrian from the breakup of Rodinia (Precambrian supercontinent). Reactivation (continuing movement) of these faults occurred in response to tectonic stresses of the Acadian Orogeny. This divided the foreland basin into zones of uplift (ridges) and depocenters, causing base level fluctuations that ultimately affected depositional sedimentation patterns across the deepening Appalachian Basin (i.e. variations in the distribution, and thickness of sediment intervals) (Engelder & Lash, 2008; Bruner & Smosna, 2011).
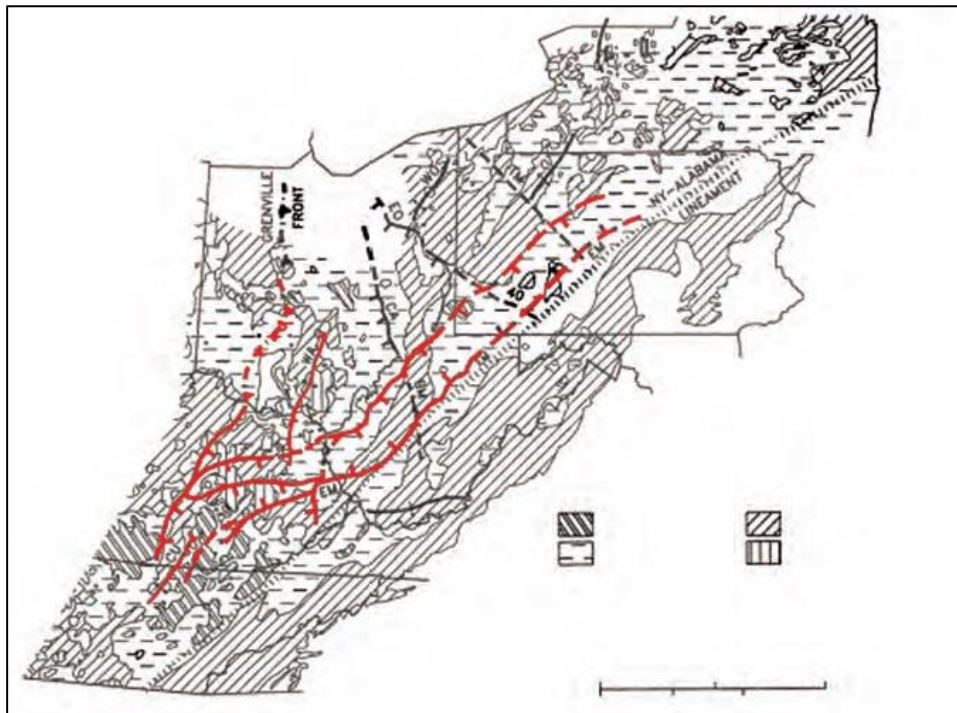
Figure 3. Rome Trough from Kentucky through Pennsylvania (Bruner & Smosna, 2011). Basement faults indicated in red.

14

The Marcellus Shale is composed of three stratigraphic intervals. The Union Springs Member (lower Marcellus) is an organic-rich, naturally radioactive (due to presence of uranium and thorium), blackish-gray to black shale interval, with reduced clay and high quartz and pyrite abundances. The Oatka Creek Member (upper Marcellus) is composed of two distinct intervals: a radioactive, carbonate-rich black shale interval that sits below a gray shale (organic-lean; mixed with intermittent carbonate layers). These intervals are separated by the Cherry Valley Member (also known as Purcell Limestone in West Virginia), a thin layer of limestone, shale and sandstone nodules. The Marcellus lies above the Onandaga Formation, and is overlain by the Mahantango Formation (also named the Skaneateles Formation), a variable mix of mudstone, sandstone, limestone, and conglomerate. Both the Marcellus and Mahantango Formations are subgroups of the Hamilton Group (Sageman et al., 2003; Engelder & Lash, 2011; Bruner & Smosna, 2011). Radiometric dating analysis of the Tioga Ash Bed, which occurs at or near the base of the Marcellus, dates the onset of formation to 390 ± 0.5 Ma (Middle Devonian Period) (Roden, et al., 1990).

Marcellus Shale mineralogy is composed of predominantly non-expanding clay (illite), quartz and calcite (Hosterman & Whitlow, 1983; Laughrey et al., 2011; Chalmers et al., 2012). Calcite is present throughout the basin, with highest concentrations found in western New York, northeastern Ohio and southwestern Pennsylvania (Hosterman & Whitlow, 1983). Carbonate concretions present within organic-rich intervals of the Marcellus are thought to have been formed during diagenesis (< 1 meter below the surface) by precipitation within matrix pores before shale compaction (Bruner & Smosna, 2011).

Marcellus Shale Mineral Composition	
Mineral(s)	**Abundance (%)**
Clay	10-35
Quartz	10-60
Calcite, Dolomite, Siderite	3-50
Pyrite	5-13
Mica	5-30
Feldspars	0-4

Table 3. Characteristic mineral composition of the Marcellus Shale (data from Bruner & Smosna, 2011).

Marcellus Shale Clay Abundances		
Mineral	**Average Abundance (%)**	**Expandability**
Illite	70	Non-expanding
Chlorite	15	Non-expanding
Illite/Smectite (mixed-layer)	15	Non-expanding/Expanding
Illite/chlorite (mixed-layer)	Trace	Non-expanding

Table 4. Clay mineral distribution of the Marcellus Shale (Hosterman & Whitlow, 1983).

Average porosity within the Marcellus Shale is approximately 6 - 10 %. Porosity can be attributed to: 1) interparticle (matrix porosity); 2) natural open fractures; and 3) nanopore- to micropore-shale voids within kerogen, bitumen, and pyrobitumen. (Soeder, 1988; Bruner & Smosna, 2011; Laughrey et al., 2011). In addition to the Marcellus being predominantly mesoporous (2 - 50 nm) and microporous (< 2 nm) pores, shale pore throat sizes range from approximately 0.1 - 0.005 μm (Nelson, 2009; Chalmers et al., 2012). Marcellus Shale permeabilities are in the microdarcy to nanodarcy range (Soeder, 1988; Bruner & Smosna, 2011; Lee et al., 2011).

1.5.2 Petroleum Geochemistry

The Marcellus Shale consists of predominantly Type II (sapropelic) kerogen, with an abundance of the single genus *Tasmanites* (marine green algae) (Ryder et al., 2013). Small input from Type III, terrestrial organic matter (fresh and/or oxidized woody material), can be found in the eastern portion of the basin associated with the evolution and diversification of higher land plants during late Marcellus deposition (Bruner & Smosna, 2011).

Maximum paleotemperatures for the Marcellus range from approximately 100 - 200 $^{\circ}$C (increasing progressively eastward and southeastward across the basin) (Bruner & Smosna, 2011), and reflectance values range from approximately 1.5 - 3.0 %R_o throughout much of the core region of the basin (approximately 5,000 - 8,000 ft below sea level), placing the formation outside of the oil window (> 150 $^{\circ}$C) (Milici & Swezey, 2006).

High maturity levels are suggested to be associated with: 1) migration of hot fluids from fault structures beneath the Marcellus associated with the Rome Trough; and/or 2) overburden pressure associated with greater burial depth. Longer burial time may have also contributed to the degradation of organic matter, even if higher temperatures were not reached. (Milici & Swezey, 2006; Engelder & Lash, 2008; Bruner & Smosna, 2011).

Organic richness of the Marcellus Shale varies regionally and stratigraphically across the basin, with average TOC values ranging from approximately 2 - 10 %. Highest values are found in the lowest 50 ft of the formation (Union Springs Member). Geographically, TOC values are generally highest in the central region of

17

the basin, decreasing to the east and west (in New York), and south along the basin axis (from New York to West Virginia). Localized variations in organic richness may have resulted from movement of basement structures (continued tectonic deformation) that created localized zones of uplift and subsidence during basin formation, ultimately affecting patterns of TOC accumulation (Milici & Swezey, 2006; Bruner & Smosna, 2011).

The Marcellus Shale has become an extremely productive natural gas-producing formation in the Appalachian basin, currently producing over 14 bcf (billions of cubic feet) of natural gas per day (U.S. EIA, 2014).
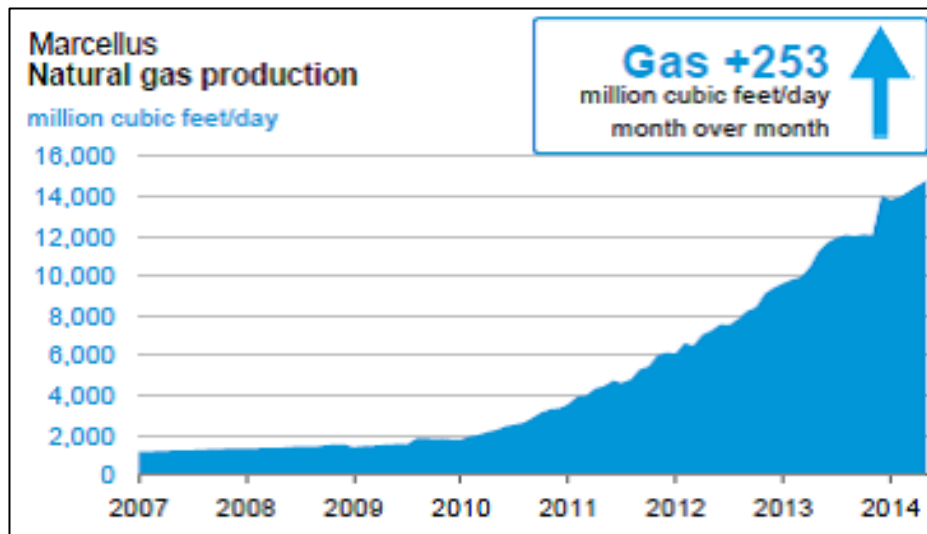
Figure 4. Natural gas productivity of the Marcellus Shale (U.S. Energy Information Administration, April 2014). An increase in natural gas production of 253 MMcf (millions of cubic feet) per day was seen from April to May of 2014.

Injection of CO_2 is not currently used in the Marcellus Shale. However, knowledge of the type and quantity of hydrocarbons that could be mobilized with CO_2, and of the important factors influencing recovery from inorganic and organic shale matrices, will be important if industrial-scale use of CO_2 is someday used as an alternative fracturing fluid in unconventional shale reservoirs.

1.6 Supercritical Fluid Extractions

1.6.1 Principles of Supercritical Fluid Extractions

Supercritical fluid extractions use high-density gases such as CO_2, ethane, propane, toluene or water, to extract a wide array of both volatile and nonvolatile organic compounds (Rudzinksi & Aminabhavi, 2000). These gases exist in a supercritical state beyond the critical point on the boiling point curve (liquid-gas equilibrium), where there is no longer any distinction between liquid or gas phases. The term fluid describes a behavior that is characteristic of all liquids, gases, and supercritical fluids.

A more appropriate name for this technique would be a 'dense gas extraction' to emphasize two major points: 1) the importance of high densities needed for efficient solvent strength (Williams, 1981); and 2) the solvent is a gas (i.e. it fills any available volume) even if liquid-like behavior is exhibited under certain pressure-temperature conditions in the supercritical region.

Supercritical fluids can have a high, liquid-like density that can thus enhance their solvent strength, or dissolving power. However, by virtue of the solvent being a gas, it still maintains higher diffusivity, lower viscosity and lower surface tension (between the solvent and other solids or liquids present) compared to conventional liquid solvents (i.e. those used in Soxhlet extractions), improving mass transfer through the sample matrix and increasing extraction rates (Williams, 1981; Monin et al., 1987; Li et al., 1997; Rudzinksi & Aminabhavi, 2000).

	Gas ($T_{ambient}$)	Supercritical Fluid (T_c, P_c)	Liquid ($T_{ambient}$)
Density,ρ (kg/m^3)	1.0	100 - 800	1,000
Viscosity, η (Pa·s)	0.001	0.005 - 0.01	0.05 - 0.1
Diffusivity, D (m^2/s)	10^{-5}	10^{-7}	10^{-9}

Table 5. Comparison of physical properties of gases, liquids and supercritical fluids (data from Kemmere & Meyer, 2005).

Carbon dioxide exists in a supercritical state at temperatures and pressures greater than its critical point of 30.978 ± 0.015 ^{o}C (critical temperature, T_c) and 7.3773 ± 0.0030 MPa (critical pressure, P_c) (Span & Wagner, 1996). The associated critical density is 467.6 ± 0.6 kg/m^3 (Span & Wagner, 1996). Many advantages of using CO_2 over other supercritical fluid extraction solvents owe to its nonflammable and nontoxic nature, availability in purified form, and low critical temperature, which allows for easy separation from extracted compounds at atmospheric conditions (Williams, 1981; Li et al., 1997).
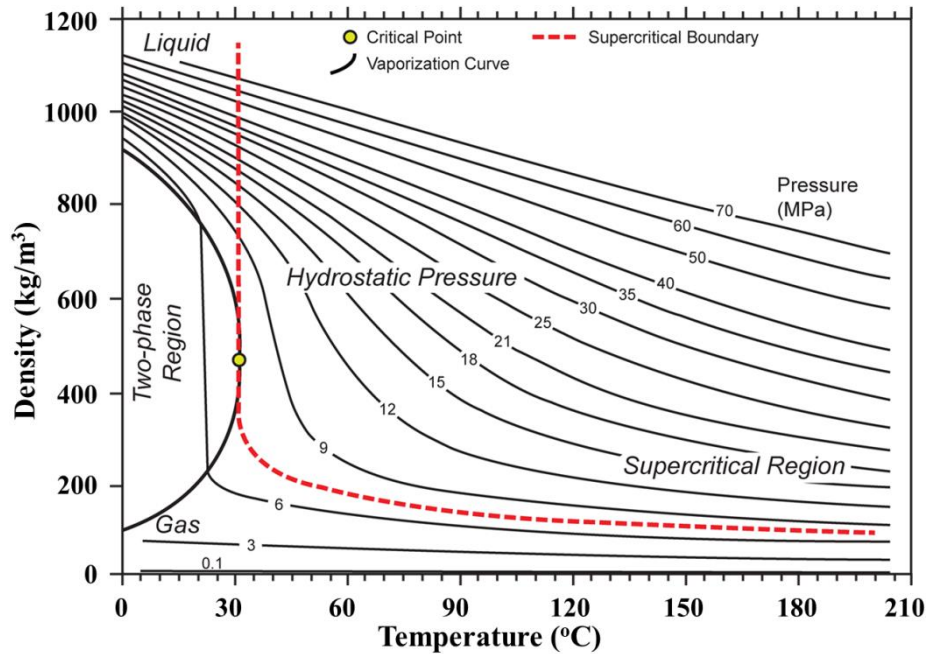
Figure 5. Relationships among density, pressure and temperature of CO_2 in sedimentary basins (modified from Bachu, 2003). Density ranges shown are suggested to be characteristic of worldwide sedimentary basins under varying surface temperature and geothermal gradient conditions, assuming hydrostatic and lithostatic pressures.

In a supercritical phase, density can be varied continuously with changes in pressure or temperature without CO_2 going through a phase change. By virtue of its liquid-like density, supercritical CO_2 can subsequently act as a solvent. Increasing temperature in this region requires greater pressure to achieve the same density. Thus, supercritical extractions are typically carried out at temperatures within approximately 100° above the critical temperature, where solvent density is maximized (Williams, 1981).

1.6.2 Solvent Strength of Supercritical Carbon Dioxide

Solvent strength is primarily a function of solvent density, which is controlled by changes in pressure and temperature in the supercritical region. Increasing solvent strength observed with increasing density results from intermolecular forces of attraction of closely-packed solvent molecules around target solutes. Higher solvent densities observed in the supercritical region also enhance the solvent's ability to vaporize nonvolatile compounds at temperatures below their normal boiling points (Maddocks et al., 1979). At low to moderate pressures, an increase in temperature above the critical threshold leads to: 1) a reduction in solvent density (and thus solubility of the solute); and subsequently 2) an increase in vapor pressure of the solute. However at higher pressures, any decrease in density due to increasing temperature is minimized, such that the increasing vapor pressure of the solute increases its concentration in the supercritical solvent (Williams, 1981; Brogle, 1982).

1.6.3 Solute Selectivity in Supercritical Carbon Dioxide

Solubility in supercritical fluids is not only dependent upon solvent density, but upon the chemical and physical properties of the solvent and potentially extractable compounds. Selectivity of target compounds can be enhanced via changes in extraction pressure and temperature, which affect solvent density and polarity (Williams, 1981; Monin et al., 1987; Li et al., 1997; Rudzinksi & Aminabhavi, 2000). Although CO_2 is a nonpolar molecule with a zero net charge, it has a quadrupole moment. Thus, certain high-pressure (high-density) conditions, such as those encountered in the supercritical region, can cause a momentary distortion of electron distribution within CO_2, creating weak intermolecular forces of attraction (London dispersion forces) among neighboring CO_2 molecules and inducing slight solvent polarity. For example, at 600 kg/m^3, CO_2 acts like a nonpolar solvent. However, at 1,000 kg/m^3, intermolecular forces of attraction may polarize CO_2, enhancing its affinity for moderately polar compounds (Monin et al., 1987).

In addition, the solubility of hydrocarbons in supercritical CO_2 is also a function of the chemical composition, molecular structure (branching, degree of aromaticity, etc.) and molecular size of the target compounds. A general trend is observed in solubility with physical structure (Monin et al., 1987):

iso-aliphatics > n-aliphatics > napthenes > aromatics

Despite this trend, differences in molecular size or polarity are found to be more important for determining solubility in CO_2 than are differences in structure, aromaticity, or degree of saturation. Solubility of n-aliphatic hydrocarbons decreases with increasing carbon number (Williams, 1981; Monin et al., 1987). Additionally, at

22

characteristic extraction pressures (8.1 - 60.8 MPa), supercritical CO_2 does not effectively extract highly polar compounds, unless a polar modifier fluid (i.e. methanol) is added (Rudzinksi & Aminabhavi, 2000). Even at high densities, supercritical CO_2 may have difficulty efficiently solvating: 1) thermally-stable, low volatility compounds, such as extremely large, aggregated hydrocarbon compounds; and 2) highly polar molecules (i.e. compounds with a high concentration of NSO heteroatoms) that may have greater affinity to charged, polar inorganic matrices. Thus, optimum use of supercritical CO_2 is found in the extraction of other low- to moderate-molecular weight, nonpolar compounds.

1.6.4 Literature Review: Supercritical Fluid Extraction of Source Rocks

Extensive research on supercritical fluid extractions in the petroleum industry has been on-going for use in the: 1) separation of crude oil and bitumen into SARA class fractions; 2) extraction and characterization of petroleum from different source rock matrices (i.e. shale, coal, oil shale, and tar sands); and 3) identification and decontamination of PAHs in soil (Li et al., 1997; Rudzinksi & Aminabhavi, 2000; Rudyk et al., 2013). Supercritical CO_2 extractions have successfully recovered a wide range of nonpolar PAHs and aliphatic hydrocarbons from shale and coal under varying extraction parameters (Monin et al., 1987; Greibrokk et al., 1992; Jaffè et al., 1997; Li et al., 1997; Rudzinksi & Aminabhavi, 2000; Kolak & Burruss, 2003). The molecular size of CO_2, 2.8 Å, enables it to access micropores of coal and shale matrices (Walker et al., 1988; Nelson, 2009).

A comparison of extraction techniques from Monin et al. (1987) found optimum extraction of n-aliphatic hydrocarbons ranging from n-C_{10} to n-C_{34} from shale with

supercritical CO_2 (at 40 ^{o}C and 20 MPa). Li et al. (1997) extracted similar ranges of aliphatic and aromatic hydrocarbons as did Monin et al. (1997) at 120 ^{o}C and 20.3 MPa, but focused on quantifying the recovery of more volatile (C_6 to C_{14}) hydrocarbons, with yields ranging between 0.01 to 0.2 wt %. However, their quantitative results were normalized to the mass of shale, with no report of TOC content. Additionally, neither study mentioned the thermal maturity, mineralogy or sample particle size of the extracted shale.

1.7 Statement of the Problem

Supercritical fluid extraction is a complex process, with many parameters that are dependent upon geochemical characteristics of the sample matrix, molecular characteristics of the potentially extractable compounds, and chemicophysical properties of the extracting solvent (Jaffè et al., 1997; Rudzinksi & Aminabhavi, 2000). Numerous *ex situ* supercritical fluid extraction studies have assessed the effects of pressure, temperature, time and addition of co-solvents on the quantity and distribution of extractable hydrocarbons from different source rock matrices. However, the effect of sample matrix particle size (sieve size) has not been sufficiently documented, especially with regard to the extraction of shale gas or shale oil.

Supercritical CO_2 extractions of shale oil from crushed oil shale of 0.212 mm, 0.710 mm and 1.000 mm mean sample particle sizes (Allawzi et al., 2011), oil from crushed paprika samples of approximately 0.2 - 1.5 mm in size (Nagy & Simándi, 2008) and cocoa butter from ground cocoa nibs of 0.07 mm, 0.25 - 0.50 mm, and 1.00

24

- 2.00 mm sizes (Asep et al., 2008), all showed an increase in recovery of different organic oils with decreasing sieve size. Authors of each of these studies attributed this trend to an increase in exposed sample surface area associated with smaller particles, which enhances accessibility of the solvent to the extractable compounds, creates shorter diffusion paths, enhances mass transfer through the sample matrix, and thus ultimately increases overall extraction rates.

However, other authors have pointed out that there may be a sample particle size (sieve size) threshold in supercritical fluid extractions, with optimum sizes ranging from 0.25 - 2.00 mm. If sieve sizes are too small, channeling can occur that causes the solvent to flow in particular paths within its bulk movement through the extraction cell. Created by channels among the sample particles, these directed flow paths reduce interactions between the solvent to extractable compounds, resulting in decline in extraction efficiency and overall recovery (Reverchon & De Marco, 2006; Martìnez, 2008). Furthermore, the process of grinding samples into smaller size fractions could lead to loss of volatile compounds (Reverchon & De Marco, 2006), also reducing expected extraction yields.

Thus, a deeper investigation into the controls on hydrocarbon recovery from shale of different sample matrix particle sizes in supercritical fluid extractions is needed. Investigation of the effect of sample particle size on hydrocarbon mobilization with supercritical CO_2 will contribute to a better understanding of the mechanisms of CO_2-hydrocarbon interactions within fractured shale matrices.

The aim of my research is to determine the quantity and distribution of n-aliphatic hydrocarbons that can be extracted from Marcellus Shale samples with supercritical CO_2 as a function of sample matrix particle size, under estimated *in situ* temperature and pressure conditions. Temperature and pressure conditions used in this study, 80 ^{o}C and 20.7 MPa (3,000 psi), respectively, were chosen to represent approximate *in situ* reservoir conditions at depth (6,300 - 7,500 ft) for the selected samples, based on a geothermal gradient of 30 ^{o}C/km (with an average surface temperature of 20 ^{o}C) and subsurface pressurized gradient of 10.5 MPa/km (0.465 psi/ft) (Burke, 2011). At 80 ^{o}C and 20.7 MPa (3,000 psi), the density of CO_2 is 600 kg/m^3 (Bachu, 2003; Ouyang, 2011). Under these conditions, I propose the following scientific working hypotheses:

1. The distribution of potentially recoverable hydrocarbons from samples of Marcellus shale, extracted with supercritical CO_2, will contain quantifiable concentrations of low- to moderate-molecular weight n-aliphatic hydrocarbons ranging from predominantly n-C_{10} to n-C_{34}.

2. There will be a statistically significant increase in n-aliphatic hydrocarbon recovery with decreasing sample matrix particle size (sieve size). Differences in the quantity and distribution of n-aliphatic hydrocarbons extracted from different sieve size fractions will be evaluated in the context of geochemical properties of the shale matrix and extracted hydrocarbons.

Chapter 2: Methodology

2.1 Sampling

Cores from the Marcellus Shale were donated from EXCO Resources, Inc., and the Pennsylvania Geological Survey, Department of Conservation & Natural Resources. All samples are from vertically drilled wells located in central and western Pennsylvania, with depths ranging from approximately 6,300 - 8,200 ft below the surface. Thirty-one coherent pieces from different facies throughout the five cores were sampled for potential use in the supercritical CO_2 extraction experiments.
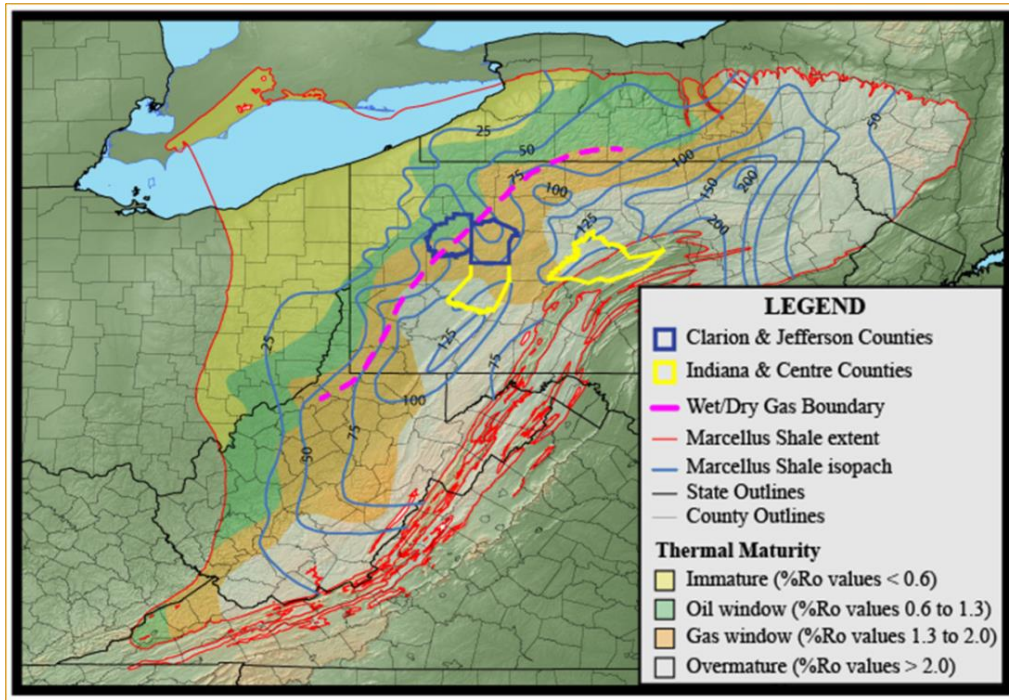
Figure 6. Map of the Marcellus Shale, with thermal maturity zones, isopach lines, wet/dry gas boundary, and sampled Pennsylvania counties. Map sources: Roen, 1984 (isopach lines; contours of structural thickness), Penn State MCOR, 2012 (wet/dry gas boundary), and East et al., 2012 (remaining figure).

Core ID	County, PA	Sampled Depth Interval (ft)
3S*	Clarion	6,283 - 6,400
4LG*	Jefferson	6,580 - 6,725
2LT*	Jefferson	7,382 - 7,490
EG**	Indiana	7,800 - 8,000
2LK*	Centre	7,952 - 8,172

Table 6. County and subsurface depth interval of sampled Marcellus cores. *Cores courtesy of EXCO. **Cores courtesy of the Pennsylvania Geological Survey, DCNR.
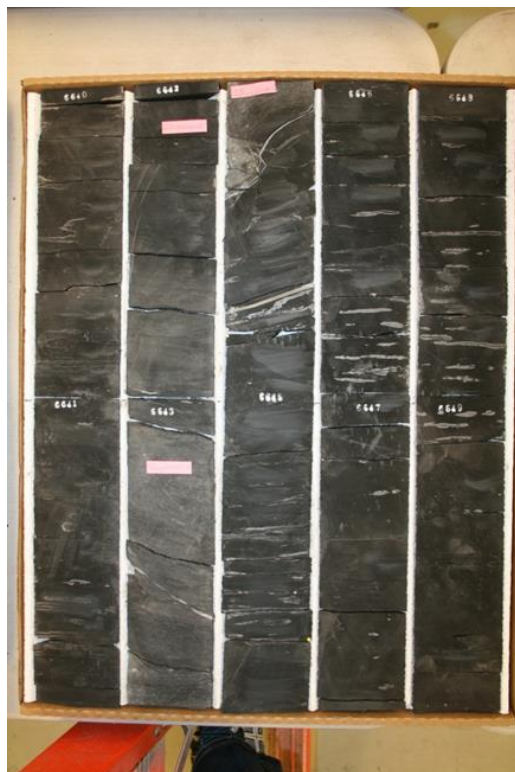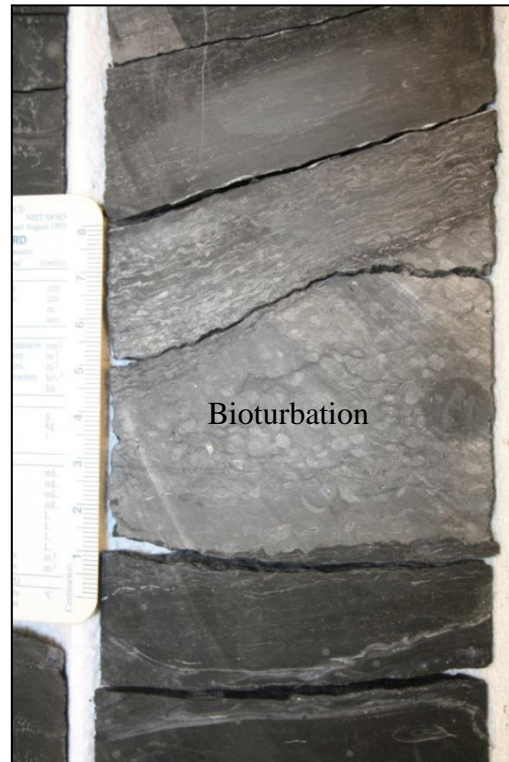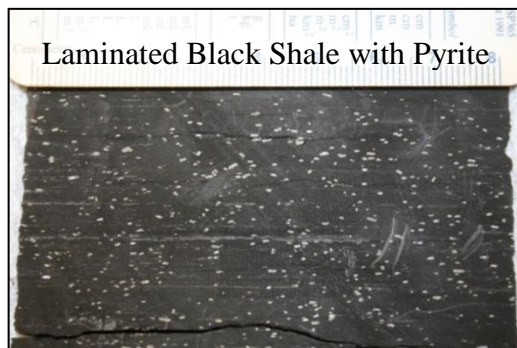
Figures 7-10. Pictures of sampled cores, highlighting the diverse lithological facies present within the Marcellus Shale. **Top-Left:** An organic-rich black shale interval with an abundance of disseminated pyrite. **Top-Right:** Bioturbated carbonate interval with a sharp transition to a more laminated black shale interval below, indicating a possible boundary between regressive and transgressive depositional processes, respectively. **Bottom-Left:** Core cuttings displayed for sample selection. **Bottom-Right:** Carbonate interval with pyrite enrichment on the lower boundary. Laminations are still visible, suggestive of a marl (lime-rich mud).

2.2 Shale Geochemical Characterization

2.2.1 Rock-Eval® Pyrolysis & Total Organic Carbon Abundance

   Rock-Eval® Pyrolysis was performed as an initial screening technique to evaluate source rock potential (based on the quantity, quality, and thermal maturity of organic matter) of the thirty-one bulk rock shale samples selected for potential use in the supercritical CO_2 extraction experiments. Analyses were performed by GeoMark Research, LTD., on a Rock-Eval II instrument, according to the following procedures. Approximately 100 mg of washed, ground (60 mesh, 250 μm) whole rock samples were pyrolyzed at 300 ^{o}C for 5 minutes, followed by programmed pyrolysis at 25 ^{o}C/min to 600 ^{o}C, where temperature then holds for 1 minute. Pyrolyzed organic compounds were detected by a flame ionization detector (FID). The first peak (S1) represents free, thermally extractable hydrocarbons (oil content) present in the rock, expressed in units of milligrams of hydrocarbon (HC) per gram of rock. The second peak (S2) represents the abundance of hydrocarbons generated from pyrolytic cracking of the remaining kerogen), expressed in units of milligrams of HC per gram of rock. The temperature recorded at the height of the S2 peak is called T_{max} (^{o}C). Any CO_2 released during pyrolysis up to 390 ^{o}C was analyzed via a thermal conductivity detector (TCD). This third peak (S3) represents the CO_2 content, expressed in units of milligrams organic CO_2 per gram of rock. A rock standard was used to calibrate the instrument prior to analysis, and to check the calibration after every 10 samples (GeoMark Research, LTD.). Acceptable uncertainty for each value is as follows:

$$T_{max} = \pm 2 \; ^{o}C$$

$$S1 \; \& \; S2 = \pm 10 \; \% \text{ variation from established value}$$

$$S3 = \pm 20 \; \% \text{ variation from established value}$$

For quantitative TOC analysis, samples were first treated with concentrated hydrochloric acid (HCl) for at least 2 hours to remove inorganic carbon. Acidified samples were then rinsed with water, filtered to remove the acid, and subsequently dried in an oven at 110 ^{o}C for at least 2 hours. Sample weights were measured before and after acidification to obtain a percent carbonate value based on mass lost. TOC analysis was then performed on a LECO C230 instrument, where the acidified samples were combusted in an oxidation oven at 1200 ^{o}C. Generated CO_2 was measured by an infrared (IR) detector, and results were reported in units of grams of carbon per gram of rock, expressed as a percentage. Calibration was achieved with standards of known carbon content, and standards were analyzed every ten samples to monitor any variations in the calibration. Duplicate analysis of project samples were performed every seven to ten samples, and acceptable standard deviations are within $\pm 3 \; \%$ (GeoMark Research, LTD).

Based on results, seven of the thirty-one samples were chosen for further geochemical characterization analyses and the supercritical CO_2 extractions (Table 7). Chosen samples were considered the most organically rich and had the greatest extraction potential, with selection criteria based on the highest S1 (> 0.70 mg HC/g rock) and S1/TOC (mg HC/g TOC) values.

Core ID	County, PA	Sample ID	Vertical Depth (ft)	Depth Between Samples (ft)
3S	Clarion	3S-8	6,312	88
		3S-29	6,400	
2LT	Jefferson	2LT-12	7,438	33
		2LT-19	7,471	
4LG	Jefferson	4LG-3	6,589	54 (4LG-3 to 4LG-18); 9 (4LG-18 to 4LG-25)
		4LG-18	6,643	
		4LG-25	6,662	

Table 7. Marcellus Shale samples selected for further geochemical characterization and supercritical CO_2 extractions.

2.2.2 Sample Preparation: Crushing & Sieving

Each core sample was crushed to a powder with a stainless steel mortar and pestle. Crushed samples were subsequently dry-sieved by using a nested stack of U.S.A. Standard sieves into the following size fractions: 1000 - 500 µm (18 - 35 mesh), 250 - 125 µm (60 - 120 mesh), and 63 - 25 µm (230 - 500 mesh). The 1000 - 500 µm and 250 - 125 µm size fractions were chosen to represent coarse and fine sand-size grains, respectively, and the 63 - 25 µm fraction was chosen to represent silt-size grains. Sample splits of each sieve size were then taken following the 'cone and quarter' technique (Schumacher et al., 1990). Sample splits were reserved for the supercritical CO_2 extractions, and for the following characterization analyses: 1) organic petrography (reflectance); 2) stable carbon isotopes; 3) X-ray diffraction; 4) Brunauer, Emmett and Teller surface area; and 5) scanning electron microscopy imaging. All size fractions and samples splits were stored in glass jars that were previously baked in a high temperature muffle furnace and sealed with Polytetrafluoroethylene (Teflon) lined lids until ready for use.

2.2.3 Stable Carbon Isotope Analysis

Carbon isotopic composition can be correlated with source (or type) of organic matter present in ancient rocks (Zielinksi, 1977; Maynard, 1981). Analysis was performed in the Stable Isotope Laboratory at UMD with a Eurovectar Elemental Analyzer (EA) interfaced with an Isoprime Isotope Ratio Mass Spectrometer (IRMS).

Prior to analysis, ground bulk rock samples are first acidified with 3 M HCl to remove inorganic carbon, followed by rinses with Milli-Q water to remove the water and subsequent drying in a low temperature oven (60 ^{o}C). Organic carbon of the residual samples was converted to CO_2 via oxidative combustion in the EA. Combustion products were carried via a flow of helium (He) carrier gas through a reduction column to reduce any N_xO_x gases to N_2 and remove excess O_2, then through a chemical trap (magnesium perchlorate) to remove water, and ultimately into a gas chromatography (GC) column to separate gaseous components. Separated CO_2 was sent to the IRMS, where isotopic constituents were separated and collected on the basis of differing mass/charge (m/z) ratios: 44 for $^{12}C^{16}O_2$, and 45 for $^{13}C^{16}O_2$. Isotopic ratios ($^{13}C/^{12}C$) were measured relative to a reference gas standard. Results are expressed in delta notation, in per mil (‰, parts per thousand) units, relative to the universal Vienna Pee Dee Belemnite (V-PDB) standard.

$$\delta^{13}C\ (‰) = [(R_{sample} - R_{standard})/R_{standard}]\ x\ 1{,}000,$$

$$\text{where } R = {^{13}C}/{^{12}C}.$$

Urea standards, with an expected $\delta^{13}C$ value of -29.39 ‰, were also analyzed in the EA-IRMS between batches of 10 samples to correct for instrumental drift. Acceptable uncertainties are within $\pm$ 0.1 ‰ variation from the established value.

2.2.4 Reflectance Analysis

Reflectance analysis, performed in accordance with ASTM D7708, was used to confirm the thermal maturity of the samples and to potentially identify the type of organic matter present. One sample from each core (3S-8, 2LT-12, and 4LG-3) was analyzed due to the minor depth interval (< 90 ft) between samples with each core (Table 7). Reflectance measurements were made on a Leica DMRX incident light microscope equipped with a tungsten halogen discharge light source and a photomultiplier detector. Results were recorded as the percentage of incident white light reflected from the sample, $\%R_o$. Measurements were taken by using an oil immersion objective lens to increase microscope resolution, and calibrated against a glass standard (1.314 $\%R_o$). Average values were reported based on a total of between 21-24 measurements for each core sample with reported uncertainties within $\pm$ 0.5 $\%R_o$. QA/QC was performed on a Hilgers microscope system with LED light source and digital camera detector.

Prior to analysis, ground shale samples (1000 - 500 μm) were mounted in a heat-setting thermoplastic to create pellets in a Buehler Simplimet 3000 Automatic Mounting Press, and subsequently polished with a Buehler Ecomet 4 according to ASTM D2797.

2.2.5 X-Ray Diffraction

X-ray Diffraction (XRD) was performed at the U.S. Geological Survey (USGS) to determine the major, minor, and trace mineral abundances (%) within each of the samples. Results were used to evaluate variations in hydrocarbon recovery among samples.

Prior to analysis, powdered shale samples (63 - 25 µm) were dried at 100 ^{o}C (to remove water from clay minerals) and then low temperature ashed (LTA) to obtain a loss on ignition (LOI) value (Pontolillo & Stanton, 1994). The LTA process uses an ionized oxygen plasma to combust each sample's organic matter at 100 ^{o}C under vacuum, with generated CO_2 and H_2O gases removed by a vacuum pump, thus removing organic matter from the sample matrix and isolating the mineral content. The LOI value is a measure of TOC expressed as a percentage of weight lost from the LTA process. Ashed samples were mounted as 25 mm pellets. XRD analyses were performed on a PANalytical X'Pert PRO X-ray diffractometer, where the sample pellets were irradiated with monochromatic X-ray beams generated from a copper anode. Diffraction angles (*2θ*) and corresponding intensities of diffracted X-rays were measured and calibrated according to the method of least squares. Mineral phase identification and abundances were achieved by comparing the sample X-ray diffraction patterns against a user-supplied library of reference mineral standards (Hosterman & Dulong, 1989; Biscaye, 1964). Acceptable accuracy for this method is within ± 2 % and absolute uncertainties within ± 1 % (1 σ) (Smith et al., 2013).

A diffraction angle (*2θ*) is related to the interlayer spacing in a mineral's crystalline structure according to Bragg's Law, given by

$$n\lambda = 2d\sin\theta, \text{ where}$$

n = order of reflection,

λ = wavelength of incident X-ray beam (1.54 Å for Cu anode),

d = interplanar spacing of crystalline lattice, and

θ = incidence angle of X-ray beam.

Diffraction angles and their corresponding intensities create an X-ray diffraction pattern that is characteristic of a given crystalline structure, enabling mineral phase identification.

2.3 Microwave-Assisted Extractions

Microwave-assisted extractions were performed on a CEM MARS X® Microwave Accelerated Reaction System, as an initial semi-quantitative screening of the distribution of potentially extractable hydrocarbons present in the samples. This extraction technique uses microwave radiation to heat and extract solutes from a solid sample matrix in a closed vessel. Extraction parameters are listed in Table 8.

Microwave-Assisted Extraction Parameters	
Sample Mass	5.0 g
Extraction Solvent	Acetone/Dichloromethane (50/50)
Method	GreenChem PAH3000
Maximum Temperature	200 $^{\circ}$C
Maximum Pressure	200 psi
Power	300 Watts
Stage 1 (Increasing T & P)	8 minutes
Stage 2 (P still increasing @ target T)	15 minutes

Table 8. Microwave-assisted extraction parameters. Method parameters chosen as specified in the CEM instrument operations manual.

Solvent mixtures for the extractions must have at least one component capable of absorbing microwave energy. Thus, acetone was selected as the polar solvent that can strongly absorb microwave energy and dissipate heat to surrounding molecules, and dichloromethane (DCM) as the nonpolar solvent used to extract nonpolar hydrocarbons. Once the extraction was complete, extracts were filtered from the sample and the solvent was subsequently evaporated by using a nitrogen evaporator (N-EVAP). The dried, extracted residue was then re-introduced into hexane to a final

1-ml volume prior to analysis via Gas Chromatography-Mass Spectrometry (GC-MS). Results were used to determine the appropriate GC-MS method and hydrocarbon standards necessary for quantitative analysis of extractable n-aliphatic hydrocarbons from the samples.

A quantitative microwave-assisted extraction of each sample (1000 - 500 μm fraction) was later performed after initial supercritical CO_2 extractions were complete to provide a rough estimate of extraction efficiency. GC-MS analysis of these extracts was performed in accordance with the procedures listed in Section 2.4.3 below.

2.4 Supercritical Carbon Dioxide Extractions

2.4.1 ISCO SFX^TM 220 Supercritical Fluid Extraction System

Hydrocarbon extractions of all samples and sieve sizes were performed on an ISCO SFX^TM 220 Supercritical Fluid Extraction System coupled with an ISCO 260D model syringe pump at the USGS. Extraction method parameters were adapted from USGS Open-File Report 2006-1054 (Kolak, 2006).

Supercritical CO_2 Extraction Parameters	
Sample Mass	1.0 g
Extraction Solvent	100 % CO_2 (Bone Dry, 99.9 % minimum purity)
Temperature	80 ^{o}C
Pressure	20.7 MPa (3,000 psi)
Extraction Mode – Step 1	Static, 15 minutes
Extraction Mode – Step 2	Dynamic, 60 minutes
Restrictor (outlet line) Temperature	100 ^{o}C
Collection Solvent	100 ml chilled hexane (in ice water bath, 0 ^{o}C)

Table 9. Supercritical CO_2 extraction parameters.

Selected temperature and pressure values were chosen to represent approximate *in situ* reservoir conditions for the samples. A high restrictor temperature, generally ranging between 100 - 150 ^{o}C, are chosen to minimize precipitation of heavy hydrocarbons or ice that could plug the line and reduce hydrocarbon recovery yield (Monin et al., 1987; Li et al., 1997). Optimum temperature of the collection solvent, ranging between 0 to -5 ^{o}C, is found to minimize loss of volatile hydrocarbons, while also preventing plugging of the restrictor line (which has been observed at very low temperatures of -40 ^{o}C) (Li et al., 1997). The volume of CO_2 dispensed in each extraction ranged between approximately 70 - 90 ml (at 80 ^{o}C and 20.7 MPa), with a flow rate of approximately 1.0 - 1.5 ml/min during the dynamic extraction step.

Temperature settings in the extractor are controlled by a Fuji electric sensor with a manufacturer accuracy of $\pm$ 1 ^{o}C. The temperature sensor was calibrated using an alcohol thermometer, and the expected accuracy was confirmed. Pressure is also digitally controlled by the extractor, but was calibrated by using an external NIST-certified pressure gauge to within a reported accuracy of $\pm$ 3 % ($\pm$ 0.69 MPa, 100 psi) from the target pressure (20.7 MPa, 3,000 psi).

Once extractions were complete, total (unfractionated extracts) were subsequently concentrated to approximately 10 ml in a 125-ml pear flask by using a vacuum rotary evaporator (ROTAVAP). Each extract was then transferred to a volumetric concentrator tube for concentration of the extract to a final 5-ml volume by using a nitrogen evaporator (N-EVAP). Each pear flask was rinsed three times with hexane, and all rinses added to the concentrator tube. Final 1/5 and 1/10 (extract/hexane)

dilutions were necessary for the 3S-8 and 3S-29 extracts prior to analysis to prevent hydrocarbon peaks from saturating the GC-MS detector.

Accuracy for the entire extraction method was evaluated with method blanks and surrogate standards. Baked quartz sand was used as a method blank at the start of each batch of extractions (daily) to monitor for contamination. Surrogate standards, which monitor the entire analytical performance (from sample preparation, through the CO_2 extraction, all subsequent extract concentration and dilution steps, and GC-MS analysis), were used as an estimate of extraction efficiency. Each sample and method blank was spiked with a known volume of 10,000 µg/ml stock surrogate solution (see Table 10 for volumes and concentrations) just prior to the start of each extraction. The surrogate solution contains deuterated n-aliphatic hydrocarbon standards (decane-d_{22}, $C_{10}D_{22}$, and tetracosane-d_{50}, $C_{24}D_{50}$) in hexane, encapsulating the range of expected extractable hydrocarbons. Decane-d_{22} was chosen to monitor recovery of lower molecular weight, volatile hydrocarbons. Tetracosane-d_{50} was chosen to monitor recovery of higher molecular weight, low-volatility hydrocarbons.

Extract Dilutions	Volume Injected of Surrogate Stock (µl)	Expected Final Concentration of Surrogate in Extract (µg/ml)
1/10 (10X)	50	10
1/5 (5X)	10	4
None	5	10

Table 10. Injection volume and concentration of the surrogate standard solution. Percent recovery was calculated from the recovered concentration post-extraction relative to the expected concentration.
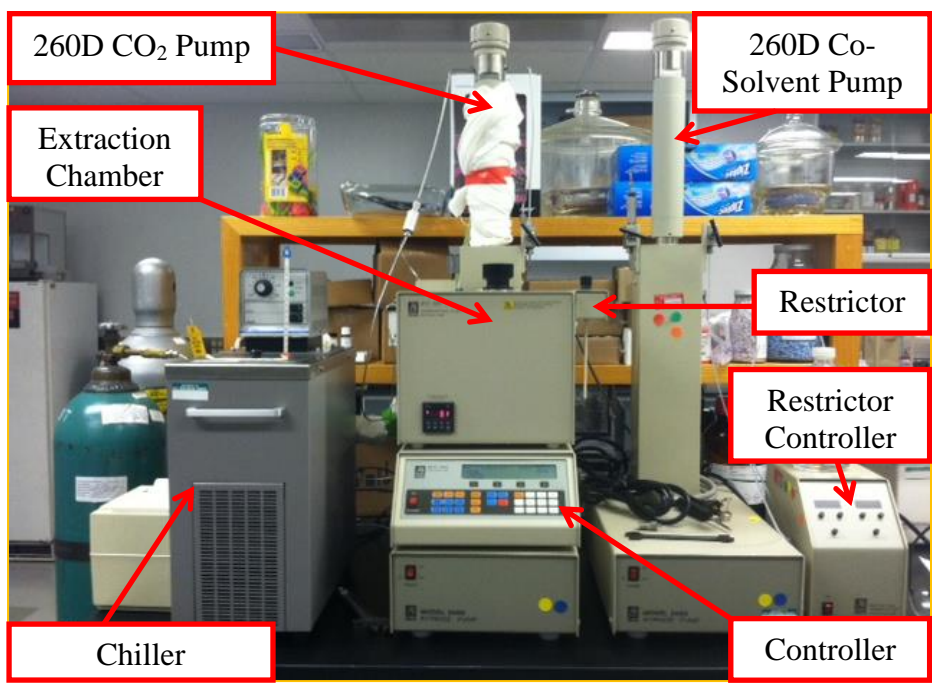
Figure 11. ISCO SFX 220^{TM} Supercritical Fluid Extraction System.
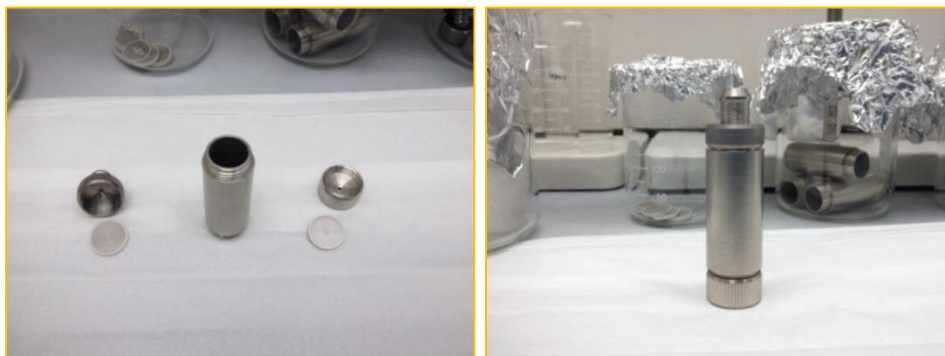
Figure 12-13. ISCO 10-ml aluminum vessel. Frit filters (with 2 µm openings) were inserted beneath the top and bottom vessel lids to prevent the sample particles from being flushed through the extractor lines. Quartz wool was loosely packed into the bottom and top of the vessel to minimize dead volume. The amount of O_2 in an empty vessel is estimated to be 2.1 ml. During extractions the vessel is approximately 90 % filled with the sample and quartz wool; thus, the O_2 content decreases by approximately 1 order of magnitude (2 % of total volume).

Figure 14. Top-down view of the extraction chamber.

39

2.4.2 Open Column Chromatography

Open column chromatography tests were performed on bulk extracts from the initial supercritical CO_2 test extractions (one sample from the 2LT and 4LG cores) to determine whether separation of hydrocarbon compounds into aliphatic, aromatic and polar hydrocarbon class fractions would improve resolution of the n-aliphatic hydrocarbons and separate the overlapping hydrocarbons, unresolved complex mixture (UCM), prior to analysis via GC-MS. None of the 3S samples were tested since there was no visible interference in the bulk extract chromatograms.

A 200-ml glass chromatography column was first assembled on a ring-stand with a polytetrafluoroethylene (PTFE) stopcock at the bottom. A small layer of glass wool was inserted, followed by the following reagents: 2.5 g neutral alumina, 2.5 g silica grade 62, and 5.0 g silica grade 923. Analytical methods for preparing those reagents and performing the extract separation were adapted from USGS Open-File Report 2006-1054 (Kolak, 2006).

Figure 15. Open column chromatography test.

Hydrocarbon Class Fraction	Eluting Solvent
Aliphatics	Hexane
Aromatics	30D – 30 % v/v DCM in Hexane
NSO's/Resins (Polars)	30M – 30 % v/v Methanol in Hexane

Table 11. Open column chromatography solvents. Eluting solvents were chosen to separate hydrocarbon class fractions within bulk extracts.

Each class fraction was collected in a 125-ml pear flask, evaporated under ROTAVAP to approximately 10 ml, and then transferred to a graduated concentrator tube. Each pear flask was rinsed three times with the corresponding solvent for that fraction, and all rinses added to the concentrator tube. The aliphatics fraction was subsequently concentrated down to a 1-ml volume by using a nitrogen evaporator (N-EVAP), and the aromatics and polar fractions to a 2-ml volume, prior to GC-MS analysis. The aromatics and polar fractions were only qualitatively evaluated by the GC-MS, since hydrocarbon standards and analytical methods were only set up for quantifying the aliphatics fraction.

2.4.3 Gas Chromatography-Mass Spectrometry Analysis

Quantitative analysis of total resolvable n-aliphatic hydrocarbons from all sample extracts was performed on a Hewlett Packard/Agilent 6890 Series Gas Chromatograph (GC) interfaced with a Hewlett Packard/Agilent 5973 Mass Selective Detector (MSD). Automatic sample injection was performed with a Hewlett Packard/Agilent 7683 Series Automatic Injector, operating in splitless mode to maximize resolution of trace compounds. Analytical method parameters were adapted from USGS Open-File Report 2006-1054 (Kolak, 2006).

GC-MS Parameters	
Injector Temperature/Mode	280 ^{o}C/Splitless
Injection Volume	1 µl
Carrier Gas/Flow Rate	He / 0.9 ml/min (constant flow)
GC Column	HP-5MS, 30 m x 0.25 mm x 0.25 µm
GC Oven Program	50 ^{o}C, hold for 1.5 minutes; Ramp to 315 ^{o}C @ 10 ^{o}C/min; 315 ^{o}C, hold for 15 minutes
MSD Conditions	Full scan, 35-500 amu
Solvent Delay Time	4.5 minutes

Table 12. GC-MS method parameters for the analysis of extracted n-aliphatic hydrocarbons.

Aliphatic hydrocarbons were identified by their GC retention times in the Total Ion Current (TIC) Chromatogram (compared to hydrocarbon standards), and the mass spectrum of each component's resolved fragmentation pattern of m/z fragment intensities (compared to reference libraries). Quantitative measurements were made by the TIC signal intensity (total ion counts/second) for the area under the peak of the user-defined target ion (also called the base peak, or most abundant m/z fragment for the compound). Tables of all calibrated standards and target n-aliphatic hydrocarbons are listed in Appendix A.

Prior to injection on the GC-MS, a known amount of internal standard solution (25 μl of 1,000 μg/ml stock) was added to each 5-ml extract (final 5 μg/ml concentration) so that quantitative measurements could be made via an internal standard method of calibration. A 5 μl-volume of the internal standard solution was also added to the 1 ml-aliphatics extracts (from the open-column chromatography tests) to achieve the same final concentration. The internal standard solution includes a range of deuterated n-aliphatic hydrocarbons dissolved in hexane: dodecane-d_{26}, $C_{12}D_{26}$, hexadecane-d_{34}, $C_{16}D_{34,}$ nonadecane-d_{40}, $C_{19}D_{40}$ and triacontane-d_{62}, $C_{30}D_{62}$. A 7-point calibration curve of Response Ratios (sample/internal standard) against Amount Ratios (sample/internal standard) was generated for an n-aliphatic hydrocarbon standard solution (n-C_9 to n-C_{40}). Calibration levels include the following concentrations: 0.25, 0.5, 1.0, 2.5, 5.0, 7.5, and 10.0 μg/ml. Levels were diluted with hexane from the original 1,000 μg/ml stock solution. A quadratic regression model was found to be the best fit relationship between Amount and Response Ratios, with coefficient of determination (r^2) values $\geq$ 0.999 for n-C_9 through n-C_{30}.
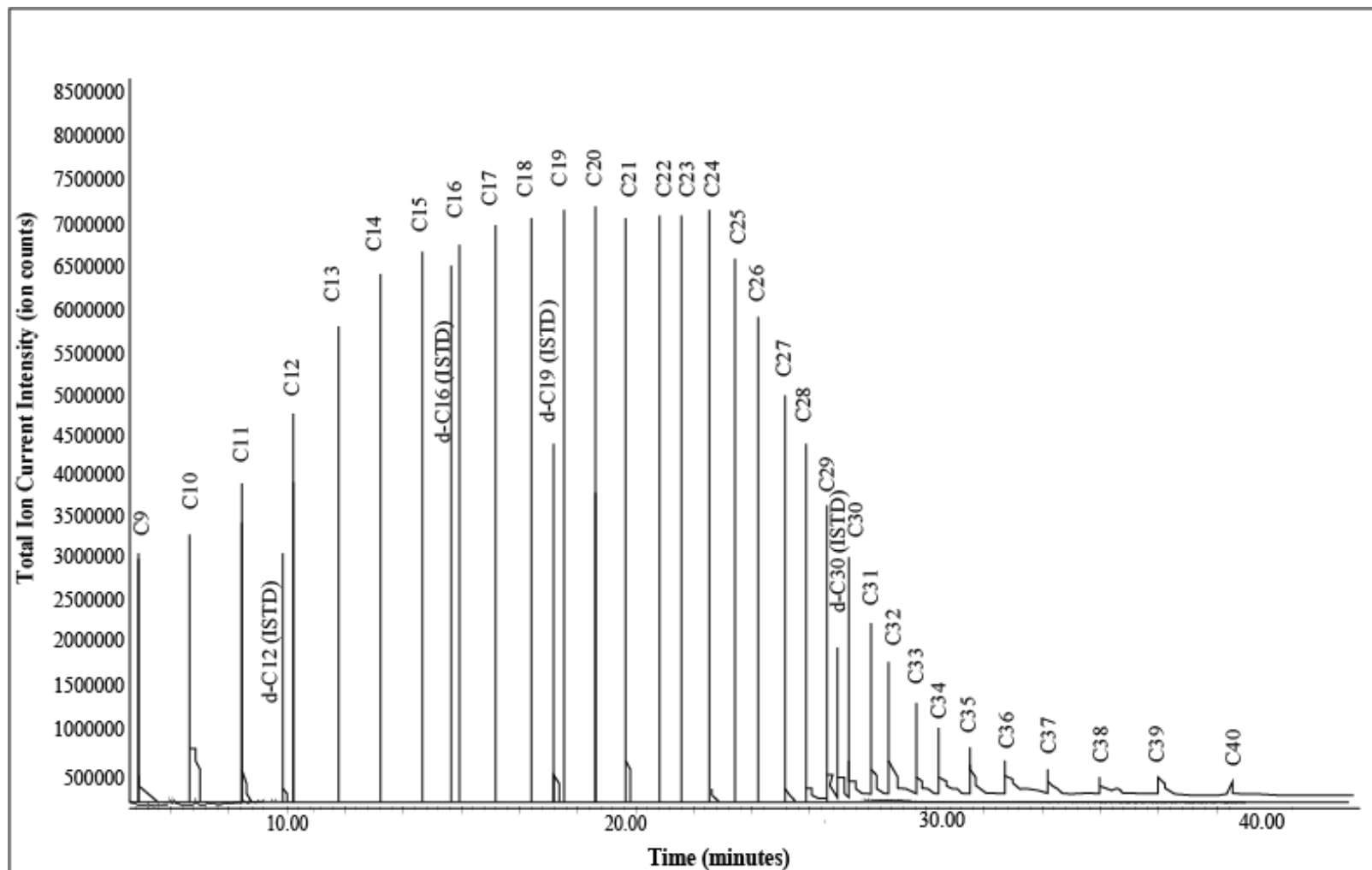
Figure 16. TIC chromatogram of the n-C$_9$ to n-C$_{40}$ hydrocarbon standard solution (5.0 µg/ml).

43

2.5 Particle Size Characterization

2.5.1 Surface Area Analysis

Specific surface area was measured on a subset of the ground shale samples to evaluate if differences in surface area were influencing hydrocarbon yields from the different sieve size fractions. One sample from each core (3S-8, 2LT-12, and 4LG-3), and each sieve size fraction (1000 - 500 μm, 250 - 125 μm, and 63 - 25 μm) within that sample, was analyzed.

Surface area analyses were performed by Particle Technology Labs on a Micromeritics® TriStar II 3020 static pressure (volumetric) analyzer, with N_2 as the adsorbate gas. Prior to analysis, each sample was heat conditioned for 3 hours at 300 ^{o}C to remove atmospheric contaminants physically bonded to the surface and pores (outgassing). Static pressure adsorption and desorption analyses were then performed on 2.0 - 2.5 g of each sample at a constant temperature of -195.8 ^{o}C. Samples were incrementally dosed with a known volume of N_2 into the evacuated sample chamber until saturation pressure was reached, followed by incremental reduction in N_2 pressure. Throughout the analytical process, measurements of the volume of N_2 physically adsorbed onto the solid sample (adsorbent), and the equilibrium pressure of N_2 at each dosing, were recorded at constant temperature. Accuracy for the surface area results have been reported to within $\pm$ 0.24 m^2/g ($\pm$ 1 %), which is within the range of accepted instrumental accuracy of $\pm$ 3.45 % (at the 99.7 % confidence level). Uncertainties, determined from triplicate analyses, have been reported to within $\pm$ 0.3 m^2/g ($\pm$ 1 %, $\pm$ 1 σ_m).

Surface area was evaluated from a 10-point interval on the adsorption isotherm, following the Brunauer-Emmet-Teller (BET) multilayer gas adsorption model. Specific surface area results, expressed in units of area per mass of sample (m^2/g), were calculated by using the BET adsorption isotherm equation:

$$\frac{1}{V(\frac{P_o}{P-1})} = \frac{C-1}{V_m * C} * \frac{P}{P_o} + \frac{1}{V_m * C} \text{ , where}$$

P = Absolute pressure of N_2 in equilibrium with the surface at -195.8 ^oC (Pa),

P_o = Saturation pressure of N_2 (Pa),

P/P_o = Relative pressure (dimensionless),

V = Volume of N_2 adsorbed at standard temperature and pressure (m^3/g STP),

V_m = Volume of N_2 adsorbed at STP to form a monolayer on the surface (m^3/g STP),

STP = 0 ^oC and 0.1 MPa, and

C = BET constant related to enthalpy of adsorption of N_2 on sample (dimensionless).

The BET value $\frac{1}{V\frac{P_o}{(P-1)}}$ is plotted against P/P$_o$ for each data point according to the equation above. The resulting plot should be linear within a relative pressure range of 0.05-0.30 (Sing et al., 1985). From the plot, the slope, and y-intercept can be evaluated as follows

$$slope = \frac{C-1}{V_m * C} \quad , \quad y - intercept = \frac{1}{V_m * C} \quad .$$

Then V_m and C are calculated from the following equations

$$V_m = \frac{1}{slope + y - intercept} \quad , \quad C = \frac{slope}{y - intercept} + 1 \quad .$$

Upon solving for V_m, the specific surface area is calculated from

$$a_s\ (BET) = \frac{V_m * L * a_m}{2.24\ x\ 10^{-2}}\ , \text{where}$$

a_s = Specific surface area (m^2/g),

V_m = Monolayer capacity of N_2 (m^3/g STP),

L = Avogadro's Number (6.022 x 10^{23} molecules/mole N_2),

a_m = Molecular cross-section of N_2 at -195.8 ^{o}C = 1.62 x 10^{-19} m^2 (Sing et al., 1985),

and

2.24 x 10^{-2} = Volume occupied by 1 mol N_2 at STP (m^3).

2.5.2 Scanning Electron Microscopy Imaging

Scanning electron microscopy imaging was performed on a JEOL 8900 Electron Probe Microanalyzer to visualize and characterize the surface of sample particles within each sieve size fraction. Prior to analysis, samples were mounted on carbon tape and then coated with a thin layer of carbon to make the sample surface electrically conductive (minimize charging at the surface). Each sample was then irradiated with an electron beam (electron probe), and images were made from interactions of the beam with the sample. Secondary Electron (SE) images, which give information on surface topography and 3-D structure, are produced from secondary electrons emitted by atoms within the sample that are excited by the initial electron beam. Back-Scatter Electron (BSE) images, which give information on chemical composition, are produced from initial X-ray beam electrons reflected from different atomic constituents within the sample. Both SE and BSE images were taken of the 1000 - 500 μm and 250 - 125 μm fraction of sample 4LG-3.

Chapter 3: Results

3.1 Shale Geochemical Characterization

3.1.1 Rock-Eval® Pyrolysis & Total Organic Carbon Abundance

Rock-Eval® pyrolysis results were used to evaluate the quantity, quality and thermal maturity of the organic matter in thirty-one shale samples. Quantity of organic matter, or organic richness, was evaluated based on three parameters: TOC, S1, and S2. TOC ranged from 0.2 - 7.6 wt % for all samples. Note that some TOC values were considered to indicate 'Good' to 'Excellent' hydrocarbon resource potential (Table 13) according to the definitions of Peters and Cassa, 1994.

Resource Potential Parameters			
Hydrocarbon (HC) Potential	**TOC (wt %)**	**S1 (mg HC/g rock)**	**S2 (mg HC/g rock)**
Poor	0 - 0.5	0 - 0.5	**0 - 2.5**
Fair	0.5 - 1	**0.5 - 1**	2.5 - 5
Good	**1 - 2**	**1 - 2**	5 - 10
Very Good	**2 - 4**	**2 - 4**	10 - 20
Excellent	**> 4**	> 4	> 20

Table 13. Resource parameters to evaluate hydrocarbon resource potential of sedimentary rocks (Peters & Cassa, 1994). Sample values are in **Bold**.

Results for the seven samples used in the supercritical CO_2 extractions, shown in Tables 14 and 15, had the highest S1 and S1/TOC values. The S1/TOC value, which normalizes oil content to TOC, is referred to as the 'oil saturation index', and is used as an indication of *in situ* source rock potential (Jarvie & Baker, 1984; Jarvie, 2012). Therefore, these values were used as the criteria for the selection of samples for the extraction experiments.

Sample ID	Quantity: Resource Potential			Quality: Type of Organic Matter			Thermal Maturation
	TOC	S1	S2	S3	HI	OI	PI
3S-8	4.8	2.8	0.7	0.4	14.6	7.9	0.8
3S-29	6.2	0.7	0.7	0.3	11.5	5.2	0.5
2LT-12	3.2	0.8	0.5	0.2	16.4	6.3	0.6
2LT-19	3.7	0.7	0.6	0.3	16.0	8.4	0.5
4LG-3	3.9	0.9	0.4	0.3	9.6	7.5	0.7
4LG-18	1.5	1.0	0.3	0.6	17.1	38.2	0.8
4LG-25	5.6	1.2	0.4	0.2	7.5	3.0	0.7

Table 14. Rock-Eval® Pyrolysis results (GeoMark Research, LTD). Units: TOC (wt %), S1 & S2 (mg HC/g rock), S3 (mg CO_2/g rock), HI (mg HC/g TOC), OI (mg CO_2/g TOC), T_{max} (^{o}C).

Sample ID	TOC (wt %)	S1 (mg HC/g rock)	S1/TOC (mg HC/g TOC)
3S-8	4.8	2.8	58.8
3S-29	6.2	0.7	11.8
2LT-12	3.2	0.8	24.3
2LT-19	3.7	0.7	19.0
4LG-3	3.9	0.9	23.8
4LG-18	1.5	1.0	64.5
4LG-25	5.6	1.2	20.9

Table 15. Rock-Eval® Pyrolysis quantity results (GeoMark Research, LTD). Results were used as criteria for selecting samples for the supercritical CO_2 extractions.

Very low Hydrogen Index (HI ≡ S2/TOC) values (< 50 mg HC/g TOC) and oxygen index (OI ≡ S3/TOC) values (< 39 mg CO_2/g TOC) were found for all samples. A modified Van Krevelen diagram (cross plot of HI versus OI indices) suggests that the type of kerogen present could be oxidized, highly mature, or Type IV kerogen (Peters, 1986; Peters & Cassa, 1994). However, a modified Van Krevelen diagram of Devonian shales from the Appalachian Basin (Figure 17) suggests that the principal source of organic matter is Type II kerogen. Low HI values (0 - 100) and OI

values (5 - 30) in this region are suggested to represent original Type II converted to Type IV (inert solid bitumen) by a high degree of thermal maturation (Ryder et al., 2013).
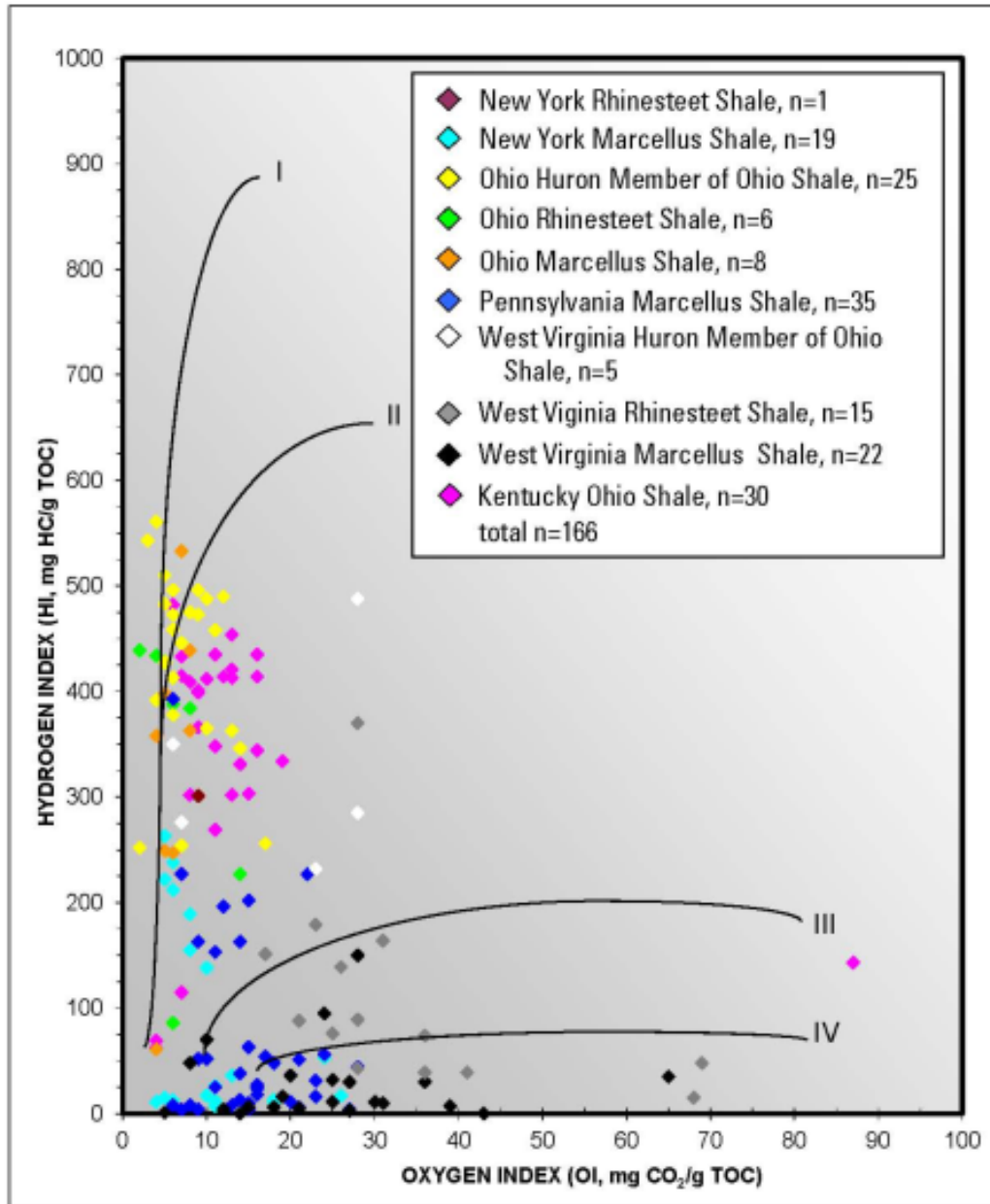
Figure 17. Modified van Krevelen diagram of Devonian shales (Ryder et al., 2013).

Thermal maturity can be roughly estimated from the modified van Krevelen diagram, T_{max}, and production index (PI ≡ S1/(S1+S2)) measurements. PI indicates the degree to which kerogen is transformed into free hydrocarbons (Espitalié et al., 1977). PI values for the samples ranged from 0.5 - 0.8, which suggests they are in a late-mature/post-mature stage of hydrocarbon generation, the dry gas window, occurring at subsurface paleotemperatures of approximately 150 - 200 ^{o}C (Peters, 1986).

Maturity Level		T_{max}	PI
	Immature	< 435	< 0.01
Mature	Early	435 - 445	0.10 - 0.15
	Peak	445 - 450	0.25 - 0.40
	Late	450 - 470	> 0.40
	Post-mature	> 470	-

Table 16. Thermal maturity evaluation parameters (Peters & Cassa, 1994).

However, standard interpretations of PI values and T_{max} for the 4LG samples are not in agreement. Ultimately, due to the low and broad (or lack of) S2 peak, thermal maturity and original kerogen type could not be accurately determined for all samples and needed further evaluation.

3.1.2 Stable Carbon Isotope Analysis

Carbon isotopic composition can be used as a diagnostic tool to aid in identifying the source of organic matter present in ancient rocks (Zielinksi, 1977; Maynard, 1981). Very negative δ^{13}C compositions, ranging from -29.2 to -30.9 ‰, were measured on the organic fraction of each sample (the bulk shale residue analyzed after acidification removed any existing inorganic carbon). This range of values suggests photosynthetic incorporation of carbon from CO_2 for the generation of

organic matter, favoring enrichment of ^{12}C relative to ^{13}C. Yet it is also documented that algal and land-plant sources of sedimentary organic matter cannot be differentiated by using the $^{13}C/^{12}C$ alone, but should be used together with atomic C/N abundance ratios (Meyers, 1994).

Plots of $\delta^{13}C$ values against C/N ratios also aid in identifying C3 versus C4 photosynthentic pathways (Meyers, 1994). In C3 photosynthesis, plants, green algae, and cyanobacteria use the enzyme ribulose 1,5-bisphosphate carboxylase/oxygenase (RuBisCO) to fix CO_2 into two 3-carbon molecules of 3-phosphoglycerate (3-PGA). In C4 photosynthesis, inorganic carbon is initially fixed into a 4-carbon compound (oxaloacetate) by the enzyme phosphoenolpyruvate (PEP) carboxylase in mesophyll cells of plant leaves. PEP carboxylase has no competing oxygenase activity, and thus fixes CO_2 more quickly and efficiently, but at a higher energy cost, than the C3 photosynthetic pathway.

Although total nitrogen abundances were not analyzed on this sample set, the $\delta^{13}C$ values do coincide with those found in other Devonian-age shales located in the central/western Appalachian Basin, which authors suggest is associated with an algal-derived, marine source of organic matter (plankton) (Zielinksi, 1977; Maynard, 1981), relative to more of a terrestrial source of organic matter with $\delta^{13}C$ values of approximately -25 to -26 ‰ (Maynard, 1981).

3.1.3 Reflectance Analysis

Reflectance measurements of the observable organic matter ranged from 2.2 - 2.6 ($\pm$ 0.5) %R_o (Table 17), confirming a high degree of thermal maturity and placing the sampled Marcellus shale in a post-mature stage of hydrocarbon generation (the dry gas window, 150 - 200 $^{\circ}$C). These reflectance values are slightly higher than those reported on regional thermal maturity maps (approximately 1.3 - 2 %R_o) for Appalachian Basin Devonian shales in the counties wherein these cores were drilled (Repetski et al., 2008; East et al., 2012; Ryder et al., 2013). However, given the uncertainties for these measurements, there is no significant difference among thermal maturity values. Thermal maturity zones reported across the Appalachian Basin are also compiled from both reflectance (%R_o) and conodont color alteration index (CAI) measurements taken on different sample within the basin, and currently there is no conversion factor between the two indices (East et al., 2012).

Reflectance Analysis				
Sample ID	# of Measurements (N)	Mean (% R_o)	Uncertainty ($\pm$ %R_o)	Relative Uncertainty (%)
3S-8	24	2.3	0.3	15
2LT-12	21	2.6	0.5	18
4LG-3	23	2.2	0.4	17

Table 17. Reflectance measurements of solid bitumen (pyrobitumen). Uncertainties are reported as $\pm$ 1 σ.

Reflectance also revealed the predominant organic matter was in the form of solid pyrobitumen, as evidenced by its pore-lining and pore-filling texture, and growth around mineral grains (Figures 18 and 19). A few inertinite macerals were recognized by their angular shapes and high reflectance (Figure 20). Inertinite macerals are

produced from highly degraded terrestrial plant matter or woody tissue, considered to be highly oxidized (or possibly burnt) in nature prior to deposition (Hutton, 1994; Peters et al., 2005). However, the identification of the original maceral composition of the pyrobitumen could not be determined due to the high degree of thermal maturity. The predominant type of original organic matter, Type II kerogen (*Tasmanites* algae, a telalginite maceral, and bituminite macerals), had to be inferred from studies of other low-maturity Marcellus Shale and Devonian-age shales elsewhere in the Appalachian Basin (Bruner & Smosna, 2011; Ryder et al., 2013). Telalginite and bituminite macerals are part of the liptinite maceral group, derived from algae, plankton or spores.
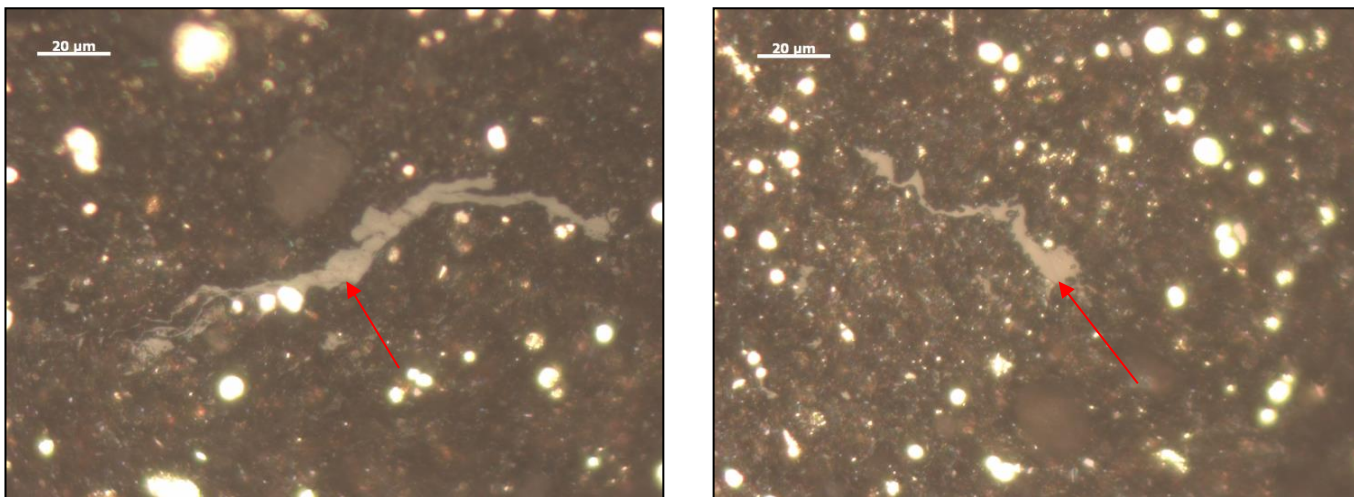
Figure 18-19. Reflectance images of pyrobitumen. Pyrobitumen indicated by red arrow. Bright framboidal pyrite structures are dispersed throughout. **Left:** 3S-8, with a reflectance value of 2.6 %R_o. **Right:** 2LT-12, with a reflectance value of 3.0 %R_o.

Figure 20. Reflectance image of inertinite maceral. Inertinite (from sample 4LG-3) indicated by red arrow.

3.1.4 X-Ray Diffraction

XRD results showed that all samples were composed of predominantly quartz and clay (mainly illite) minerals. Carbonate minerals were also abundant in samples 3S-29 and 4LG-18. Minor mineral constituents include feldspars, chlorite, and pyrite. The mineralogy is similar to that reported for other Marcellus Shale samples (Tables 3 and 4) (Hosterman & Whitlow, 1983; Bruner & Smosna, 2011).

Sample ID	QTZ	FLD	CARB	I/S	ILLITE	KAOL	CHLR	PY	OTHR	ΣCLY
3S-8	40.4	1.8	1.8	0.0	37.0	0.0	8.5	9.6	0.8	45.5
3S-29	34.1	1.5	46.3	0.0	12.3	0.0	0.0	4.3	0.0	12.3
2LT-12	28.9	1.9	0.6	0.0	51.3	0.0	10.8	6.0	0.0	62.1
2LT-19	33.0	2.2	5.9	0.0	45.4	0.0	2.0	9.7	0.3	47.4
4LG-3	39.7	2.7	4.7	0.0	36.0	0.0	9.4	7.1	0.0	45.4
4LG-18	24.4	0.7	35.7	0.0	27.7	0.0	4.8	5.8	0.0	32.5
4LG-25	36.1	2.4	1.4	0.0	43.1	0.0	6.0	9.8	0.6	49.1

Table 18. Major (≥ 50 %), minor (< 10 % and ≥ 5 %), and trace (< 5 %) phase mineralogy.

XRD Uncertainties									
	QTZ	FLD	CARB	I/S	ILLITE	KAOL	CHLR	PY	OTHR
Uncertainty ($\pm$ %)	0.7	0.5	0.2	0.0	0.4	0.0	0.5	0.8	0.1

Table 19. XRD uncertainties for each mineral phase. Uncertainties are reported within $\pm 1 \sigma$.

Label ID	Mineral Name(s)	Mineral Formula(s)
QTZ	Quartz	SiO_2
FLD	K-feldspar & Plagioclase (Albite to Anorthite)	$KAlSi_3O_8$ & $NaAlSi_3O_8$ (Albite) to $CaAl_2Si_2O_8$ (Anorthite)
CARB	Calcite, Ankerite, Dolomite, & Siderite	$CaCO_3$, $Ca(Fe^{2+}, Mg)(CO_3)_2$, $CaMg(CO_3)_2$, & $FeCO_3$
I/S	Illite/Smectite	$K_yAl_4(Si_{8-y},Al_y)O_{20}(OH)_4$ ($1 < y < 1.5$) / $(\frac{1}{2}Ca,Na)(Al,Mg,Fe)_4(Si,Al)_8O_{20}(OH)_4*nH_2O$
KAOL	Kaolinite	$Al_2Si_2O_5(OH)_4$
CHLR	Chlorite	$Mg_2Al_2SiO_5(OH)_4$
PY	Pyrite, Marcasite, & Sphalerite	FeS_2, FeS_2, & $(Zn,Fe)S$
OTHER	Trace (low level qualitative ID match)	N/A

Table 20. Nomenclature for XRD results.
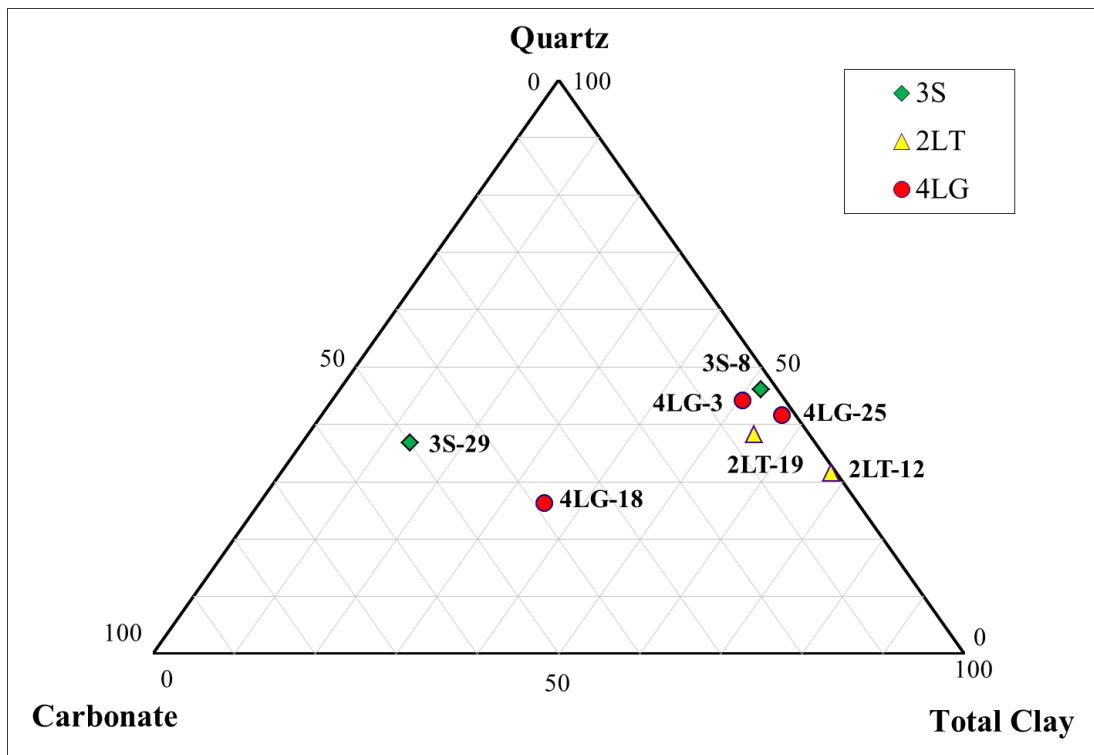
Figure 21. Ternary diagram showing the relative proportions of total clay, carbonate and quartz.

3.2 Microwave-Assisted Extractions

Results from the initial semi-quantitative microwave-assisted extractions showed successful extraction of resolvable n-aliphatic hydrocarbons from all samples. However, an additional UCM of hydrocarbons was observed in the GC-MS chromatograms for the 2LT samples. A UCM is a mixture of co-eluting, overlapping compounds observed as a broad peak in gas chromatograms of petroleum hydrocarbons. Its composition, size and shape are dependent upon the composition of petroleum source(s). UCMs are composed of recalcitrant petroleum compounds most resistant to weathering and biodegradation processes, and could contain a diverse mixture of aliphatic (linear, branched and cyclic), PAH, and alkylbenzene hydrocarbons. Open column chromatography tests were performed on the bulk extracts in an attempt to separate the UCM. Although the UCM did elute in the aliphatics fraction, hydrocarbon peaks could not be fully resolved. If separation is required in future extractions, a higher resolution analytical method would be required (i.e. two-dimensional GC x GC-MS) (Frysinger et al., 2003).

Follow-up quantitative microwave-assisted extractions performed on the 1000 - 500 μm fraction for each sample demonstrated successful extraction of resolvable n-aliphatic hydrocarbons from n-C_{11} through n-C_{22}. The UCM was also observed in both 2LT sample extracts in the range of n-C_{18} to n-C_{23}. A few discernible n-aliphatic hydrocarbon peaks were visible at the top of the UCM, but could not be fully resolved and thus were only qualitatively identified. Highest recovery was achieved from the 3S samples. Quantity of total resolvable n-aliphatic hydrocarbons ranged from approximately 0.01 - 3 mg hydrocarbon/g TOC.

Comparisons to the distribution and quantity of resolvable n-aliphatic hydrocarbons from the supercritical CO_2 extraction are made in Section 3.4.1 (Figure 25 and Table 31).
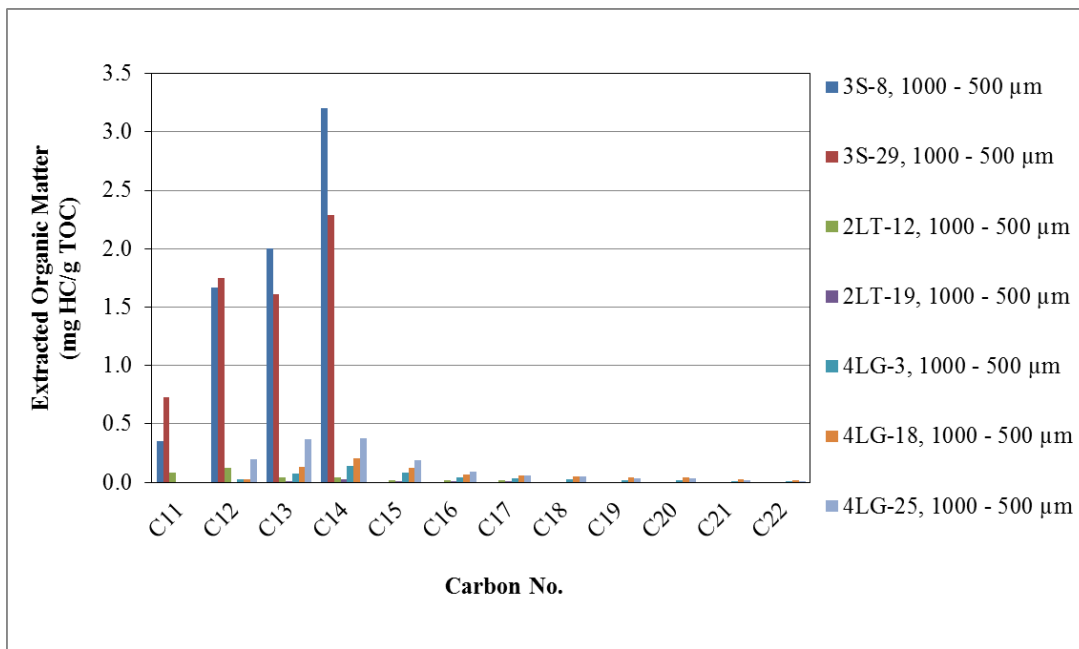
Figure 22. Distribution of resolvable n-aliphatic hydrocarbons extracted from the microwave-assisted extractions. Quantity extracted is plotted as a function of hydrocarbon chain length (carbon number) for the 1000 - 500 μm sieve size fraction of each sample.

3.3 Supercritical Carbon Dioxide Extractions

3.3.1 Distribution of Extracted Aliphatic Hydrocarbons

Supercritical CO_2 extractions of the 1000 - 500 μm, 250 - 125 μm, and 63 - 25 μm sieve size fractions from each sample were performed according to the experimental conditions in Section 2.4.1. Sieving was performed dry, and resulted in significant adherence of fine particles on the larger particles within the designated sieve size range. Therefore, the relationship between sieve size and particle size is complex. The predominant distribution of resolvable n-aliphatic hydrocarbons extracted from each

sample is listed in Table 21, with greatest recovery in the range of n-C_{12} through n-C_{15}. Sample extract TIC chromatograms, representative of each core, are attached in Appendix C.

Sample ID	Resolvable n-Aliphatic Hydrocarbon Distribution	Unresolved Complex Mixture*
3S-8	n-C_{11} through n-C_{14}	---
3S-29	n-C_{11} through n-C_{14}	---
2LT-12	n-C_{11} through n-C_{14}	n-C_{18} through n-C_{23}
2LT-19	n-C_{11} through n-C_{14}	n-C_{18} through n-C_{23}
4LG-3	n-C_{11} through n-C_{21}	---
4LG-18	n-C_{11} through n-C_{21}	---
4LG-25	n-C_{12} through n-C_{21}	---

Table 21. Distribution of extracted n-aliphatic hydrocarbons for each sample. *Hydrocarbons listed had discernible peaks at the top of the UCM, but could only be quantified.

There was no significant difference in the distribution of extracted n-aliphatic hydrocarbons among sieve size fractions within samples of a given core. However, a few distinctions in distribution were noticeable among cores. In addition to the quantifiable recovery of n-C_{11} through n-C_{14} hydrocarbons for all of the 2LT sample extracts, a UCM was observed in the range of n-C_{18} through n-C_{23}. These peaks could not be isolated, and thus were only qualitatively identified based upon retention time and fragmentation pattern. The 4LG sample extracts were characterized by a Gaussian-like distribution of hydrocarbon recovery, with progressive decline in recovery for the lightest ($< C_{14}$) and heaviest (C_{15+}) molecular weight hydrocarbons.

3.3.2 Quantity of Extracted Aliphatic Hydrocarbons

Quantity of total resolvable n-aliphatic hydrocarbons ranged from approximately 0.01 - 0.6 parts per thousand by weight (mg HC/g rock), or 0.3 - 12 (mg HC/g TOC). Results have been normalized to the mass of TOC (Tables 22 - 27 and Figure 23). Results also indicate an order of magnitude increase in recovery from the 3S samples (all sieve size fractions), in comparison to that recovered from the 2LT and 4LG samples. Total recovery by carbon number for each sample and sieve size fraction is attached in Appendix D.
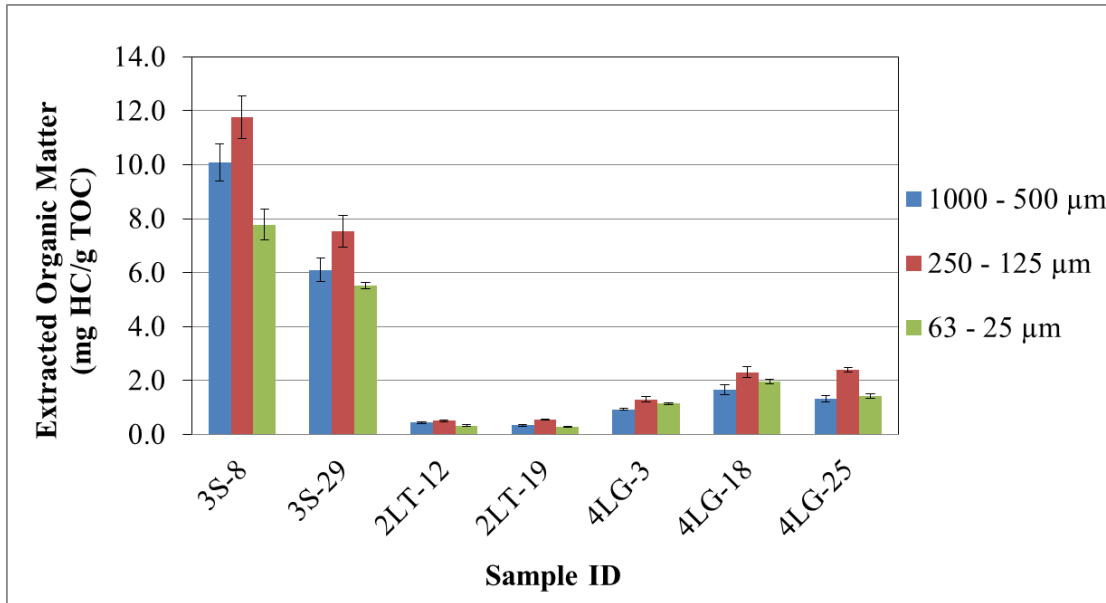
Figure 23. Supercritical CO_2 extractions: Total quantity of resolvable n-aliphatic hydrocarbons extracted from each sample as a function of sieve size. Error bars are $\pm$ 1 σ_m.

Sieve Size Fraction: 1000 - 500 µm			
Sample ID	Quantity Extracted (mg HC/g TOC)	Uncertainty (± mg HC/g TOC)	Relative Uncertainty (%)
3S-8	10.1	0.7	7
3S-29	6.1	0.4	7
2LT-12	0.44	0.03	8
2LT-19	0.33	0.03	8
4LG-3	0.93	0.03	3
4LG-18	1.7	0.2	11
4LG-25	1.3	0.1	8

Sieve Size Fraction: 250 - 125 µm			
Sample ID	Quantity Extracted (mg HC/g Org C)	Uncertainty (± mg HC/g org C)	Relative Uncertainty (%)
3S-8	11.8	0.8	7
3S-29	7.5	0.6	8
2LT-12	0.5	0.04	7
2LT-19	0.5	0.01	3
4LG-3	1.3	0.1	7
4LG-18	2.3	0.2	9
4LG-25	2.4	0.1	3

Sieve Size Fraction: 63 - 25 µm			
Sample ID	Quantity Extracted (mg HC/g Org C)	Uncertainty (± mg HC/g org C)	Relative Uncertainty (%)
3S-8	7.8	0.6	8
3S-29	5.5	0.1	2
2LT-12	0.33	0.03	8
2LT-19	0.28	0.02	8
4LG-3	1.14	0.04	3
4LG-18	1.97	0.08	4
4LG-25	1.42	0.08	6

Tables 22-24. Quantity of resolvable n-aliphatic hydrocarbons extracted from each sieve size fraction. Results are averaged from triplicate extractions. Uncertainties are reported as $\pm$ 1 σ_m.

Precision was evaluated by calculating the relative uncertainty, ratio of the standard error of the mean (σ_m) to the average, expressed as a percent. For most of the extractions, n-C_{11} through n-C_{13} had the highest deviation and contributed the largest source of error to the overall results. Slight fluctuation in the volume of CO_2 dispensed in each extraction (70-90 ml) among replicate extractions may have also contributed a source of variability.

Surrogate standard recovery totals for all extractions (samples and method blanks) averaged 47 ± 3 % for decane-d_{22} ($C_{10}D_{22}$) and 97 ± 2 % for tetracosane-d_{50} ($C_{24}D_{50}$). Uncertainties for surrogate standards are reported as $\pm 1 \sigma_m$. Higher volatility of the lower molecular weight standard ($C_{10}D_{22}$), and of target hydrocarbons of similar molecular weight, may make them more sensitive to loss in post-extraction (solvent evaporation) steps in this extraction method, accounting for lower-than-expected yields.

Comparison of results for each sieve size fraction within a given sample show that recovery of total resolvable n-aliphatic hydrocarbons increased between approximately 15 - 58 % from the 250 - 125 µm sieve size in comparison to that extracted from the 1000 - 500 µm fraction for each sample. However, recovery is maximized for the 250 - 125 µm sieve size fraction, with lower yields for the 63 - 25 µm fraction from all sample extracts (Tables 25 - 27).

Sample ID	1000 - 500 μm (mg HC/g TOC)	250 - 125 μm (mg HC/g TOC)	% Difference
3S-8	10.1	11.8	15
3S-29	6.1	7.5	21
2LT-12	0.44	0.5	14
2LT-19	0.33	0.5	49
4LG-3	0.93	1.3	33
4LG-18	1.7	2.3	33
4LG-25	1.3	2.4	58

Sample ID	250 - 125 μm (mg HC/g TOC)	63 - 25 μm (mg HC/g TOC)	% Difference
3S-8	11.8	7.8	41
3S-29	7.5	5.5	31
2LT-12	0.5	0.33	43
2LT-19	0.5	0.28	65
4LG-3	1.3	1.14	13
4LG-18	2.3	1.97	16
4LG-25	2.4	1.42	51

Sample ID	1000 - 500 μm (mg HC/g TOC)	63 - 25 μm (mg HC/g TOC)	% Difference
3S-8	10.1	7.8	26
3S-29	6.1	5.5	10
2LT-12	0.44	0.33	29
2LT-19	0.33	0.28	18
4LG-3	0.93	1.14	20
4LG-18	1.7	1.97	18
4LG-25	1.3	1.42	7

Table 25-27. Percent difference of n-aliphatic hydrocarbon recovery between the two sieve size fractions in the first two columns is presented in the third column.

3.3.3 Open Column Chromatography Tests

Open column chromatography tests were performed on bulk extracts from the supercritical CO_2 extractions (one sample extract from each of the 2LT from 4LG cores) to see if separation of hydrocarbons into aliphatic, aromatic and polar class fractions prior to GC-MS analysis would improve resolution of extracted n-aliphatic hydrocarbons and separate the UCM present in the 2LT sample extracts. Test results revealed that there was no improvement in resolution (separation) of the UCM. Thus, for the most efficient use of time, open column chromatography was not used as a post-extraction step for any of the extractions reported in this document. All GC-MS analyses were performed on the bulk extracts, and hydrocarbons that were qualitatively identified in the UCM were not included in the quantitative recovery results. However, it is noted that if this extraction method is to be used on different shale, or other source rock, samples, open column chromatography may be a necessary post-extraction step prior to analysis.

Sample ID	Quantity Extracted (mg HC/g TOC)	% Difference
4LG-25 (Bulk Extract)	1.3	7
4LG-25 (Aliphatics Fraction)	1.4	
2LT-12 (Bulk Extract)	0.4	2
2LT-12 (Aliphatics Fraction)	0.4	

Table 28. Percent difference in n-aliphatic hydrocarbon recovery between bulk extract and aliphatic fractions. Each open column chromatography test was performed on one of the bulk extracts from each sample listed (1000 - 500 μm).

3.3.4 Statistical Analysis

To determine if there was a statistically significant difference in hydrocarbon recovery among sieve size fractions of the crushed samples, a single-factor analysis of variance (ANOVA) was performed for the data set.
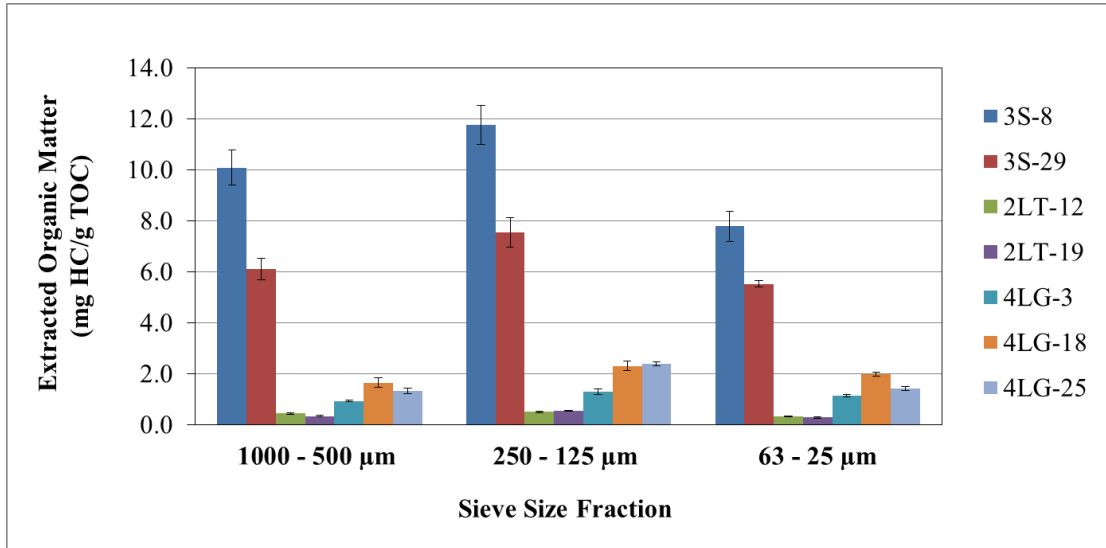
Figure 24. Total resolvable n-aliphatic hydrocarbons extracted as a function of sieve size distribution. Error bars are $\pm 1 \sigma_m$.

ANOVA evaluates two types of variance, *within group variance* (error) and *among group variance* (treatment plus error) to determine if there is a difference in hydrocarbon recovery among the populations from which the samples have been taken. The nomenclature used in this analysis is listed in Table 29 and below.

Treatments (Sieve Size)	1000 - 500 µm	250 - 125 µm	63 - 25 µm
Replicates/Sample in each Treatment	3S-8, 3S-29, 2LT-12, 2LT-19, 4LG-3, 4LG-18, 4LG-25	3S-8, 3S-29, 2LT-12, 2LT-19, 4LG-3, 4LG-18, 4LG-25	3S-8, 3S-29, 2LT-12, 2LT-19, 4LG-3, 4LG-18, 4LG-25
# of Replicates/Treatment	7	7	7

Table 29. Nomenclature for the single-factor ANOVA.

Within group (error) variance is measured from the dispersion of replicates around their respective treatment means, whereas the *among group (treatment) variance* is calculated from the dispersion of each treatment mean from the grain mean. W*ithin group variance* is calculated from the equation

$$Error\ Mean\ square\ (error\ variance) = \sum \frac{(X_i - TM)^2}{DF}, where$$

X_i = Average hydrocarbon recovery (mg HC/g TOC) from each sample,

TM = Treatment Mean, and

DF = Sum of degrees of freedom for each treatment (DF = 18).

Among group variance is calculated from the following equation

$$Mean\ square\ (treatment\ variance) = \sum \frac{(TM - GM)^2 * t}{DF}, where$$

t = Number of replicates for each treatment (t = 7),

DF = Degrees of freedom for the total number of treatments (DF = 2),

TM = Treatment Mean, and

GM = Grand Mean.

$$Grand\ Mean = \frac{\sum X_i}{n}, where$$

X_i = Average hydrocarbon recovery (mg HC/g TOC) from each sample, and

n = Total number of replicates from all treatments (n = 21).

Once both types of variance are calculated, the *F statistic* is calculated as follows

$$F\ statistic = \frac{Among\ group\ variance}{Within\ group\ variance}$$

The calculated *F statistic* is compared to a critical F value, given a 5 % significance level ($\alpha = 0.05$). If the calculated *F statistic* is greater than the critical value for the appropriate degrees of freedom, the treatments are significantly different and are thus unlikely to have come from the same population. Given the appropriate degrees of freedom for each type of variance, the critical *F statistic* ($F_{2,18}$) for the single-factor ANOVA used in this study is: **3.56.** Results revealed that there was no significant difference in n-aliphatic hydrocarbon recovery among the sieve size fractions.

Source of Variation	Sum of Squares	DF	Mean Square (Variance)	$F_{2,18}$ Statistic
Among groups (treatment)	4.7	2	2.3	0.17
Within groups (error)	241.4	18	13.4	
Total	246.1	20		

Table 30. Results summary for the single-factor ANOVA.

3.4 Method Validation

3.4.1 Solvent Extraction Comparison

Extraction efficiency was estimated by comparing total resolvable n-aliphatic hydrocarbon recovery between the supercritical CO_2 extractions and microwave assisted extractions for the 1000 - 500 µm fraction of each sample. Predominantly the same distribution of extracted hydrocarbons was found in both extraction methods. An increase in recovery was observed in the supercritical CO_2 extractions for all samples except 3S-29 and 4LG-25. However, the percent difference in recovery for 3S-29 and 4LG-25 samples was ≤ 7 %). Differences in extraction parameters most likely contribute to differences in recovery.
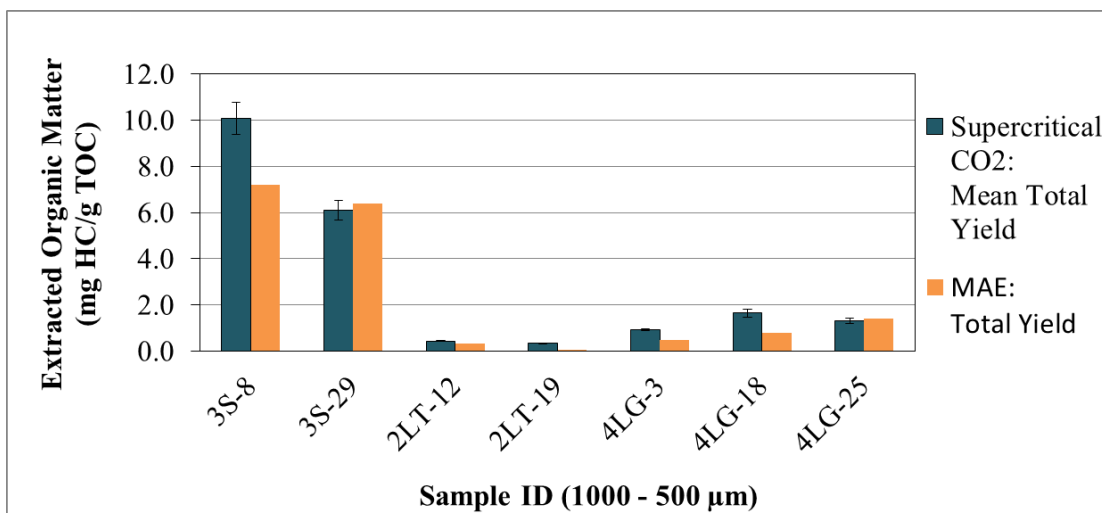
Figure 25. Supercritical CO_2 and microwave-assisted extraction comparison. Recovery of total resolvable n-aliphatic hydrocarbons from the 1000 - 500 μm fraction are reported for each sample. Mean yields from the supercritical CO_2 extractions were calculated from triplicate extractions, with reported uncertainties of ± 1 σ_m. Only one microwave-assisted extraction was performed on each sample.

Total Resolvable n-Aliphatic Hydrocarbons (mg HC/g TOC): 1000 - 500 μm Sieve Size Fraction			
Sample ID	**Supercritical CO_2 Extractions: Mean Total Yield**	**Microwave-Assisted Extractions: Total Yield**	**% Difference**
3S-8	10.1	7.2	33
3S-29	6.1	6.4	4
2LT-12	0.4	0.3	26
2LT-19	0.3	0.1	137
4LG-3	0.9	0.5	65
4LG-18	1.7	0.8	73
4LG-25	1.3	1.4	7

Table 31. Supercritical CO_2 and microwave-assisted extraction comparison. Differences in recovery of total resolvable n-aliphatic hydrocarbons are reported.

3.4.2 Time Study

To examine whether the time parameter used in the supercritical CO_2 extractions (15-minute static step, followed by a 1-hour dynamic step) had an effect on the quantity of hydrocarbons extracted from the samples, a series of extractions were

performed wherein the length of the dynamic step was changed to 30 minutes, 2 hours, and 3 hours. Sample splits from the 4LG-25, 250 - 125 μm fraction were used in each extraction.

Results identified highest recovery from the 1-hour dynamic step, where the average volume of CO_2 dispensed in the triplicate extractions was approximately 86 ml. Lowest recovery was from the 30-minute dynamic step, where only half (43 ml) of CO_2 was dispensed during the extraction.
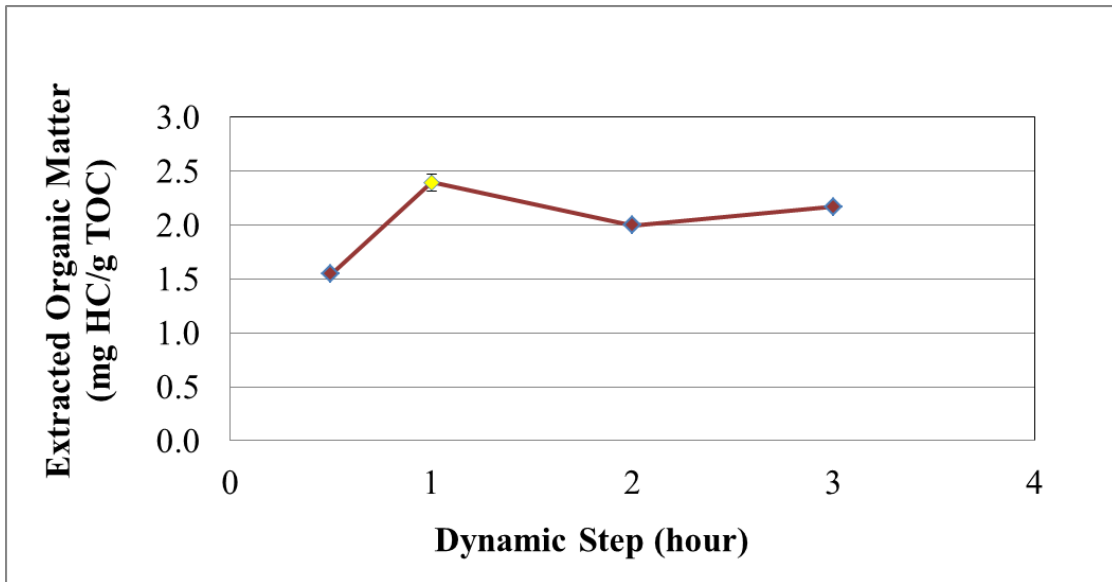
Figure 26. Time study for the supercritical CO_2 extractions. The length of the dynamic (flow through) step of was varied for sample 4LG-25, 250 - 125 μm. The reported value for the 1-hour extraction is an average value from triplicate extractions with an uncertainty of ± 0.1 mg HC/g TOC (± 1 σ_m). Only one extraction was performed for the 30-minute, 2-hour and 3-hour extractions.

Extracted Organic Matter (mg HC/g TOC)		
30 min	**1 hr**	**% Difference**
1.5	2.4	43
1 hr	**2 hr**	**% Difference**
2.4	2.0	18
2 hr	**3 hr**	**% Difference**
2.0	2.2	8
1 hr	**3 hr**	**% Difference**
2.4	2.2	10

Table 32. Percent difference in recovery as a function of time.

69

3.4.3 Re-Crushing & Re-Extraction Tests

To further evaluate if an increase in sample surface would enhance recovery, a test was performed whereby three previously extracted shale samples were crushed further and then re-extracted under the same initial extraction conditions. One sample from each core (the 1000 - 500 µm size fraction of 3S-8, 2LT-12, and 4LG-3) was chosen for this test. A 10 % increase in recovery was observed from the 3S-8 sample. No quantifiable results were achieved for the 2LT-12 and 4LG-3 sample extracts. Low signal peaks were qualitatively identified by the GC-MS for these samples, but concentrations were below the lowest calibration standard (0.25 µg/ml).

3.5 Characterization of Sieve Size Fractions

3.5.1 Surface Area Analysis

Surface area results did not reveal any significant variation or consistent trend among sieve sizes as was anticipated (Table 33 and Figure 27). BET surface area plots for each sample and sieve size are attached in Appendix E.

Specific Surface Area Results				
Sample ID	Sieve Size (µm)	Specific Surface Area (m^2/g)	Uncertainty ($\pm m^2/g$)	Relative Uncertainty (%)
3S-8	1000 - 500	24.2	0.3	1
	250 - 125	23.7	0.3	1
	63 - 25	24.3	0.3	1
2LT-12	1000 - 500	18.1	0.3	2
	250 - 125	19.5	0.3	2
	63 - 25	20.8	0.3	1
4LG-3	1000 - 500	21.4	0.3	1
	250 - 125	21.2	0.3	1
	63 - 25	22.4	0.3	1

Table 33. Specific surface area results. Reported uncertainties are $\pm$ 1 σ_m.
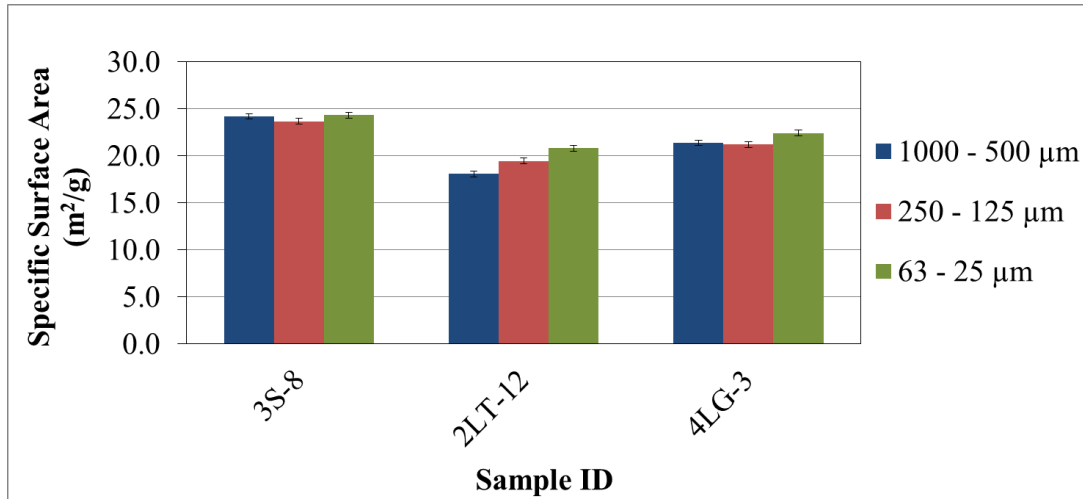
Figure 27. Specific surface area results. Results from each sample are reported as a function of sieve size. Error bars are ± 1 σ_m.

3.5.2 Scanning Electron Microscopy Imaging

A scanning electron microscope was used to image both 1000 - 500 μm and 250 - 125 μm fractions of the 4LG-3 samples in an attempt to get an explanation for why no clear inverse relationship was observed between surface area and sieve size. Secondary Electron (SE) images revealed that individual crushed shale particles were coated in a layer of smaller adhered fine particles.

Figure 28-30. Secondary Electron images of 4LG-3, 1000 - 500 µm sieve size fraction. Magnification from left to right: 40X, 250X, 1000X.
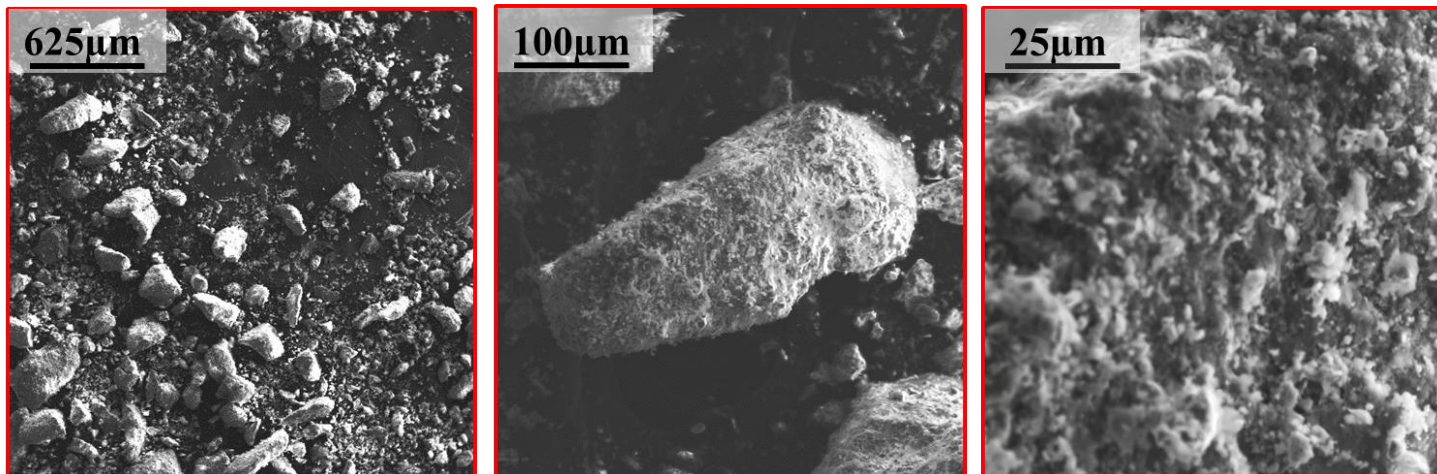
Figure 31-33. Secondary Electron images of 4LG-3, 250 - 125 µm sieve size fraction. Magnification from left to right: 40X, 250X, 1000X.

3.6 Aliphatic Hydrocarbon Recovery Trends

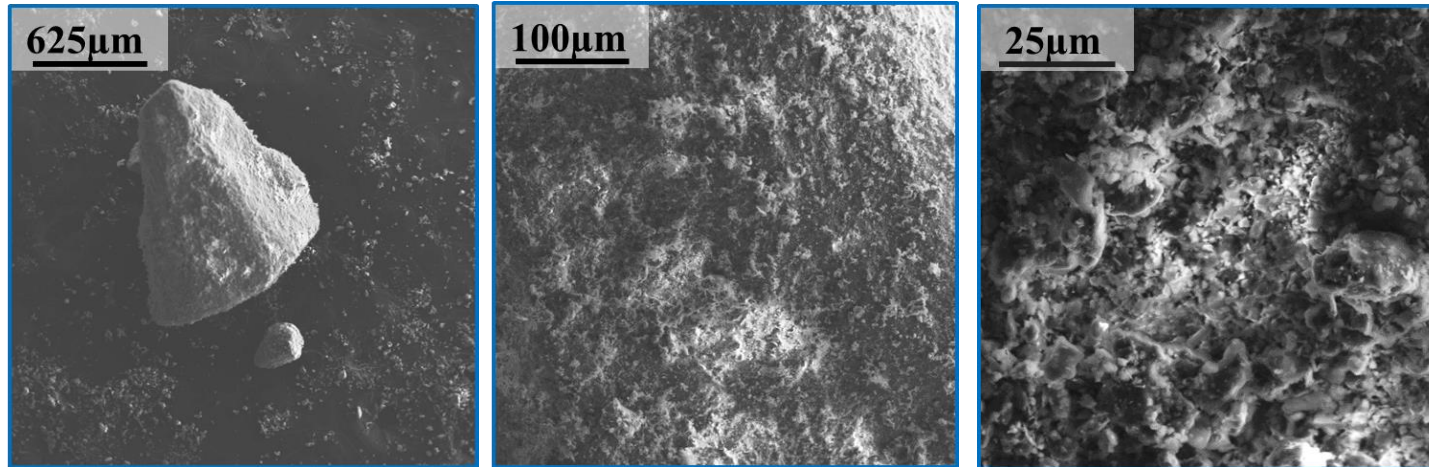The scanning electron microscopy images revealed that the sieve size fractions extracted are merely sieve size ranges and not a true indication of rock matrix grain size distribution. Nevertheless, a few trends were observed among sample extracts that could suggest other controls on hydrocarbon recovery from the supercritical CO_2 extractions.

3.6.1 Hydrocarbon Recovery vs. Surface Area

Despite there being no significant differences in hydrocarbon recovery between sieve size fractions, recovery plotted as a function of surface area suggests that there is an overall trend of increasing recovery with increasing exposed sample surface area.
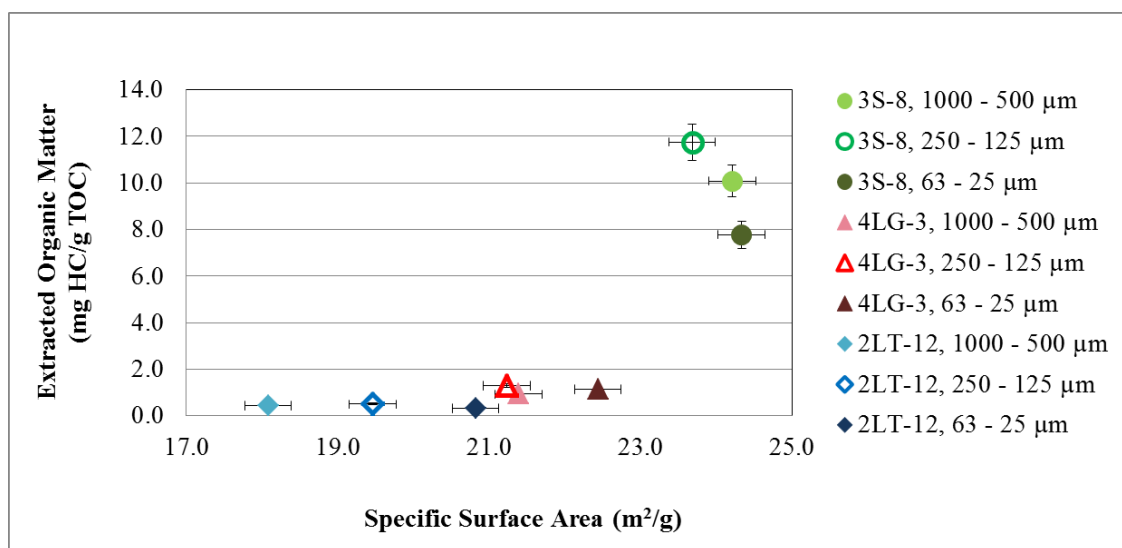
Figure 34. Hydrocarbon recovery as a function of surface area. Results are only reported for the subset of samples analyzed for specific surface area. Vertical and horizontal error bars are $\pm$ 1 σ_m.

3.6.2 Hydrocarbon Recovery vs. Free Hydrocarbon Content

A plot of recovery as a function of S1 (free hydrocarbon content of each sample) does suggest a positive correlation between the two abundances. However, it is noted that this is an imperfect trend controlled mainly by sample 3S-8. Additionally, only one sample (3S-29) does not follow this suggested trend. The only differentiating feature of this sample is its low total clay content (12 %) compared to all other samples (> 30 %).
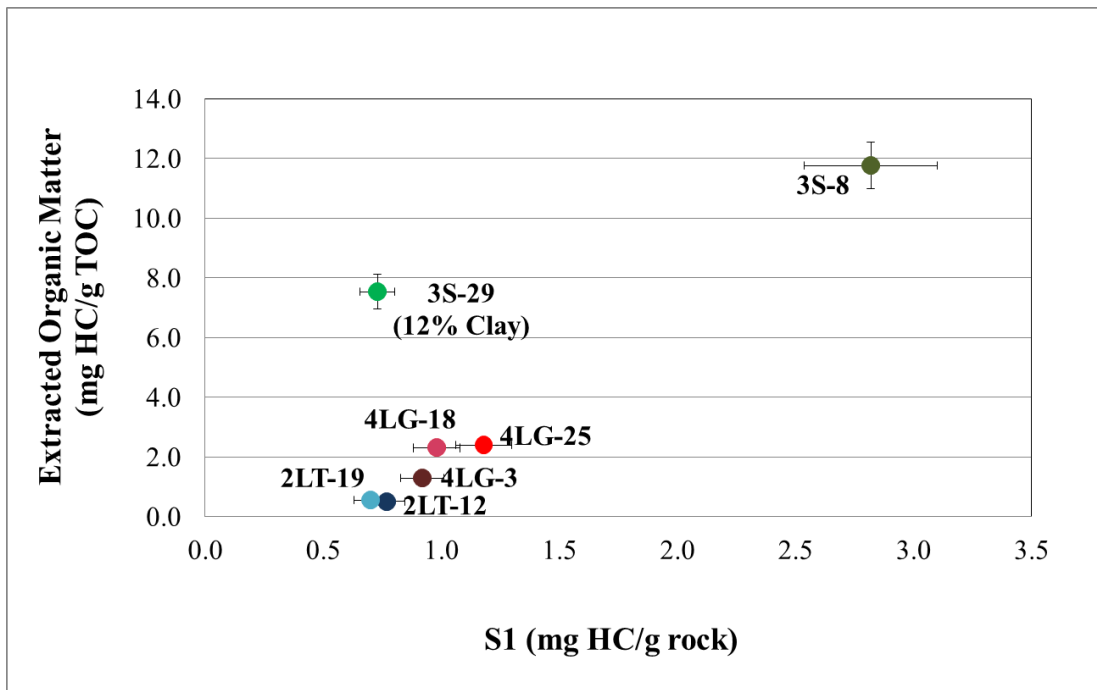
Figure 35. Hydrocarbon recovery as a function of S1abundance. Plotted results are from the 250 - 125 μm sieve size fraction. Vertical error bars are ± 1 σ_m. Horizontal error bars are ± 1 σ.

74

3.6.3 Hydrocarbon Recovery vs. Mineralogy

No major trends were observed among samples when comparing hydrocarbon recovery to mineral abundances (quartz, total clay, illite, total carbonate and pyrite). For the 3S and 2LT samples, recovery does slightly increase with an increasing clay/carbonate abundance ratio, which could suggest a greater association of free hydrocarbons with clay minerals. However, this pattern was not observed with the 4LG samples.
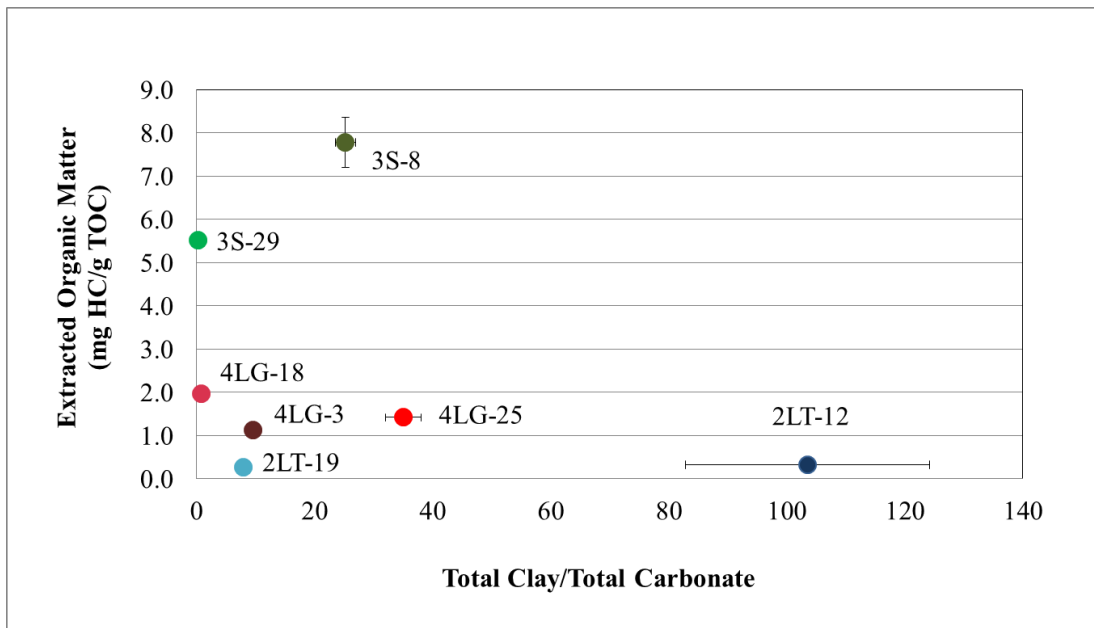
Figure 36. Hydrocarbon recovery as a function of clay/carbonate abundance ratio. Abundance ratios, calculated from the XRD measurements, were performed on the 63 - 25 μm sieve size fraction. Both horizontal and vertical error bars represent ± 1 σ_m.

Chapter 4: Results Interpretation & Discussion

4.1 Distribution of Extracted Aliphatic Hydrocarbons

High-density carbon dioxide extracted n-aliphatic hydrocarbons in the range of predominantly $n-C_{11}$ through $n-C_{21}$ (diesel-range) from the samples of Marcellus Shale, with highest yields between $n-C_{12}$ and $n-C_{15}$. Higher recovery of these lower molecular weight hydrocarbons is also as expected given the high sample maturity. A higher proportion of aliphatic hydrocarbons with carbon number $< C_{19}$ are generated with high maturity samples, relative to heavier C_{19+} hydrocarbons associated with lower maturity samples, due to the increasing degree of thermal degradation, or 'cracking' of organic matter' associated with increasing maturity level (Ryder et al., 2013). The distribution of hydrocarbons found in this study is also comparable to previous supercritical CO_2 extraction studies wherein organic matter was extracted from petroleum source rocks under similar extraction conditions (Monin et al., 1987; Greibrokk et al., 1992; Li et al., 1997).

There was no statistically significant difference in distribution of extracted n-aliphatic hydrocarbons (including both resolvable hydrocarbons and the unresolvable UCM) between sieve size fractions for a given sample, or between samples within a given core.

A difference in the distribution of hydrocarbons extracted was observed among cores. The expected Gaussian distribution of resolvable n-aliphatic hydrocarbons (~ $n-C_{11}$ through $n-C_{21}$) was detected in all 4LG sample extracts. The 2LT samples had a tighter distribution range of resolvable n-aliphatic hydrocarbons ($n-C_{11}$ through $n-C_{14}$), yet a broad UCM peak of co-eluting petroleum compounds was present in all of

the sample extracts with qualitative identification of n-aliphatic peaks from approximately n-C_{18} through n-C_{23}. The source and chemical composition of the UCM is unknown, but may have resulted from petroleum compounds resistant to chemical and biological degradation, or from different sources of petroleum contamination (Frysinger et al., 2003).

Only n-C_{11} through n-C_{14} peaks were identified in the 3S sample extracts. All 2LT and 4LG sample extracts had a more complex hydrocarbon extract (visible branched aliphatic hydrocarbons). Given that there were no major differences in sample depth, mineralogy, or organic matter content (in terms of quantity, quality, and thermal maturity), this could indicate a different petroleum source or contaminant (i.e. drilling fluids or the presence of nonindigenous hydrocarbons), or a difference in pore structure.

4.2 Quantity of Extracted Aliphatic Hydrocarbons

4.2.1 Overall Yield

The total yield of extracted n-aliphatic hydrocarbons ranged from approximately 0.3 - 12 mg HC/g TOC, with lowest recovery from the 2LT samples and highest recovery from the 3S samples. Although recovery for the supercritical CO_2 extractions was lower than that predicted by the oil saturation index (S1/TOC ratios in Table 15), pyrolysis (thermal extraction) and supercritical fluid extractions are different types of extractions that can yield different quantities and distributions of hydrocarbons (Jarvie & Baker, 1984). Additionally, only the resolvable n-aliphatic hydrocarbons, a fraction of the bulk extract, were quantified in the supercritical CO_2

extractions. However, results from the supercritical CO_2 extractions were comparable to those from the microwave-assisted extractions. Results from the time study also suggest that recovery was optimized at the time parameters chosen for the supercritical CO_2 extractions.

4.2.2 Evaluation of Recovery between Sieve Size Fractions

Statistical analyses indicated that there was no significant increase in hydrocarbon recovery with a decrease in sieve size between the 1000 - 500 μm, 250 - 125 μm, and 63 - 25 μm size fractions extracted in this study. BET surface area results confirmed that there was no significant increase in surface area with decrease in sieve size fraction. The scanning electron microscopy images revealed the presence of adhered fines coating the individual shale particles, and that sieve sizes were not an accurate indication of crushed rock matrix grain size distribution. This could ultimately be the main reason why no significant variation in recovery was found between the extracted sieve size fractions.

Although no significant differences in recovery were found, a similar pattern was observed with highest recovery from the intermediate (250 - 125 μm) sieve size fraction, followed by a drop in expected extraction yields from the 63 - 25 μm sieve size fraction from all sample extracts, an observation that warrants further investigation. The decrease in expected recovery from the smallest size fraction could be influenced by many factors including loss of volatile compounds upon crushing the shale samples, and channeling effects that can occur in supercritical fluid extractions. If sample matrix particle sizes are too small, solvent can flow through

78

channels created among sample particles instead of interacting with extractable compounds, reducing extraction rates and overall recovery. Optimum sample particle sizes (sieve sizes) for supercritical fluid extractions are suggested to be within the range of 2.00 mm to 250 µm (Reverchon & De Marco, 2006; Martìnez, 2008). Lower extraction efficiencies sometimes encountered with sieve sizes below this range has also been associated with particle aggregation (Kolak and Burruss, 2003), with and higher capillary entry pressures, which can require more force to extract hydrocarbons from porous media (Al-Marouqi et al., 2009).

Additionally, although the 63 - 25 µm fraction is not an accurate indication of true crushed rock matrix grain size distribution, crushed particles within (and below) this size range are within the range of actual shale grain sizes. The Marcellus and other Devonian shales are predominantly mesoporous, with pore and pore throat sizes on the order of 10^{-1} to 10^{-3} µm in diameter (Nelson, 2009; Chalmers et al., 2012). Although, the molecular size of CO_2, 2.8 Å (2.8 x 10^{-4} µm), enables it to access micropores of coal and shale matrices (Walker et al., 1988), petroleum hydrocarbons have molecular diameters of approximately the same order of magnitude, 10^{-2} to 10^{-4} µm, as characteristic shale pore and pore throat sizes (Nelson, 2009). Thus, a threshold of hydrocarbon extraction may have been reached accounting for the lower recoveries from the 63 - 25 µm sieve size fraction in all sample extracts.

4.2.3 Evaluation of Recovery among Samples

No major differences in hydrocarbon recovery were observed among samples with regard to the type and thermal maturity of the organic matter, mineralogy, depth or lithology, which could explain any variation in hydrocarbon recovery among the three

79

cores. Nevertheless, a few trends were observed that warrant further investigation. First, a slight increase in hydrocarbon yield was noticed with an increase in the clay/carbonate ratio for the 3S and 2LT samples, which could suggest a greater association of free hydrocarbons with clay minerals. However, since this trend was not observed for the 4LG samples, there could be other prevailing controls on hydrocarbon recovery. Additionally, overall hydrocarbon recovery increased as a function of S1 abundance and surface area (regardless of sieve size). An increase in exposed sample surface area may provide greater access of supercritical CO_2 to the extractable free hydrocarbons within the shale matrix. Extractions from a larger sample set would be needed to further evaluate these suggested trends and controls on hydrocarbon recovery within the Marcellus Shale.

Chapter 5: Conclusions

5.1 Summary

Results show that supercritical CO_2 has the potential to liberate diesel-range n-aliphatic hydrocarbons, in the range of n-C_{11} through n-C_{21}, from high-maturity shale at estimated *in situ* reservoir pressure and temperature condition. A higher proportion of aliphatic hydrocarbons with carbon number $< C_{19}$ are generated in high maturity samples, relative to heavier C_{19+} hydrocarbons associated with lower maturity samples, due to an increasing degree of thermal degradation of organic matter linked to increasing maturity level (Ryder et al., 2013).

Overall recovery of extracted hydrocarbons ranged between 0.3 - 12 mg HC/g TOC. No significant differences in recovery were found between sieve sizes. However, the scanning electron microscopy images revealed that crushed rock particle size (or sieve size) was not an accurate indication of rock matrix grain size distribution for the size ranges analyzed.

Although no significant variation was found between sieve size fractions, overall trends in hydrocarbon recovery were observed among all samples that warrant further investigation. First, recovery reached a maximum threshold with the intermediate 250 - 125 µm size fraction. Second, recovery increased as a function of S1 (free hydrocarbon content) and specific surface area, regardless of sieve size.

Potential avenues for future work could involve expanding the sample set to improve resolution and further evaluate the observed trends. Characterizing the actual mineral grain sizes of the shale itself could be performed to see if the matrix is different from sample to sample. Additionally, characterization of the matrix pore structure may also reveal hydrocarbon distributions within both organic and inorganic pore spaces, which could present additional controls on hydrocarbon recovery and explain the observed variations in recovery among cores. Modification of sample preparation prior to extractions could also be attempted, to see if extraction efficiency improves with the removal of adhered particle fines. However, washing could still lead to loss of soluble hydrocarbons and introduce new sources of unanticipated error.

New avenues for the extractions themselves could involve the use of water as a co-solvent modifier. Although these extractions are not an exact simulation of *in situ* hydrocarbon extraction techniques, this could help evaluate the impact of formation water (or brine) on hydrocarbon mobilization. Finally, a series of supercritical CO_2 extractions could also be done across the wet/dry gas boundary in the Marcellus to evaluate the gradation in recovery from lower maturity samples. Test extractions were attempted on a lower maturity sample from the Woodford Shale Formation (extract TIC in Appendix F). However, the only detectable hydrocarbons were present as a UCM (approximately n-C_{11} through n-C_{24}) that could not be resolved by open column chromatography separation methods. These extractions may produce more tangible results if higher-resolution separation and analytical tools are available (i.e. GC x GC-MS) (Frysinger, 2013).

5.3 Scientific Importance & Application

Knowledge that supercritical CO_2 can liberate diesel-range hydrocarbons from high-maturity shale has potential applications in exploration, extraction, and sequestration initiatives. It is acknowledged that different mechanisms of extraction may be involved *in situ* due to the presence of brine, variability in subsurface pressures and temperatures, and longer injection/drilling time periods, which may all affect CO_2's solvent strength and extraction capabilities. However, results will hopefully contribute to a better understanding of the interactions of high-density CO_2 within fractured shale matrices and controls on hydrocarbon mobilization throughout surfaces and pores of exposed fractures and particle fines. If CO_2 is ever to be used as an extraction fluid in EGR and EOR initiatives within the Marcellus or other unconventional source rocks, these interactions need to be more fully understood.

Appendix A: Target & Standard n-Aliphatic Hydrocarbons

Hydrocarbon, C_nH_{2n+2}	Boiling Point (°C) @ 1 bar	Physical State @ 25°C, 1 bar	GC RT (min)	MS Target Ion	MS Qualifier Ions*	Molecular Mass/Ion (M⁺)
Nonane, C_9H_{20}	150.8	Liquid	5.3	57	43, 71, 85	128.26
Decane, $C_{10}H_{22}$	174.1	Liquid	6.9	57	43, 71, 85	142.28
Undecane, $C_{11}H_{24}$	195.9	Liquid	8.5	57	43, 71, 85	156.31
Dodecane, $C_{12}H_{26}$	216.3	Liquid	10.0	57	43, 71, 85	170.33
Tridecane, $C_{13}H_{28}$	235.4	Liquid	11.5	57	43, 71, 85	184.36
Tetradecane, $C_{14}H_{30}$	253.5	Liquid	12.8	57	43, 71, 85	198.39
Pentadecane, $C_{15}H_{32}$	270.6	Liquid	14.1	57	43, 71, 85	212.41
Hexadecane, $C_{16}H_{34}$	286.8	Liquid	15.3	57	43, 71, 85	226.44
Heptadecane, $C_{17}H_{36}$	302.2	Solid	16.4	57	43, 71, 85	240.47
Octadecane, $C_{18}H_{38}$	316.7	Solid	17.5	57	43, 71, 85	254.49
Nonadecane, $C_{19}H_{40}$	330.6	Solid	18.5	57	43, 71, 85	268.52
Eicosane, $C_{20}H_{42}$	343.8	Solid	19.5	57	43, 71, 85	282.55
Heneicosane, $C_{21}H_{44}$	356.6	Solid	20.4	57	43, 71, 85	296.57
Docosane, $C_{22}H_{46}$	368.7	Solid	21.3	57	43, 71, 85	310.60
Tricosane, $C_{23}H_{48}$	380.1	Solid	22.1	57	43, 71, 85	324.63
Tetracosane, $C_{24}H_{50}$	391.4	Solid	23.0	57	43, 71, 85	338.65
Pentacosane, $C_{25}H_{52}$	402.0	Solid	23.8	57	43, 71, 85	352.68
Hexacosane, $C_{26}H_{54}$	412.2	Solid	24.6	57	43, 71, 85	366.71
Heptacosane, $C_{27}H_{56}$	422	Solid	25.3	57	43, 71, 85	380.73
Octacosane, $C_{28}H_{58}$	431.7	Solid	26.0	57	43, 71, 85	394.76
Nonacosane, $C_{29}H_{60}$	440.9	Solid	26.7	57	43, 71, 85	408.79
Triacontane, $C_{30}H_{62}$	449.7	Solid	27.3	57	43, 71, 85	422.81
Hentriacontane, $C_{31}H_{64}$	458	Solid	28.0	57	43, 71, 85	436.84
Dotriacontane, $C_{32}H_{66}$	467.1	Solid	28.6	57	43, 71, 85	450.87
Tritriacontane, $C_{33}H_{68}$	474	Solid	29.4	57	43, 71, 85	464.89
Tetratriacontane, $C_{34}H_{70}$	285.1 @ 0.003bar	Solid	30.2	57	43, 71, 85	478.92
Pentatriacontane, $C_{35}H_{72}$	490.1	Solid	31.1	57	43, 71, 85	492.95
Hexatriacontane, $C_{36}H_{74}$	265 @ 0.001bar	Solid	32.2	57	71, 85, 99	506.97
Heptatriacontane, $C_{37}H_{76}$	504.1	Solid	33.5	57	43, 71, 85	521.00
Octatriacontane, $C_{38}H_{78}$	510.9	Solid	35.0	57	43, 71, 85	535.03
Nonatriacontane, $C_{39}H_{80}$	517.5	Solid	36.9	57	44, 71, 85	549.05
Tetracontane, $C_{40}H_{82}$	525	Solid	39.0	57	44, 71, 85	563.08

Table 34. Target and standard n-aliphatic hydrocarbons. Boiling point, physical state and m/z ion data compiled from *NIST Chemistry WebBook* and *Ullmann's Encyclopedia of Industrial Chemistry* (Griesbaum et al., 2013). *Each fragment corresponds to the following formula: C_nH_{2n+1}, starting with C_3H_7 (m/z = 43). Fragment ions are separated by 14 m/z units, corresponding to a loss/gain of $-CH_2-$.

Hydrocarbon, C_nD_{2n+2}	Boiling Point (°C) @ 1 bar	Physical State @ 25°C, 1 bar	GC RT (min)	MS Target Ion	MS Qualifier Ions	Molecular Mass/Ion (M⁺)*	Target HC Range
Dodecane-d$_{26}$, C$_{12}$D$_{26}$	215-217	Liquid	9.8	66	50, 82, 196	195.97 (M+26)	C$_9$-C$_{15}$
Hexadecane-d$_{34}$, C$_{16}$D$_{34}$	287	Liquid	15.0	66	50, 82, 260	259.97 (M+34)	C$_{16}$-C$_{18}$
Nonadecane-d$_{40}$, C$_{19}$D$_{40}$	330	Solid	18.2	66	50, 82, 98	307.97 (M+40)	C$_{19}$-C$_{29}$
Triacontane-d$_{62}$, C$_{30}$D$_{62}$	258-259 @ 0.004 bar	Solid	27.0	66	50, 82, 98	483.95 (M+62)	C$_{30}$-C$_{40}$

Table 35. Internal standards. Physical state and m/z ion data compiled from Sigma-Aldrich®. *(M + #) corresponds to the mass shift of the molecular ion in an MS scan due to the deuterated hydrogen atoms.

Hydrocarbon, C_nD_{2n+2}	Boiling Point (°C) @ 1 bar	Physical State @ 25°C, 1 bar	GC RT (min)	MS Target Ion	MS Qualifying Ions	Molecular Mass/Ion (M⁺)*
Decane-d$_{22}$, C$_{10}$D$_{22}$	174	Liquid	6.7	66	50, 82, 98	164.20 (M + 22)
Tetracosane-d$_{50}$, C$_{24}$D$_{50}$	391	Solid	22.7	66	50, 82, 98	388.96 (M + 50)

Table 36. Surrogate standards. Physical state and m/z ion data compiled from Sigma-Aldrich®. *(M + #) corresponds to the mass shift of the molecular ion in an MS scan due to the deuterated hydrogen atoms.

Appendix B: LOI Values

Sample ID	LOI (%)
3S-8	4.47
3S-29	6.46
2LT-12	2.84
2LT-19	3.49
4LG-3	3.27
4LG-18	1.34
4LG-25	5.95

Table 37. XRD LOI values. LOI is a measure of total organic carbon content is expressed as a percentage of weight lost from the low temperature ashing (LTA) process prior to XRD analysis. LOI values do not include water from clay minerals, as samples are dried prior to LTA.

Appendix C: Sample Extract TIC Chromatograms
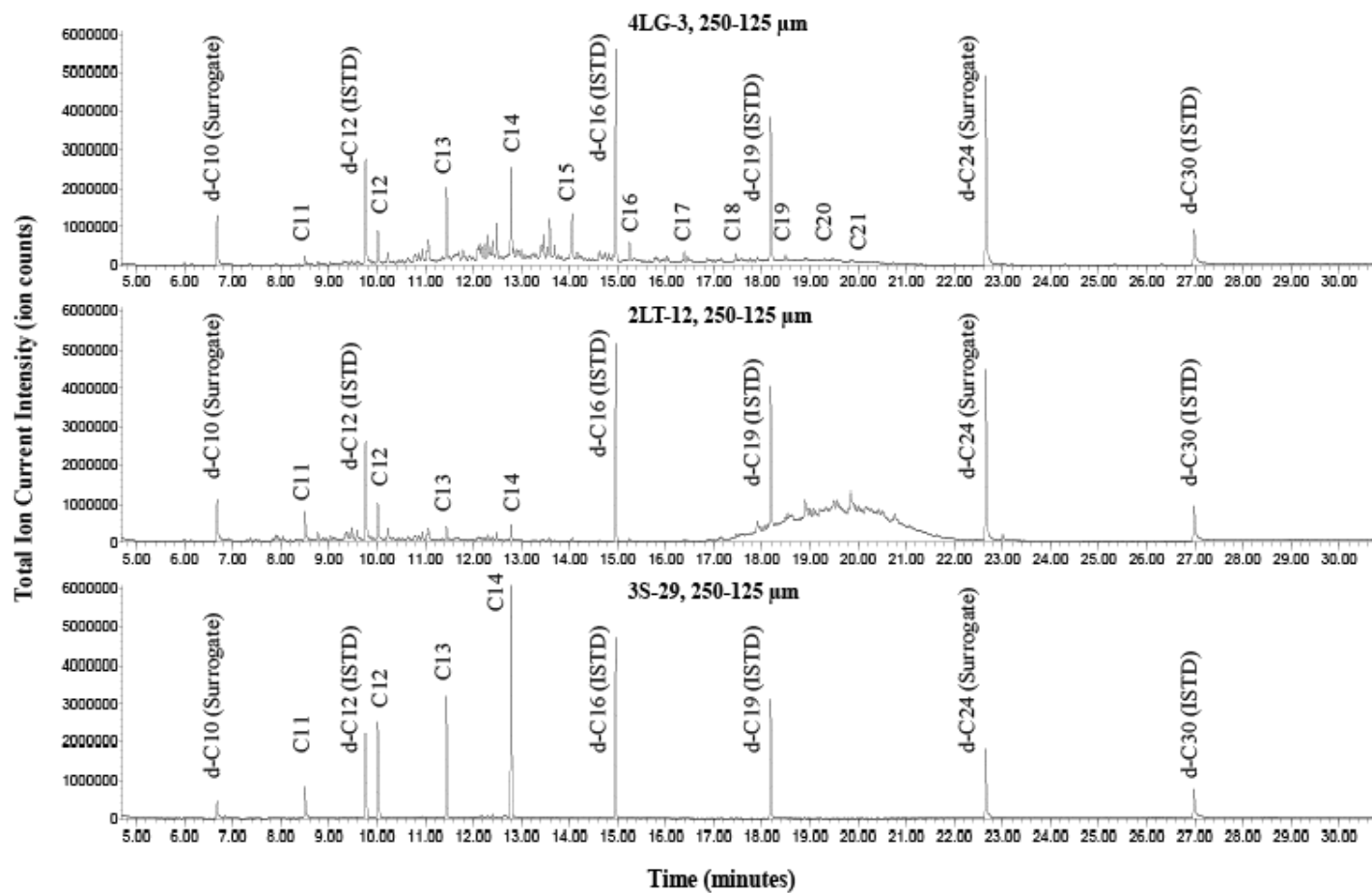
Figure 37. Sample extract TIC chromatograms. Extract chromatograms are shown for 4LG-3, 2LT-12, and 3S-8 (250 - 125 µm).

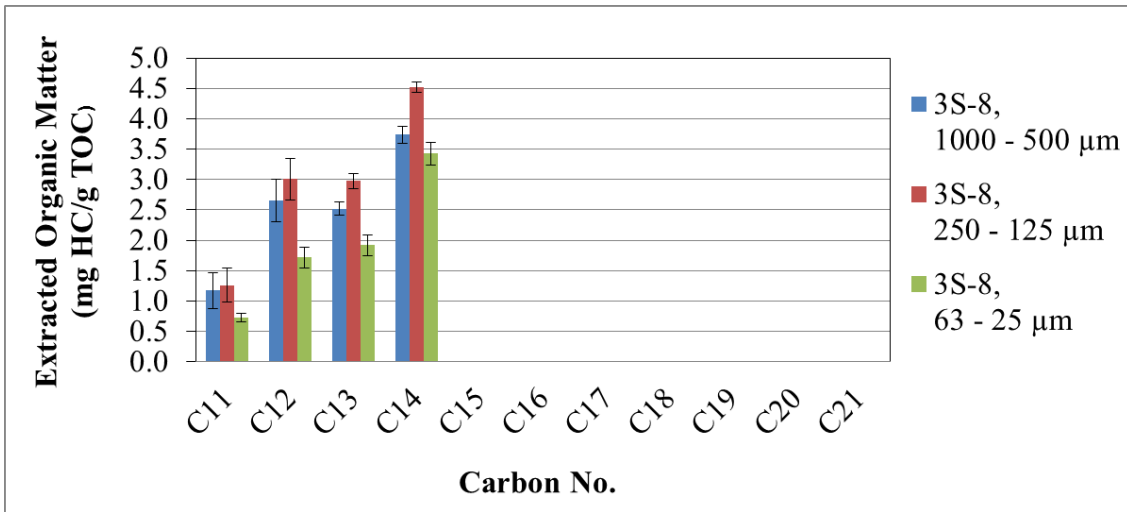# Appendix D: Extracted Hydrocarbon Distribution Plots

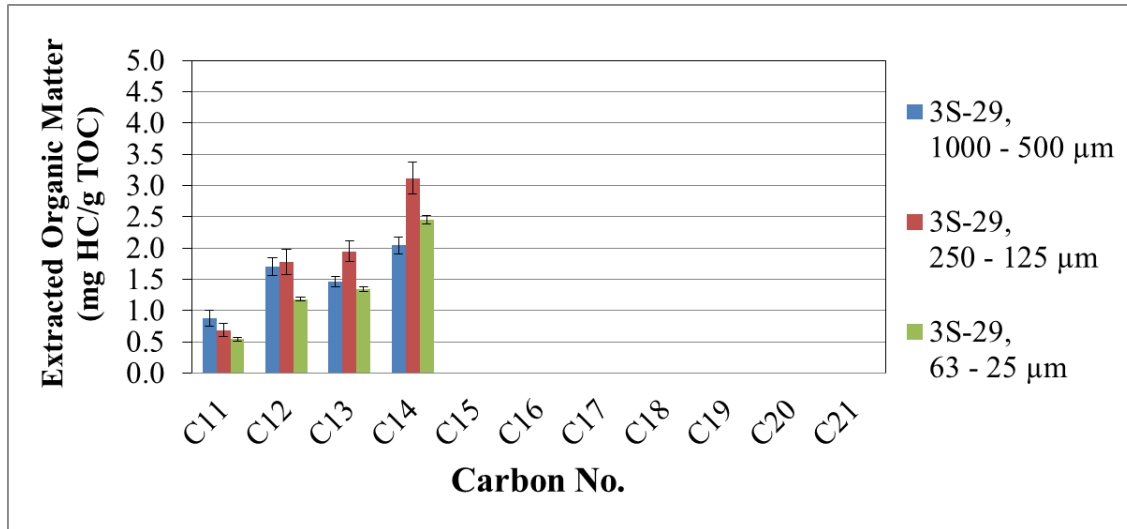**Figure 38.** Hydrocarbon distribution for 3S-8 extracts.
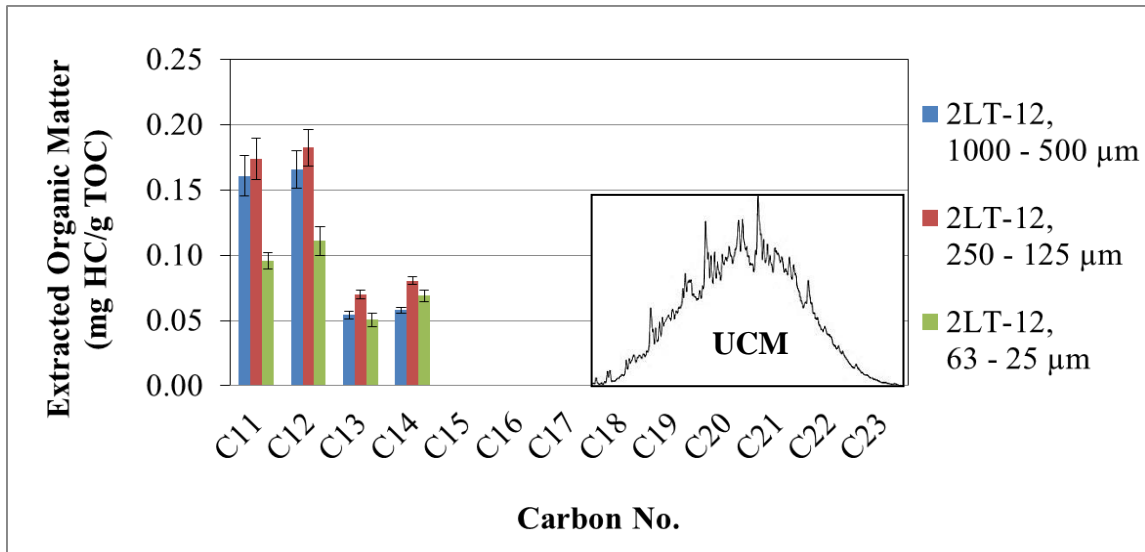

Figure 39. Hydrocarbon distribution for 3S-29 extracts.

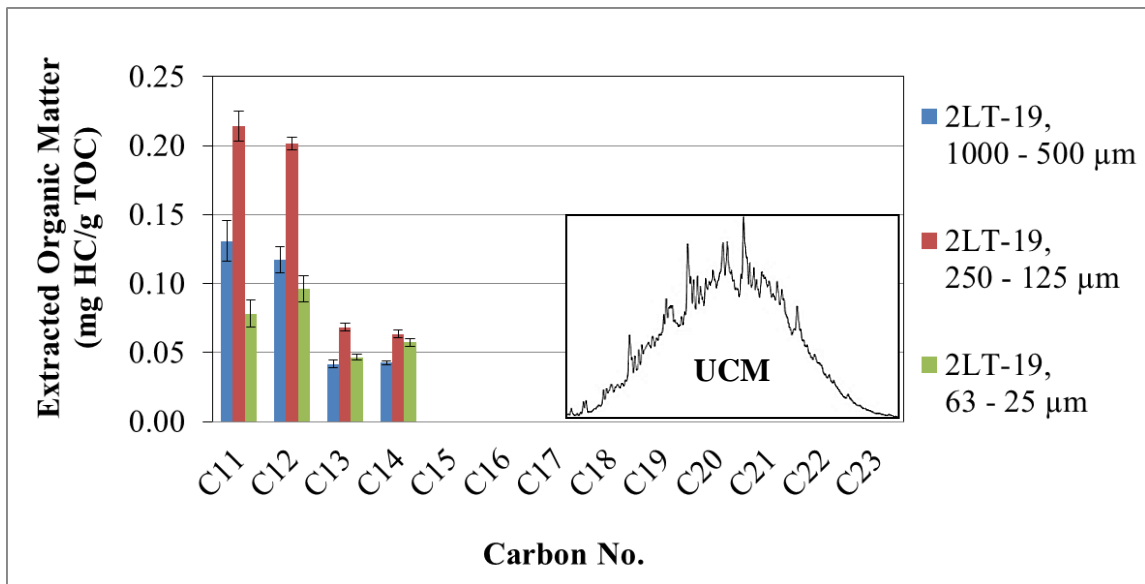**Figure 40.** Hydrocarbon distribution for 2LT-12 extracts.
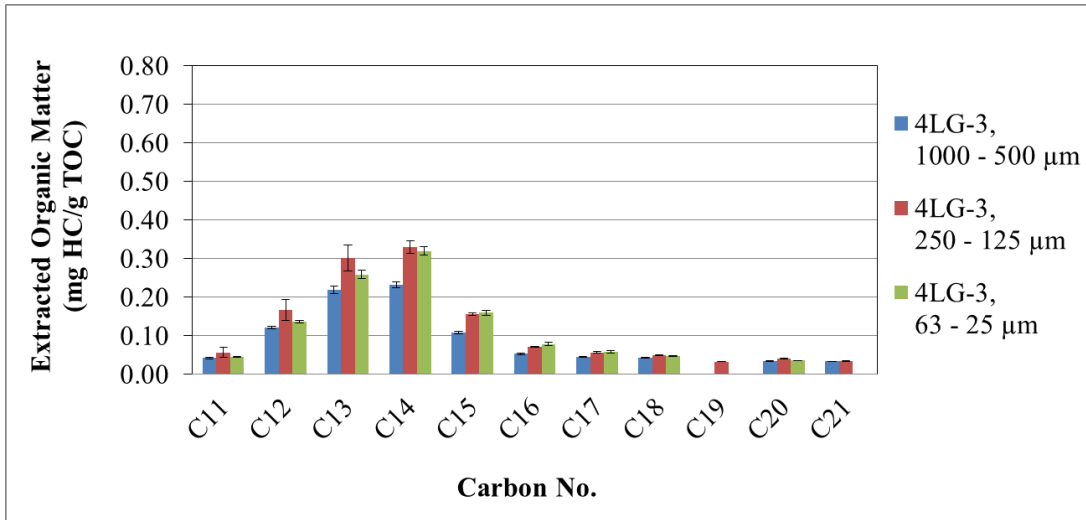

Figure 41. Hydrocarbon distribution for 2LT-19 extracts.

89

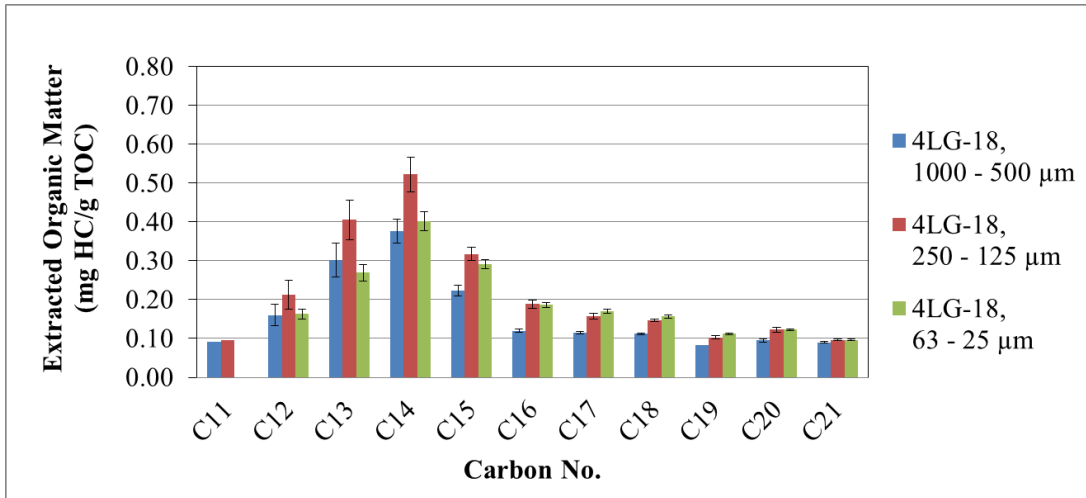**Figure 42.** Hydrocarbon distribution for 4LG-3 extracts.

Figure 43. Hydrocarbon distribution for 4LG-18 extracts.
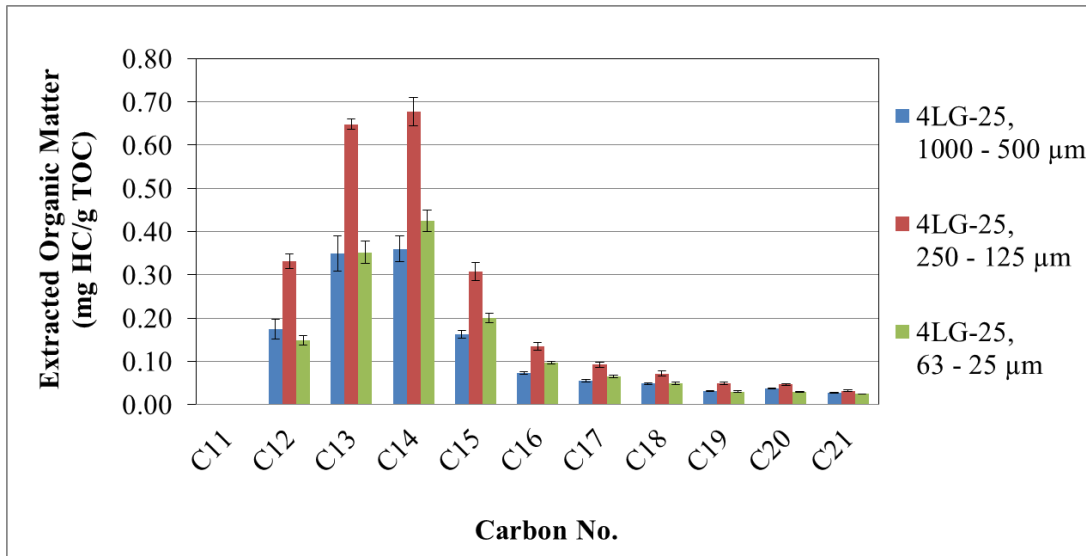

Figure 44. Hydrocarbon distribution for 4LG-25 extracts.

90

Appendix E: BET Surface Area Plots
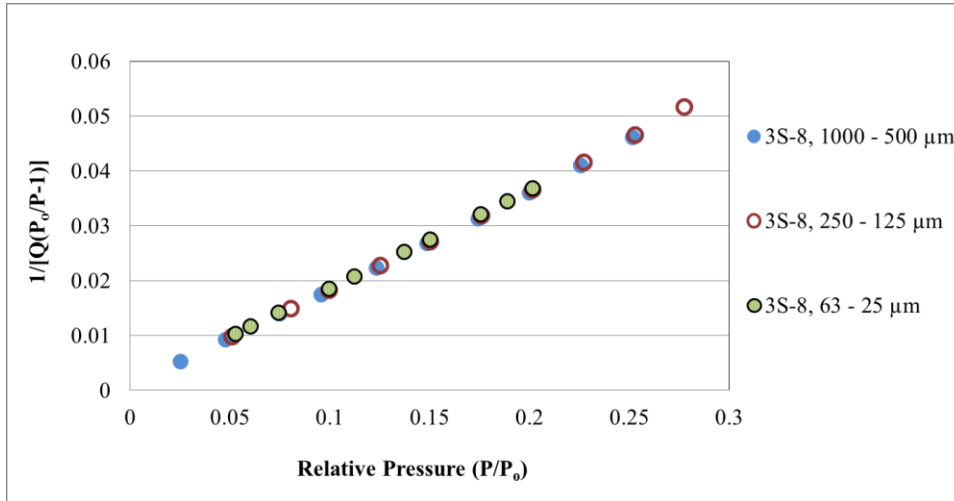
Figure 45. BET surface area plot for sample 3S-8.
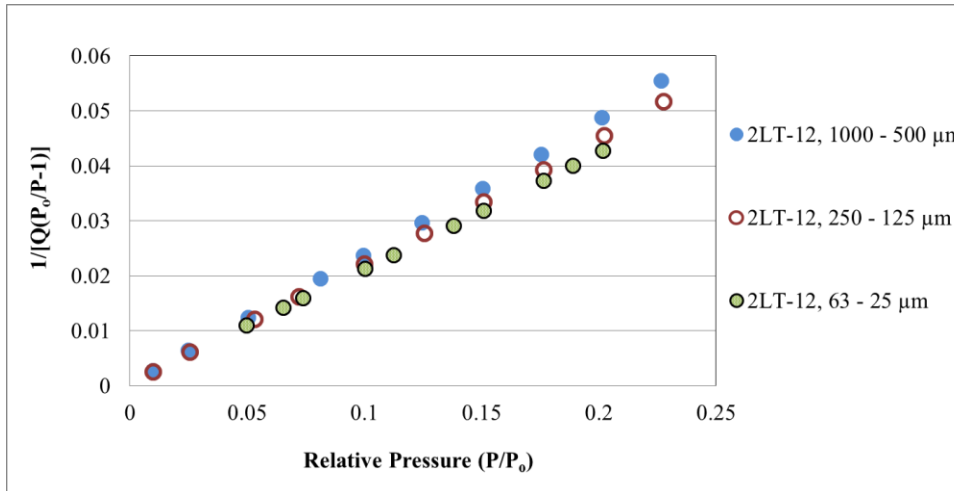

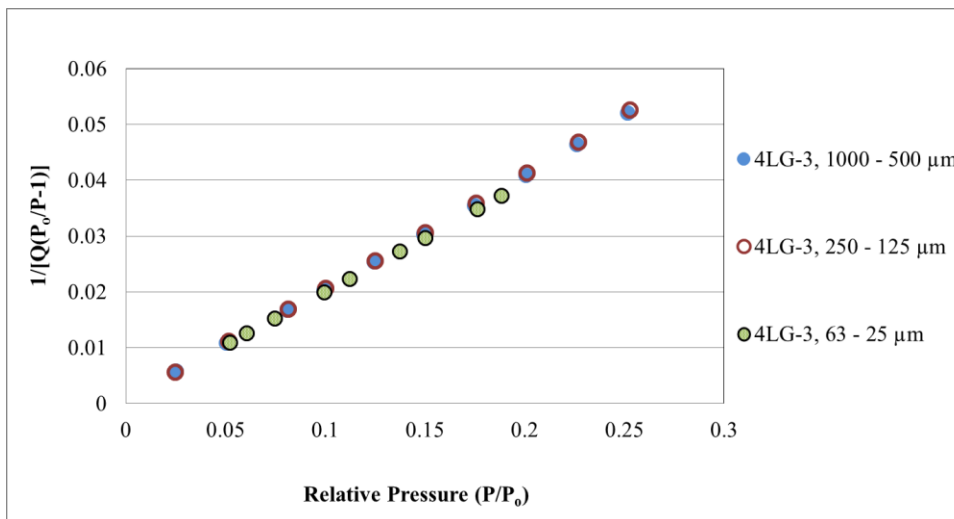**Figure 46.** BET surface area plot for sample 2LT-12.

Figure 47. BET surface area plot for sample 4LG-3.

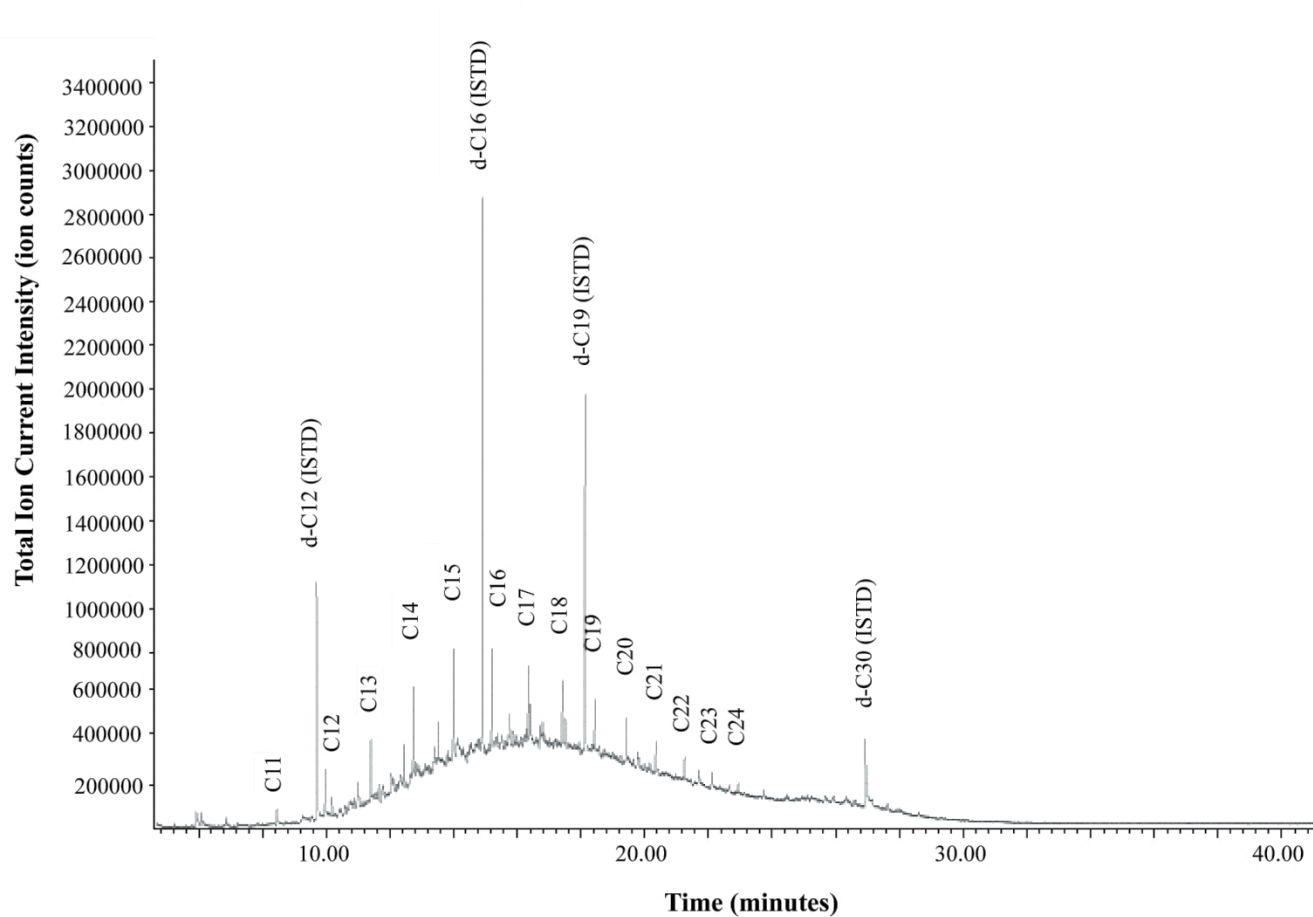91

Appendix F: Woodford Shale TIC Chromatogram

Figure 48. TIC chromatogram of the WoodFord Shale sample extract (aliphatics fraction). Internal standard (ISTD) peaks are labeled, along with qualitatively identified n-aliphatic hydrocarbon peaks at the top of the UCM.

Bibliography

Abdallah, W., Buckley, J., Carnegie, A., Edwards, J., Herold, B., Fordham, E., Graue, A., Habashy, T., Seleznev, N., Signer, C., Hussain, H., Montaron, B., and Ziauddin, M. Fundamentals of Wettability. *Schlumberger Oilfield Review* (2007) 44-61.

Akbarzadeh, K., Hammami, A., Kharrat, A., Zhang, D., Allenson, S., Creek, J., Kabir, S., Jamaluddin, A., Marshall, A., Rodgers, R., Mullins, O., and Solbakken, T. Asphaltenes-Problematic but Rich in Potential. *Schlumberger Oilfield Review* (2007) 22-43.

Allawzi, M., Al-Otoom, A., Allaboun, H., Ajlouni, A., and Al Nseirat, F. CO_2 supercritical fluid extraction of Jordanian oil shale utilizing different co-solvents. *Fuel Processing Technology* (2011) 92, 2016-2023.

American Society for Testing and Materials (ASTM). D2797 Standard Practice for Preparing Coal Samples for Microcopical Analysis by Reflected Light, *in* Annual Book of ASTM Standards: Petroleum products, lubricants, and fossil fuels; gaseous fuels; coal and coke (2011) 5, 5.06, 454-458. ASTM International, West Conshohocken, PA.

American Society for Testing and Materials (ASTM). D7708-11 Standard Test Method for Microscopical Determination of the Reflectance of Vitrinite Dispersed in Sedimentary Rocks, *in* Annual Book of ASTM Standards: Petroleum products, lubricants, and fossil fuels; gaseous fuels; coal and coke (2011) 5, 5.06, 823-830. ASTM International, West Conshohocken, PA.

Asep, E., Jinap, S., Tan, T., Russly, A., Harcharan, S., and Nazimah, S. The effects of particle size, fermentation and roasting of cocoa nibs on supercritical fluid extraction of cocoa butter. Journal of Food Engineering (2008) 85, 450-458.

Bachu, S. Screening and ranking of sedimentary basins for sequestration of CO_2 in geological media in response to climate change. *Environmental Geology* (2003) 44, 277-289.

Biscaye, P.E. Distinction between kaolinite and chlorite in recent sediments by X-ray diffraction. *American Mineralogist* (1964) 49, 1291-1289.

Boyer, C., Clark, B., Jochen, V., Lewis, R., and Miller, C. Shale Gas: A Global Resource. *Schlumberger Oilfield Review* (2011) 23, 3, 28-39.

Brogle, H. CO_2 in solvent extraction. *Chemistry and Industry* (1982) 385-390.

Bruner, K. and Smosna, R. A Comparative Study of the Mississippian Barnett Shale, Fort Worth Basin, and Devonian Marcellus Shale, Appalachian Basin. *U.S. DOE, Office of*

Fossil Energy and National Energy Technology Laboratory (2011) DOE/NETL-2011/1478.

Burke, L. Carbon Dioxide Fluid-Flow Modeling and Injectivity Calculations. *U.S. Geological Survey* (2011) Scientific Investigations Report 2011-5083.

Chalmers, G., Bustin, R., and Power, I. Characterization of gas shale pore systems by porosimity, surface area, and field electron microscopy/transmission electron microscopy image analyses: Examples from the Barnett, Woodford, Haynesville, Marcellus and Doig units. *AAPG Bulletin* (2012) 96, 6, 1099-1119.

East, J., Swezey, C., Repetski, J., and Hayba, D. Thermal Maturity Map of Devonian Shale in the Illinois, Michigan, and Appalachian Basins of North America. *USGS* (2012) Scientific Investigations Map 3214.

Engelder, T., and Lash, G. Marcellus Shale Play's Vast Resource Potential Creating Stir in Appalachia. *The American Oil & Gas Reporter* (2008).

Engelder, T., and Lash, G. Thickness trends and sequence stratigraphy of the Middle Devonian Marcellus Formation, Appalachian Basin: Implications for Acadian foreland basin evolution. *AAPG Bulletin* (2011) 95, 1, 61-103.

Espinoza, D., and Santamarina, J. Clay interaction with liquid and supercritical CO2: The relavance of electrical and capillary forces. *International Journal of Greenhouse Gas Control* (2012) 10, 351-362.

Espitalié, J., Madec, M., Tissot, B. and Leplat, P. Source Rock Characterization Method for Petroleum Exploration. Paper # OTC 2935. *Offshore Technology Conference* (1977) Houston, Texas.

Frysinger, G., Gaines, R., Xu, L., and Reddy, C. Resolving the Unresolved Complex Mixture in Petroleum-Contaminated Sediments. *Environmental Science & Technology* (2003) 37, 1653-1662.

Greibrokk, T., Radke, M., Skurdal, M. and Willsch, H. Multistage supercritical fluid extraction of petroleum source rocks: application to samples from Kimmeridge Clay and Posidonia Shale Formations. *Organic Geochemistry* (1992) 18, 4, 447-455.

Griesbaum, K., Behr, A., Biedenkapp, D., Voges, H.-W., Garbe, D., Paetz, C., Collin, G., Mayer, D., Höke, H. and Schmidt, R. Hydrocarbons. *Ullmann's Encyclopedia of Industrial Chemistry* (2013) 1-61.

Helgeson, H., Richard, L., McKenzie, W., Norton, D., and Schmitt, A. A chemical and thermodynamic model of oil generation in hydrocarbon source rocks. *Geochemica et Cosmochimica Acta* (2009) 594-695.

Hosterman, J. and Dulong, F. A computer program for semiquantitative mineral analysis of X-ray powder diffraction, *in* CMS Workshop Lectures, Quantitative Mineral Analysis of Clays, D.R. Pevear and F.A. Mumpton, eds. *The Clay Minerals Society* (1989) 1, 37-50.

Hosterman, J. and Whitlow, S. Clay mineralogy of Devonian shales in the Appalachian Basin. *Geological Survey Professional Paper 1298.* United States Printing Office (1983).

Huc, A., Nederlof, P., Debarre, R., Carpentier, B., Boussafir, M., Laggoun-Dèfarge, F., Lenail-Chouteat, A., and Bordas-Le Floch, N. Pyrobitumen occurrence and formation in a Cambro-Ordovician sandstone reservoir, Fahud Salt Basin, North Oman. *Chemical Geology.* (2000) 168, 1, 99-112.

Hutton, A., Bharati, S., and Robl, T. Chemical and Petrographic Classification of Kerogen/Macerals. *Energy & Fuels* (1994) 8, 1478-1488.

Jaffè, R., Gong, Y., and Furton, K. Temperature Effects of Supercritical Carbon Dioxide Extractions of Hydrocarbons from Geological Samples. *Journal of High Resolution Chromatography* (1997) 20, 586-590.

Jarvie, D. Shale Resource Systems for Oil and Gas: Part 2 – Shale-oil Resource Systems, *in* Shale Reservoirs: Giant Resources for the 21st Century, J.A. Breyer, ed. *AAPG Memoir* (2012) 97, 89-119.

Jarvie, D. and Baker, D. Application of the Rock-Eval III Oil Show Analyzer to the Study of Gaseous Hydrocarbons in an Oklahoma Gas Well. *187th ACS National Meeting* (1984) St. Louis, Missouri.

Kemmere, M., and Meyer, T. *Supercritical Carbon Dioxide: in Polymer Reaction Engineering*. Weinheim, Germany: Verlag GmbH & Co. Print.

Kolak, J. A Procedure for the Supercritical Fluid Extraction of Coal Samples, with Subsequent Analysis of Extracted Hydrocarbons. *U.S. Geological Survey* (2006) Open-File Report 2006-1054.

Kolak, J. and Burruss, R. An Organic Geochemical Assessment of CO_2-Coal Interactions During Sequestration. *U.S. Geological Survey* (2003) Open-File Report 03-453.

Laughrey, C., Ruble, T., Lemmens, H., Kostelnik, J., Butcher, A., Walker, G., and Knowles, W. Black Shale Diagenesis: Insights from Integrated High-Definition Analyses of Post-Mature Marcellus Formation Rocks, Northeastern Pennsylvania. *American Association of Petroleum Geologists* (2011) Search & Discovery Article #110150.

Lee, D., Herman, J., Elsworth, D., Kim, H., and Lee, H. A Critical Evaluation of Unconventional Gas Recovery from the Marcellus Shale, Northeastern United States. *KSCE Journal of Civil Engineering* (2011) 15, 4, 679-687.

Lesueur, D. The colloidal structure of bitumen: Consequences on the rheology and on the mechanisms of bitumen modification. *Advances in Colloid and Interface Science* (2009) 145, 42-82.

Lewis, R., Ingraham, D., Pearcy, M., Williamson, J., Sawyer, W., and Frantz, J. New Evaluation Techniques for Gas Shale Reservoirs. *Schlumberger Reservoir Symposium* (2004).

Li, W., Lazar, I., Wan, Y., Butala, S., Shen, Y., Malik, A., and Lee, M. Determination of Volatile Hydrocarbons in Coals and Shales Using Supercritical Fluid Extraction and Chromatography. *Energy & Fuels* (1997) 11, 945-950.

Maddocks, R., Gibson, J., and Williams, D. Supercritical Extraction of Coal. *Coal Processing Technology* (1979) 49-55.

Martìnez, Jose L. Supercritical Fluid Extraction of Nutraceuticals and Bioactive Compounds. Florida: CRC Press, Taylor & Francis Group, 2008. Print.

Maynard, J. Carbon isotopes as indicators of dispersal patterns in Devonian-Mississippian shales of the Appalachian Basin. *Geology* (1981) 9, 262-265.

McCarthy, K., Rojas, K., Niemann, M., Palmowski, D., Peters, K., and Stankiewicz, A. Basic Petroleum Geochemistry for Source Rock Evaluation. *Schlumberger Oilfield Review* (2011) 23, 2, 32-43.

Meyer, R. and de Witt, Jr., W. Definition and World Resources of Natural Bitumens. *U.S. Geological Survey Bulletin* (1990) *No. 1944*.

Meyers, P. Preservation of elemental and isotopic source identification of sedimentary organic matter. *Chemical Geology* (1994) 114, 289-302.

Milici, R. Assessment of Undiscovered Natural Gas Resources in Devonian Black Shales, Appalachian Basin, Eastern U.S.A. *U.S. Geological Survey* (2005) Open-File Report 2005-1268.

Milici, R. and Swezey, C. Assessment of Appalachian Basin Oil and Gas Resources: Devonian Shale – Middle and Upper Paleozoic Total Petroleum System. *U.S. Geological Survey* (2006) Open-File Report 2006-1237.

Monin, J., Barth, D., Perrut, M., Espitalie, M., and Durand, B. Extraction of hydrocarbons from sedimentary rocks with supercritical carbon dioxide. *Advances in Organic Geochemistry* (1987) 13, 4-6, 1079-1086.

Mort, A. and Sanei, H. Investigating laboratory-generated pyrobitumen precursors for unconventional reservoir characterization: a geochemical & petrographic approach. *Integration GeoConvention* (2013).

Nagy, B. and Simándi, B. Effects of particle size distribution, moisture content and initial oil content on the supercritical fluid extraction of paprika. *Journal of Supercritical Fluids* (2008) 46, 293-298.

Nelson, P. Pore-throat sizes in sandstones, tight sandstones, and shales. *AAPG Bulletin* (2009) 93, 3, 329-340.

Nunez-Betelu, L. and Baceta, J. Basics and Application of Rock-Eval/TOC Pyrolysis: an example from the uppermost Paleocene/lowermost Eocene in the Basque Basin, Western Pyrenees. *Ciencias Naturales* (1994) 46, 43-62.

Nuttall, B., Eble, C., and Drahovzal, J. Analysis of Devonian Black Shales in Kentucky for Potential Carbon Dioxide Sequestration and Enhanced Natural Gas Production. *Kentucky Geological Survey Final Report* (2005) DE-FC26-02NT41442.

Nuttall, B. Reassessment of CO_2 Sequestration Capacity and Enhanced Gas Recovery of Middle and Upper Devonian Black Shales in the Appalachian Basin. *MRCSP Phase II Topical Report* (2010).

Oldenburg, C., Pruess, K., and Benson S. Process Modeling of CO_2 Injection into Natural Gas Reservoirs for Carbon Sequestration and Enhanced Gas Recovery. *Energy & Fuels* (2001) 15, 293-298.

Ouyang, L. New Correlations for Predicting the Density and Viscosity of Supercritical Carbon Dioxide Under Conditions Expected in Carbon Capture and Sequestration Operations. *The Open Petroleum Engineering Journal* (2011) 4, 13-21.

Peters, K. Guidelines for Evaluating Petroleum Source Rocks Using Programmed Pyrolysis. *The American Association of Petroleum Geologists Bulletin* (1986) 70, 3, 218-329.

Peters, K. and Cassa, M. Applied Source Rock Geochemistry *in* Magoon, L.B., and Dow, W.G. (eds). The Petroleum System – From Source to Trap. *American Association of Petroleum Geologists Memoir* (1994) 60, 93-120.

Peters, K., Walters, C., and Moldowan, J. *The Biomarker Guide: Biomarkers and Isotopes in the Environment and Human History.* Vol. 1. Cambridge: Cambridge University Press, 2005. Print.

Pontolillo, J. and Stanton, R. Coal petrographic laboratory procedures and safety manual II. *U.S. Geological Survey* (1994) Open-File Report 94-631, 69.

Read, J., Whiteoak, D., and Hunter, R. The *Shell Bitumen Handbook.* 5th ed. London: Thomas Telford Publishing, 2003. Print.

Repetski, J., Ryder, R., Weary, D., Harris, A., and Trippi, M. Thermal Maturity Patterns (CAI and $\%R_o$) in Upper Ordovician and Devonian Rocks of the Appalachian Basin: A Major Revision of USGS Map I-917-E Using New Subsurface Collections. *U.S. Geological Survey* (2008) Scientific Investigations Map 3006.

Reverchon, E. and De Marco, I. Supercritical fluid extraction and fractionation of natural matter. *Journal of Supercritical Fluids* (2006) 38, 146-166.

Roden, M., Parrish, R., and Miller, D. The absolute age of the Eifelian Tioga ash bed, Pennsylvania. *Journal of Geology* (1990) 98, 282-285.

Roen, J. Geology of the Devonian black shales of the Appalachian Basin. *Organic Geochemistry* (1984) 5, 4, 241-254.

Rudyk, S., Spirov, P., & Sogaard, E. Application of GC-MS chromatography for the analysis of the oil fractions extracted by supercritical CO_2 at high pressure. *Fuel* (2013) 106, 139-146.

Rudzinksi, W. and Aminabhavi, T. A Review on Extraction and Identification of Crude Oil and Related Products Using Supercritical Fluid Technology. *Energy & Fuels* (2000) 14, 464-475.

Ryder, R., Hackley, P., Alimi, H., and Trippi, M. Evaluation of Thermal Maturity in the Low Maturity Devonian Shales of the Northern Appalachian Basin. *AAPG* (2013) Search & Discovery Article #10477.

Sageman, B., Murphy, A., Werne, J., VerStraeten, C., Hollander, D., and Lyons, T. A tale of shales: the relative roles of production, decomposition, and dilution in the accumulation of organic-rich strata, Middle-Upper Devonian, Appalachian basin. *Chemical Geology* (2003) 195, 229-273.

Schumacher, B., Shines, K., Burton, J., and Papp, M. A comparison of Soil Homogenization Techniques. *Lockheed Engineering and Sciences Company, Inc.* (1990) EPA 600//X-90/043.

Sing, K., Everett, D. Haul, R., Moscou, L. Pierotti, R., Rouquérol, J., and Siemieniewska. Reporting Physisorption Data for Gas/Solid Systems with Special Reference to the Determination of Surface Area and Porosity. *Journal of Pure and Applied Chemistry* (1985) 57, 4, 603-619.

Smith, D., Cannon, W., Woodruff, L., Solano, F., Kilburn, J., and Fey, D. Geochemical and mineralogical Data for Soils of the Conterminous United States. *U.S. Geological Survey* (2013) Data Series 801.

Soeder, D. Porosity & Permeability of Eastern Devonian Shale Gas. *SPE Formation Evaluation* (1988) 116-124.

Soeder, D. and Kappel, W. Water Resources and Natural Gas Production from the Marcellus Shale. *U.S. Geological Survey* (2009) Fact Sheet 2009-3032.

Sorenson, J., Harju, J., Hawthorne, S., Braunberger, J., Liu, G., Smith, S., and Steadman, E. Concepts for CO_2 EOR in the Bakken Formation. *19th Annual CO_2 Flooding Conference* (2013) Midland, Texas.

Span, R. and Wagner, W. A New Equation of State for Carbon Dioxide Covering the Fluid Region from the Triple-Point Temperature to 1100 K at Pressures up to 800 MPa. *Journal of Physical and Chemical Reference Data* (1996) 25, 6, 1509-1596.

U.S. Energy Information Administration. Marcellus Drilling Productivity Report (April 2014).

Vandenbroucke, M. and Largeau, C. Kerogen origin, evolution and structure. *Organic Geochemistry* (2007) 38, 719-833.

Walker, Jr., P., Verma, S., Rivera-Utrilla, J., and Davis, A. Densities, porosities and surface areas of coal macerals as measured by their interaction with gases, vapours and liquids. *Fuel* (1988) 67, 12, 1615-1623.

Wang, H., Li, G., and Shen, Z. A Feasibility Analysis on Shale Gas Exploitation with Supercritical Carbon Dioxide. *Energy Sources, Part A* (2012) 34, 1426-1435.

Werne, J., Sageman, B., Lyons, T., and Hollander, D. An Integrated Assessment of a "Type Euxinic" Deposit: Evidence for Multiple Controls on Black Shale Deposition in the Middle Devonian Oatka Creek Formation. *American Journal of Science* (2002) 302, 110-143.

Williams, D. Extraction with supercritical gases. *Chemical Engineering Science* (1981) 36, 11, 1769-1788.

Wilson, N. Organic petrology, chemical composition, and reflectance of pyrobitumen from the El Soldado Cu deposit, Chile. *International Journal of Coal Geology* (2000) 43, 53-82.

Zielinksi, R. Geochemical Characterization of Devonian Gas Shale. In *U.S. DOE Eastern Gas Shales Symposium.* ERC/SP-77/5, EGS-35 (1977).